ABSTRACT

ADAMS, VICTORIA. Myeloid Cell MHC I Expression Drives $CD8^+$ T Cell Activation in Nonalcoholic Steatohepatitis. (Under the direction of Dr. Arion Kennedy).

Activated $CD8^+$ T cells are elevated in Nonalcoholic steatohepatitis (NASH) and are important for driving fibrosis and inflammation. Despite this, mechanisms of $CD8^+$ T cell activation in NASH are largely limited. Specific $CD8^+$ T cell subsets may become activated through metabolic signals or cytokines. However, studies in NASH have not evaluated the impact of antigen presentation or the involvement of specific antigens. We hypothesize that $CD8^+$ T cell activation is dependent on antigen presentation of a unique NASH peptide. Therefore, we determined if activated $CD8^+$ T cells are dependent on MHC class I expression in NASH to regulate fibrosis and inflammation and if therapeutically blocking MHC I could prevent T cell activation.

We used H2Kb and H2Db deficient (MHC I KO*)*, Kb transgenic mice, and myeloid cell Kb deficient mice (LysM Kb KO) to investigate how MHC class I impacts $CD8^+$ T cell function and NASH. Flow cytometry, gene expression, and histology were used to examine hepatic inflammation and fibrosis. The hepatic class I immunopeptidome was evaluated by mass spectrometry. Molecular modeling and computational analysis utilizing *Pep*tide *B*inding *D*esign (PepBD) was used to develop blocking peptides.

In NASH, MHC class I isoform H2Kb was upregulated in myeloid cells. MHC I KO demonstrated protective effects against NASH-induced inflammation and fibrosis. Kb mice exhibited increased fibrosis in the absence of H2Db while LysM Kb KO mice showed protection against fibrosis but not inflammation. H2Kb restricted peptides identified a unique NASH peptide Ncf2 capable of $CD8^+$ T cell activation *in vitro*. Ncf2 reactive $CD8^+$ T cells were also detected *in vivo* through the use of an H2Kb-Ncf2 tetramer. The Ncf2 peptide was found to be

unique to NASH and was not detected during fibrosis resolution. Computational modeling and *in vitro* experimentation identified blocking peptides MHCP3 and MHCP5 to effectively block Ncf2 $CD8^+$ T cell activation and proliferation.

These results suggest that activated hepatic $CD8^+$ T cells are dependent on myeloid cell MHC class I expression in diet induced NASH to promote inflammation and fibrosis. Additionally, our studies suggest a role of NADPH oxidase in the production of Ncf2 peptide generation. Targeting H2Kb antigen presentation may be an effective treatment for NASH as blocking peptides MHCP3 and MHPC5 prevented Ncf2 $CD8^+$ T cell activation and proliferation.

Myeloid Cell MHC I Expression Drives $CD8^+$ T Cell Activation in Nonalcoholic Steatohepatitis

by
Victoria Adams

A dissertation submitted to the Graduate Faculty of
North Carolina State University
in partial fulfillment of the
requirements for the degree of
Doctor of Philosophy

Biochemistry

Raleigh, North Carolina
2024

APPROVED BY:

_____	_____
Arion Kennedy Committee Chair	Erin Baker
_____	_____
Paul Hess	Xiaojing Liu
_____	
Joe Barycki	

BIOGRAPHY

Victoria Adams obtained a B.S. degree in Biomedical Sciences from AdventHealth University in Orlando, Florida in 2018 receiving numerous scholarships that funded her undergraduate degree. While at AdventHealth she worked as a chemistry tutor and microbiology lab coordinator aiding in teaching and mentoring other students. At AdventHealth she had incredible support from mentors who helped encourage her love for science and taught her the basics of research. While working under the Santos's she was able to do microbiome research and attend her first national science conference. These experiences supported her throughout her graduate career at NC State University. At NC State University she was able to join Dr. Arion Kennedy's lab and dive into the world of immunology and metabolic diseases to better understand human health and disease.

ACKNOWLEDGMENTS

I want to start by thanking my previous teachers who encouraged and mentored me along my science journey. I want to thank Dr. Fernanda Santos and Dr. Anael Santos for being a constant pillar of support throughout my undergraduate degree and continuing to support me during my PhD. I would like to acknowledge all of those who have assisted me during my time in graduate school. Thank you to those who helped train me and provide guidance along the way.

I would like to acknowledge and thank my committee members Dr. Xiaojing Liu, Dr. Erin Baker, Dr. Paul Hess, and Dr Joe Barycki for providing input and being a part of my graduate school experience. I am thankful for my committee chair and PI, Dr. Arion Kennedy. Being one of your first students was a rollercoaster of ups and downs but I am extremely grateful for the time I got to spend here and the opportunity to do science with you. I have learned so much and it's truly been great to see how much we have both grown. I am excited to see where your lab projects go next and wish you all the best of luck.

Finally, I would like thank my husband for constantly being there for me on the good and bad days. This experience was not easy but I am so thankful that I had someone by my side to be my biggest cheerleader and constant support. I would also like to say a huge thank you to my family for all of your constant love and support.

TABLE OF CONTENTS

LIST OF TABLES

LIST OF FIGURES

CHAPTER 1: Introduction

1.1 Non-Alcoholic Fatty Liver Disease

Nonalcoholic fatty liver disease (NAFLD) represents a spectrum of liver pathologies, beginning with hepatic steatosis progressing to nonalcoholic steatohepatitis (NASH), cirrhosis, and even hepatocellular carcinoma (HCC) [1]. Hepatic steatosis is characterized by excess triglyceride accumulation in hepatocytes. Steatosis is the main feature of NAFLD and individuals have relatively low risk for developing liver-related adverse outcomes. However, about 20-30% of patients with steatosis progress to the NASH stage [2, 3]. In addition to excess lipid accumulation, NASH is characterized by hepatocyte damage (apoptosis and ballooning), inflammation, fibrosis, and immune cell infiltration **(Fig. 1.1)**.

Development of NAFLD is highly associated with metabolic diseases such as obesity, metabolic syndrome, insulin resistance, and dyslipidemia [4, 5]. With the rise of obesity, NAFLD has become more prevalent in younger individuals and even children [6, 7]. Studies have also shown strong correlations between NAFLD and the development of other diseases such as cardiovascular and kidney disease [8, 9]. Due to this high association with metabolic diseases, liver experts from 54 countries formulated a new name for NAFLD/NASH to better reflect the association with metabolic diseases. As of 2023 NAFLD has been renamed to metabolic dysfunction-associated fatty liver disease (MAFLD) and NASH has been rename to Metabolic dysfunction-associated steatohepatitis (MASH) [10, 11]. This change in nomenclature is geared towards outlining better diagnostic criterial for patients. Often times metabolic syndrome is the most common cause for fatty liver disease and is under-evaluated under the old nomenclature. When changing the name to MAFLD new diagnostic criteria were put in place and has been shown to have improved diagnostic capabilities [10].

Hepatic fibrosis is one of the strongest predictors of NASH mortality with a death rate of 12-25% NASH-related cirrhosis deaths [3]. End stage liver disease due to NASH represents the second leading cause for liver transplantation [3]. NAFLD-related cirrhosis accounts for 10-34% of HCC development in western countries. Additionally, increasing evidence suggests that about 13-49% of all HCCs develop in non-cirrhotic NASH patients [12]. Predicted prevalence of this disease is projected to increase with the rise of NAFLD stressing the need to develop effective treatment options [13]. Currently there is no FDA approved treatment for NAFLD/NASH and current treatment options rely on lifestyle interventions promoting weight loss. Additionally, the only way to clinically distinguish between NAFLD and NASH is through liver biopsy to determine the extent of liver fibrosis [9]. Future work is required to better understand the molecular mechanisms that drive NASH progression and identity potential therapeutic targets. Additional need for better diagnostic measures is also required for less invasive and earlier detection of fibrosis levels in patients.

1.2 The Immune System: Adaptive and Innate Immunity

The immune system can be classified into two types of immunity which include innate and adaptive immunity. In addition to its physical barriers, adaptive immunity is the first line of defense and acts in an antigen-independent manner that is non-specific to any particular pathogen. This process happens quickly and relies on pattern recognition receptors (PRRs) which allow innate immune cells to rapidly detect a wide range of pathogens through shared common structures known as pathogen associated molecular patterns (PAMPs). These cells can detect things such as bacterial components such as lipopolysaccharides (LPS) and viral double-stranded ribonucleic acid (RNA) [14]. Another important function of innate immunity is rapid immune

cell recruitment through the production of chemokines and cytokines in response to infection and inflammation [15]. What distinguishes adaptive from innate immunity is the ability to generate immunological memory. Adaptive immunity is antigen-dependent relying on a specific antigen to become activated and respond. Although the initial response is slow, memory cells are able to mount a more rapid and effective response to the same pathogen when exposed again to the same antigen [14, 16].

Many cells such as neutrophils, macrophages, and dendritic cells are involved in innate immune responses. Both neutrophils and macrophages are phagocytes sharing similar functions to engulf microbes and kill them. Neutrophils also contain granules and enzymes that help them eliminate pathogens and are typically short-lived cells. However, macrophages are long-lived cells that are also able to present antigens to T cells. Dendritic cells have an important role in bridging the adaptive and innate immunity as important messengers having both the phagocytosis functions and antigen presenting capabilities [17]. The adaptive immune system includes antigen-specific T cells activated by an antigen presenting cell (APC) and B cells which can differentiate into plasma cells producing antibodies. T cells are derived from bone marrow hematopoietic stem cells migrating to the thymus for maturation. These cells express T cell receptors (TCR) on their cell surface allowing for specific antigen binding to occur. Each T cell expresses a single type of TCR allowing them to recognize a wide variety of antigens [18]. Activation through antigen presentation on an APC is required for activation from cells such as macrophages, dendritic cells, or B cells. Once activated $CD8^+$ T cells become cytotoxic effector cells with the ability to target infected cells for apoptosis. Once the infection or source of inflammation is cleared most of the effector T cells die but some are retained becoming memory T cells which allow for faster reaction to the same antigen if presented it again [14, 16, 18]. B

cells are also derived from the bone marrow. These cells mature in the bone marrow and expression unique antigen binding receptors on their membranes. B cells do not require an antigen presenting cell for activation and can recognize antigens directly. B cells can also act as antigen presenting cells as well [16, 19, 20]. Although these responses are necessary for pathogen clearance, chronic activation can lead to overproduction of inflammation and aid in disease progression [14].

1.3 Immune Cells in Non-Alcoholic Steatohepatitis

NASH is characterized by immune cell infiltration, inflammation, oxidative stress, and fibrosis in the liver **(Fig. 1.2A)** [21]. During NASH, adaptive and innate immune cells such as neutrophils, macrophages, and $CD8^+$ T cells have been shown to regulate hepatic steatosis, inflammation, and fibrosis **(Fig. 1.2B)** [22-26].

Neutrophils are one of the first cells that respond to changes in inflammation and are key factors in inducing chronic inflammation by promoting macrophage recruitment [27-29]. Monoclonal Ly6G antibodies can be used to deplete neutrophils to identify their role in various diseases [30, 31]. In NASH neutrophil depletion with the Ly6G antibody led to protection against high fat diet induced NASH with reductions in body weight, inflammation, and fibrosis in mice [32]. However, neutrophil infiltration has been associated with early development of inflammation in NASH but the beneficial effects of neutrophil depletion are not seen as NASH continues to progress [33].

Macrophages are an extremely heterogeneous population with various phenotypes and functions [34]. The liver houses the largest proportion of macrophages among solid organs where they are essential for liver maintenance and homeostasis [35, 36]. Liver resident macrophages, known as Kupffer cells (KCs), originate from yok sac progenitors are self-sustaining. They play

a large role in homeostasis in the liver scavenging for cellular debris, pathogens, and gut-derived products [35]. These cells are distinguished from other macrophage types through the expression of cell surface markers such as CLEC4F and TIM4 [35, 37]. Bone marrow derived myeloid progenitors give rise to monocytes which can differentiate into monocyte-derived macrophages and macrophages. These populations are distinguished by their cell surface markers which include: monocytes (*Ly6c*$^{+}$ *CD11b*$^{+}$), monocyte-derived macrophages (*Ly6c*$^{+}$*CD11b*$^{+}$ *F480*$^{+}$*CD64*$^{+}$), and macrophages (*Ly6c*$^{-}$*CD11b*$^{+}$*F480*$^{+}$*CD64*$^{+}$). These cells are different from KCs as they are regulated by their microenvironment and can differentiate into pro-inflammatory (M1) macrophages or anti-inflammatory (M2) macrophages [34, 38].

In NASH, significant changes occur in myeloid derived cells with increased infiltration of monocytes and monocyte-derived inflammatory macrophages into the liver [39-41]. These monocyte derived macrophages are often found in close proximity to hepatic stellate cells (HSC) cells in areas of fibrosis in mice and humans suggesting they may have a role in liver fibrosis [41]. Recent studies using single-cell RNA sequencing have shown that in addition to increased infiltrating monocytes and monocyte-derived macrophages, there is a loss of embryonically derived KCs that can be partially replaced by monocyte-derived KCs permanently altering the KC pool in the liver [37, 42, 43].

In addition to macrophages, the liver contains a heterogeneous population of dendritic cells classified as conventional (cDCs) or plasmacytoid DCs [44, 45]. The role of DCs in NASH has conflicting results with studies arguing they are necessary for protection against NASH while others argue they promote NASH. This is largely due to the heterogeneity of DC populations and differences disease models. Some studies using mouse models of NASH have evidence to support cDCs having a protective role in preventing inflammation and fibrosis [46, 47]. In

contrast, cDCs were identified to infiltrate the liver in early stages of NASH due to increases in cDC1 bone marrow progenitor cells. cDC1's are associated with cross presentation of antigens to $CD8^+$ T cells and are defined by cell surface expression of CD103 and XCR1 in mice. XCR1 knockout and XCL1-blocking antibody studies showed these cells play a role in promoting inflammation and liver injury during NASH [48]. Further studies are needed to clarify the role of DCs and distinguish pathogenic vs beneficial subsets.

Intrahepatic B cells have been suggested to play a role in NAFLD progression. Infiltrating B cells have been associated with high levels of liver inflammation and fibrosis during NASH. These cells have many roles in immunity producing immunoglobulins, secreting cytokines, and presenting antigens [49]. In humans, patients with NASH show increased hepatic B cells with increased levels of circulating IgG against oxidative stress antigens [50]. Transcriptomic studies have identified a specific cluster of $CD38^+$ B cells that are altered in a diet-induced NASH model [51]. Additionally, B cell depletion in mice fed a methionine and choline deficient diet showed reductions in inflammation and fibrosis [52]. IgA^+ B cells have also been identified to play a critical role in the development of NASH-driven hepatocellular carcinoma (HCC) as the number of tumor-infiltrating B cells correlate with tumor progression in patients with HCC [51].

1.4 $CD8^+$ T Cell Functions in Disease and Resolution

$CD8^+$ T cells are comprised of heterogeneous populations that differ in phenotype and function supporting both pathogenic and beneficial functions during disease. These cells are differentiated by the cell surface markers they express making up naïve ($CD44^-CD62L^+$), effector/activated ($CD44^+CD62L^-$), and memory subsets. Memory $CD8^+$ T cells are comprised of

$CD8^+$ T cells that have responded to an antigen and persist long-term. Memory cells are capable of vigorous proliferation following reencounter with the same antigen. Memory cell subsets are categorized as T cell effector memory (*TEM, CD62L$^-$, CD44$^+$, CCR7$^-$, CXCR6$^-$)*, T cell resident memory (*TRM, CD62L$^-$, CD44$^+$, CCR7$^-$, CXCR6$^+$*) and T cell central memory (*TCM, CD6L2$^+$, CD44$^+$, CCR7$^+$*) [53, 54].

$CD8^+$ T cells can become activated through the identification of an antigen peptide presented on major histocompatibility complex (MHC) I molecules. This aids in the identification of intracellular pathogens and tumors [55]. This activates the T cell receptor (TCR) complex and mediates various intracellular signaling events that leads to T cell activation. Activated $CD8^+$ T cells can then secrete various cytokines such as granzyme B, and IFN-y and target infected cells for apoptosis [55]. In addition to antigen-dependent activation, $CD8^+$ T cells can also be activated by various cytokines such as IL-12, IL-18, and IL-15 [56-60]. $CD8^+$ T cells undergo metabolic reprogramming when they become activated, proliferate, and differentiate [61]. When naïve cells are activated, they go through a metabolic shift from oxidative phosphorylation to glycolysis to support their new energy needs [62]. Whereas memory cells rely on fatty acid oxidation as its main metabolic source **(Fig. 1.3)** [62]. Since $CD8^+$ T cells undergo metabolic reprogramming during differentiation they can also be influenced and activated through metabolites such as lactate, acetate, and extracellular ATP [56, 63].

$CD8^+$ T cells play a large role in various chronic liver diseases such as hepatitis C, NASH, and HCC. The hepatitis C virus (HCV) is one of the most common liver diseases and puts individuals at risk for developing cirrhosis and hepatocellular carcinoma [64, 65]. Patients that are able to clear the virus have HCV-specific $CD8^+$ T cells responding to specific viral epitopes. Individuals who are unable to clear the virus have impaired T cell functions, less HVC-

specific T cells, and high expression of exhaustion markers PD-1, 2B4, and KLRG1 [66-70]. Hepatocellular carcinoma (HCC) is another liver disease characterized by exhausted $CD8^+$ T cells, a feature commonly found in many cancers [71]. This is a result from the persistence of tumor antigens and the immunosuppressive tumor microenvironment [72]. Exhausted $CD8^+$ T cells express inhibitory receptors such as PD-1 and T-cell immunoglobulin and mucin-domain containing-3 (TIM3) which decrease their functional abilities. Exhausted $CD8^+$ T cells have reduced proliferation, decreased cytotoxic functions and decreased ability to release cytokines [73]. Partially exhausted $CD8^+$ T cells express only intermediate levels of inhibitory markers and their functions can be partially rescued by immune checkpoint inhibitors such as anti-PD1 [72]. Although this therapy has been approved and used in many cancers, its effectiveness in more advanced stages of HCC is only about 17-18% for complete or partial response to the anti-PD1 therapy [74, 75].

In contrast, $CD8^+$ T cells in NASH are key players in promoting hepatic inflammation and fibrosis in mice and humans [76-81]. Previous studies have shown that global knockdown or antibody depletion of $CD8^+$ T cells lead to a significant reduction in inflammation and fibrosis in the low-density lipoprotein receptor knockout (LDLRKO) NASH mouse model [81]. $CD8^+$ T cells are also known to interact with hepatocytes, HSCs, in addition to other immune cells [81]. Mechanisms for $CD8^+$ T cell activation in NASH remain elusive as there are many different subsets driving either pathogenic or beneficial effects. It is further complicated by the progressive nature of this disease as NASH can further progress to NASH-driven HCC. In contrast to NASH, as NASH-driven HCC progresses $CD8^+$ T cell infiltration and activation is significantly reduced [82]. The phenotype of these $CD8^+$ T cells significantly change as NASH transitions into HCC often associated with T cell exhaustion, auto-aggressiveness, and

expression of CXCR6 [83, 84]. Similar to the $CD8^+$ T cells found in NASH-driven HCC; one study identified a subset of resident $CD8^+$ T cells that act in an auto-aggressive manner targeting hepatocytes during NASH. These cells were characterized as expressing CXCR6, PD-1, and sensitive to metabolites such as acetate and extracellular ATP [56]. Further investigation is required as T cell exhaustion is typically associated with HCC and not early-stage NASH. Other studies have identified different T cell subsets in NASH that are activated and can directly activate HSCs during promoting liver fibrosis.

HSC cells are considered the primary source for pro-fibrotic mediators leading to NASH-associated liver fibrosis. Under homeostatic conditions HSC cells serve as the major storage site for retinol lipid droplets. When these cells become activated, they differentiate into myofibroblasts and secrete large quantities of extracellular matrix proteins [85, 86].

Interestingly, recent clinical evidence has shown that fibrosis resolution in the liver is possible through studies in patients with chronic hepatitis B virus (HBV) or HCV [87]. A study of NASH resolution in mice has shown a role for TRM $CD8^+$ T cells in resolving fibrosis. These $CD8^+$ T cells are maintained by IL-15 and attract HSC cells in a CCR5-dependent manner targeting them for apoptosis [88]. Additionally single cell TCR sequencing (scTCR-seq) identified the expansion of TCR clonal types of liver TRM cells in resolution mice suggesting they have an antigen-dependent role in fibrosis resolution [88]. Although studies have highlighted the importance of $CD8^+$ T cells in the progression and resolution of NASH, further investigation is required to better understand the mechanisms that regulate their activation.

1.5 Major Histocompatibility Complex Molecules

Major histocompatibility Complex (MHC) I molecules are expressed on all nucleated cells and are responsible for presenting short antigen peptides (8-11 amino acids in length) to $CD8^+$ T cells. MHC class I molecules are heterodimers with a glycosylated transmembrane heavy chain bound to a b2-microglobulin (b2m) subunit [89]. In mice, this region is referred to as the histocompatibility 2 (H2) complex and expresses three class I loci (K, D, and L) comparable to human class I loci HLA-A, HLA-B, and HLA-C. These genes are highly polymorphic, having numerous alleles for each locus (k, d, b, k, q), and are involved in regulating the peptide binding activities of MHC I **(Fig. 1.4)** [90]. Polymorphisms in these genes expand both the range of peptides presented and the interactions between the $CD8^+$ T cell receptor and MHC I molecule **(Fig. 1.5)** [89]. These presented peptides are typically derived from the cell's own proteins which can be altered under viral infections and disease conditions [91]. $CD8^+$ T cells can become activated when they recognize a specific peptide bound to an MHC class I molecule. Studies have even identified associations between certain MHC isoforms and susceptibility to certain diseases identifying a key way antigen presentation regulates the immune system driving disease progression [89].

1.6 MHC Class I Immunopeptidome

Peptides presented by MHC I molecules at the cell surface to $CD8^+$ T cells are known as the MHC I immunopeptidome [92, 93]. Although these peptides are critical for regulating the immune system, not much is known about its composition or how it changes in different tissues or in response to disease. The MHC I immunopeptidome contains a wide range of peptides 8-11 amino acids in length each with abundances varying between 1 and 10,000 copies per cell [92].

The composition of the immunopeptidome is further complicated by the high diversity of allelic forms of MHC I which allows different peptides to bind to the allele-specific anchor residues. Although the immunopeptidome is highly complex, mass spectrometry workflows have been very successful in identifying various MHC I peptides from human, mouse, and other species [92, 94, 95].

The immunopeptidome can be altered by disease conditions leading to altered protein expression and degradation generating new peptides called neoantigens. High fat diet (HFD) induced obesity models in mice have identified strong $CD8^+$ T cell responses to neo-antigens in adipose tissue. This study also evaluated the source of these neoantigens and discovered increased isolevuglandin (isoLG) proteins in CD206-expressing macrophages isolated from HFD fed mice [96]. IsoLGs were found to be elevated in M2 polarized macrophages and able to activate CD8+ T cells in vitro [96]. This study supports that obesity can lead to pathogenic $CD8^+$ T cell responses through a modified MHC I immunopeptidome. T cell receptor sequencing can also provide further support of altered immunopeptidome through the detection of high TCR clonality. High clonality in CD8+ T cells in patients with type 2 diabetes has identified an HLA-DR4–restricted epitope of insulin [97]. In mice and humans, obesity has shown to reduce naïve T cell pools and increase clonal T cell populations demonstrating peptide specificity [98]. Characterizing the MHC I immunopeptidome could highlight new targets and aid in the development of new T cell immunotherapies.

1.7 Immune Cell Therapy

Immunotherapy has become increasing popular over the years as we continue to further understand the roles of the immune system in diseases. Targeted immunotherapies are

particularly popular to treat various cancers. Many immune cell checkpoint inhibitor drugs are already in broad use as immune suppression of $CD8^+$ T cells often restricts their ability to clear cancer cells. These therapies utilize the patient's own cells and has had much success in cancer treatment [99]. Another form of immunotherapy called chimeric antigen receptors (CAR) T-cell therapy has also become popular. This form of immunotherapy utilizes the patents own T cells and reengineers them to respond to a specific antigen expressed typically by the cancer target [100].

In NASH $CD8^+$ T cells play a large role in disease progression; however, they also play a role in resolution [88]. Studies have shown that in resolution $CD8^+$ T cells have increased clonality suggesting they are responding to a specific peptide [88]. This could suggest that identification of a beneficial peptide could be utilized for an immunotherapy to activate specific $CD8^+$ T cells in NASH to resolve fibrosis. On the other hand, targeting and blocking pathogenic peptides in NASH could help reduce or prevent disease progression.

Overall, NASH development involves many different cellular players with various roles in promoting inflammation and fibrosis **(Table 1.1)**. Our studies aim to determine the role of antigen presentation, antigens that drive $CD8^+$ T cell activation, and peptides that block T cell activation. To address these questions flow cytometry will be utilized to detect changes in immune cell populations and activation. Lox-Cre mice will be used to alter MHC I expression and determine the role of potential antigen presenting cells. LC-MS/MS will be used to identify unique NASH peptides and flow cytometry to determine $CD8^+$ T cell reactivity. Computational modeling and flow cytometry will determine the bocking potential of blocking peptides. Targeting key cellular components such as MHC I and their antigens is essential for understanding $CD8^+$ T cell activation in NASH and identifying novel therapeutic targets.

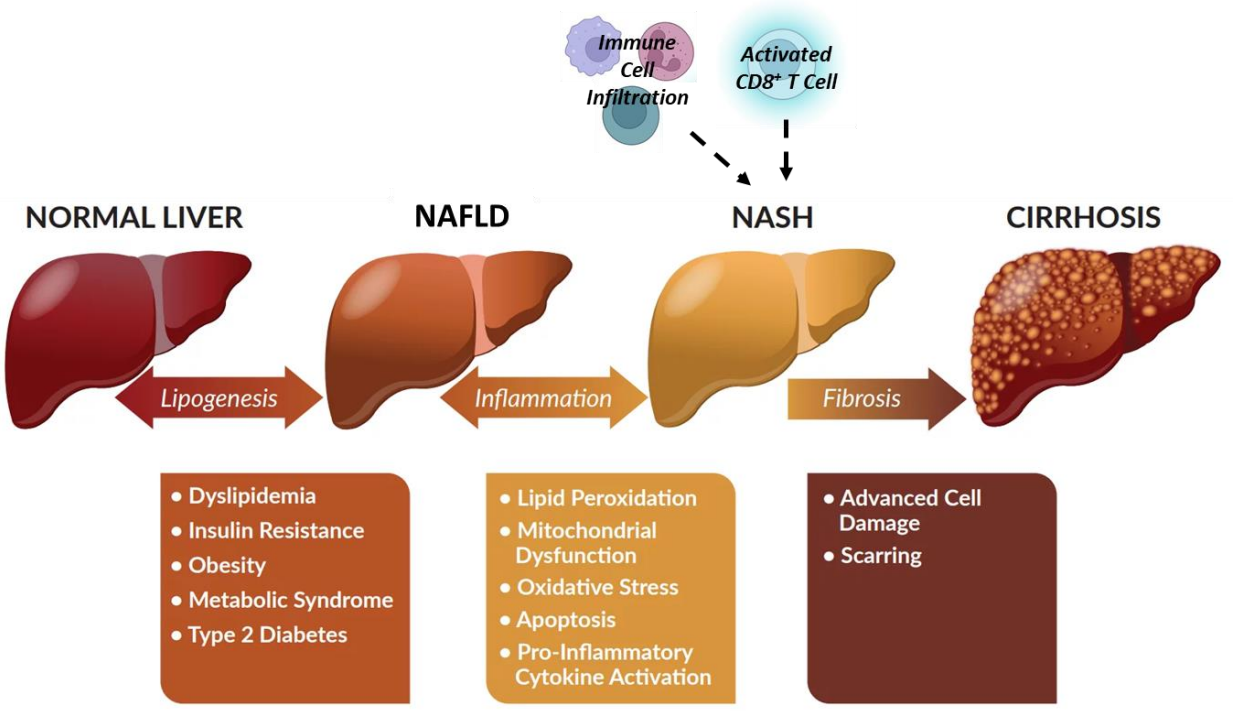

Figure 1.1. Non-Alcoholic Fatty Liver Disease Progression. Non-alcoholic Fatty Liver disease (NAFLD) is a progressive liver disorder representing a spectrum of liver pathologies. The first stage of NAFLD is characterized by excessive triglyceride accumulation called steatosis and is often associated with various metabolic diseases. The next stage of NAFLD is known as non-alcoholic steatohepatitis (NASH) and as disease progresses to NASH it is further accompanied by inflammation, fibrosis, and immune cell infiltration; most notably activated $CD8^+$ T cells. Further progression of NASH can lead to advanced cirrhosis accompanied by extensive cell damage and tissue scarring. Image modified from Cayman Chemicals Brochure [101].

A

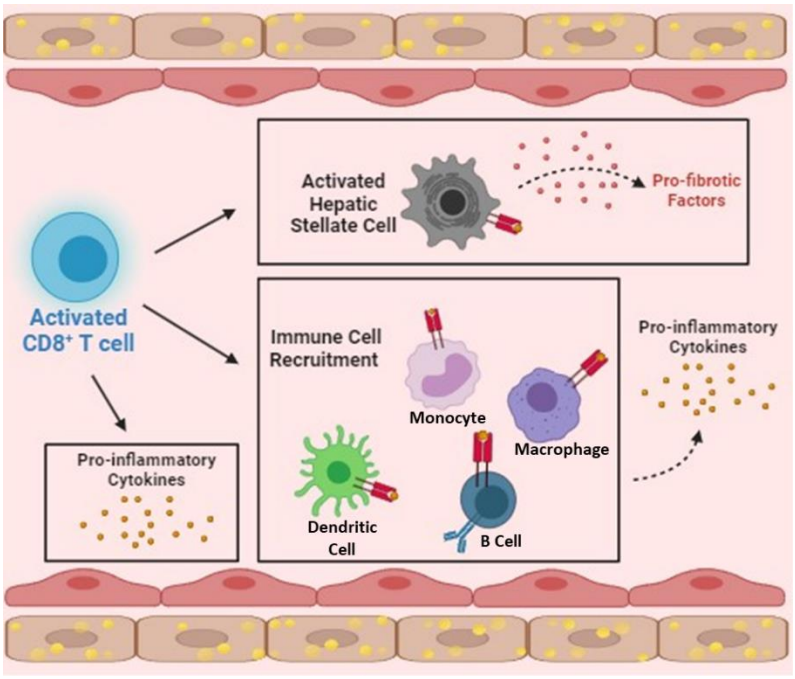

B

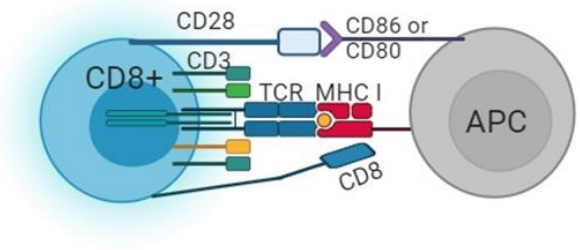

Figure 1.2 NASH Liver Immune Cell Microenvironment and CD8$^+$ T Cell Interactions. (A) Under NASH conditions CD8$^+$ T cells infiltrate the liver and are activated. Activated T cells can directly activate hepatic stellate cells (HSC), recruit other immune cells into the liver, and secrete pro-inflammatory cytokines. **(B)** CD8$^+$ T cells can become activated through MHC I antigen presentation of an antigen peptide and stimulation of its costimulatory receptors CD3 and CD28. MHC I is expressed on any nucleated cell including various immune cells such as macrophages, dendritic cells, and B cells. Figures were generated using BioRender.

Figure 1.3. Schematic diagram of $CD8^+$ T cell subsets and metabolic transitions. $CD8^+$ T cells subsets are defined by their functional and metabolic signatures. Single cell sequencing studies have identified specific genes upregulated during differentiation. Naïve $CD8^+$ T cells have low proliferation levels expressing gene markers such as CCR7. These cells show a preference for oxidative phosphorylation. Naïve cells can become activated and differentiate into cytotoxic effector T cells. These cells express genes such as CX3CR1 and have high proliferation levels in response to specific antigens. These cells shift to a metabolic preference for glycolysis. Memory $CD8^+$ T cells are derived from effector T cells and differentiate into three types: tissue resident memory (TRM), central memory (TCM), and effector memory (TEM). Both naïve and effector $CD8^+$ T cells have the potential to convert into a dysfunctional state leading to T cell exhaustion. This results in low levels of cytotoxic functions and an immunosuppressive phenotype. Image adapted from Zhong et al, 2023, Biomed. Pharmacother [102].

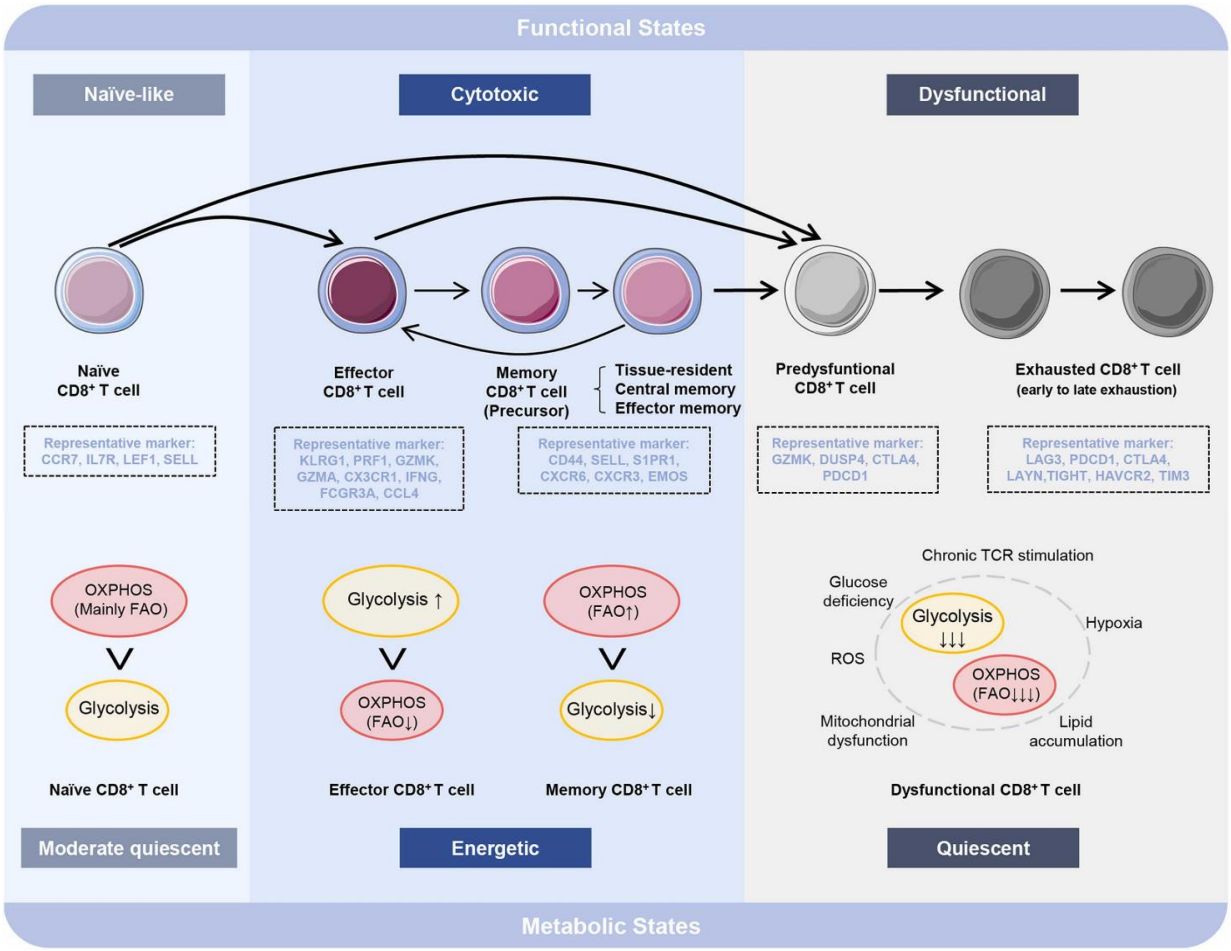
Functional States
Naïve-like
Cytotoxic
Dysfunctional
Naïve CD8+ T cell
Effector CD8+ T cell
Memory CD8+ T cell (Precursor)
Tissue-resident
Central memory
Effector memory
Predysfuntional CD8+ T cell
Exhausted CD8+ T cell (early to late exhaustion)
Representative marker: CCR7, IL7R, LEF1, SELL
Representative marker: KLRG1, PRF1, GZMK, GZMA, CX3CR1, IFNG, FCGR3A, CCL4
Representative marker: CD44, SELL, S1PR1, CXCR6, CXCR3, EMOS
Representative marker: GZMK, DUSP4, CTLA4, PDCD1
Representative marker: LAG3, PDCD1, CTLA4, LAYN,TIGHT, HAVCR2, TIM3
OXPHOS (Mainly FAO)
Glycolysis
Glycolysis ↑
OXPHOS (FAO↓)
OXPHOS (FAO↑)
Glycolysis↓
Chronic TCR stimulation
Glucose deficiency
Glycolysis ↓↓↓
Hypoxia
ROS
OXPHOS (FAO↓↓↓)
Mitochondrial dysfunction
Lipid accumulation
Naïve CD8+ T cell
Effector CD8+ T cell
Memory CD8+ T cell
Dysfunctional CD8+ T cell
Moderate quiescent
Energetic
Quiescent
Metabolic States

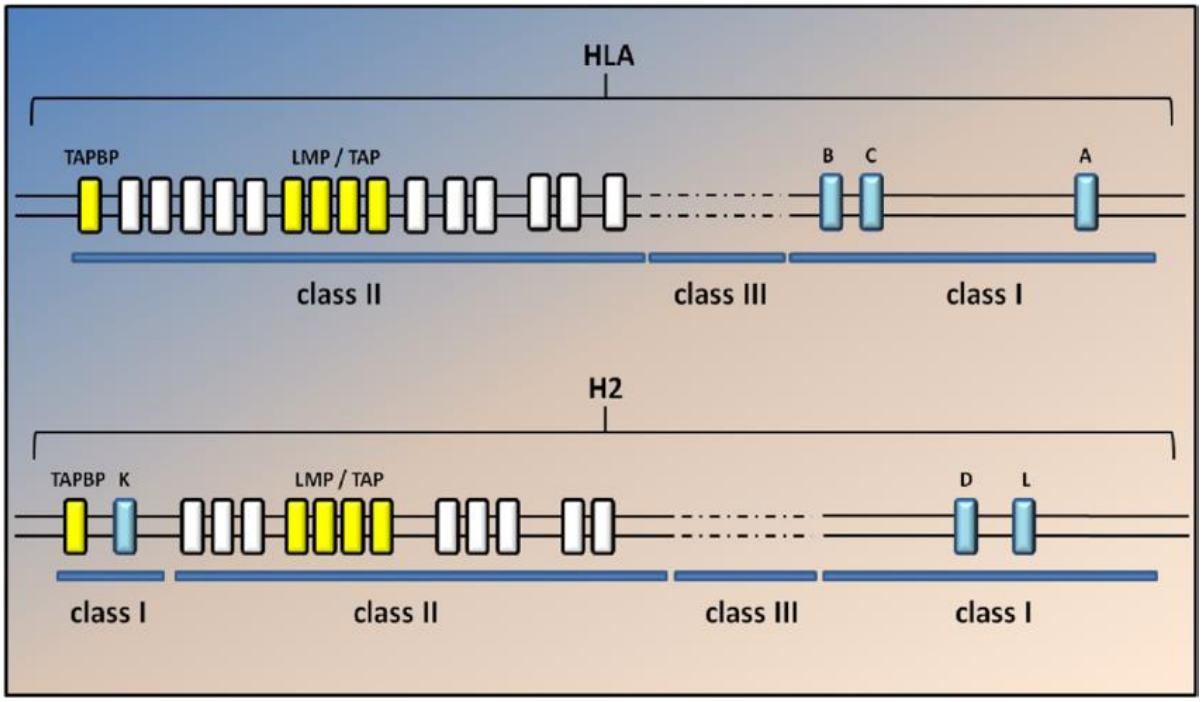

Figure 1.4. Simplified map of the human and mouse MHC class I genomic region. Human and mouse MHC I regions span about 3.6 mb and located on chromosomes 6 (human) and 17 (mice). MHC I regions are referred to as the human leukocyte antigens (HLA) in humans and histocompatibility 2 (H2) in mice. Other genes involved in MHC I antigen presentation are also encoded on the same chromosome including two TAP genes (Tap1 and Tap2) and immunoproteasome genes (Lmp2 and Lmp7). The beta-2-microglobin (b2m) light chain subunit of MHC I is encoded on a separate chromosome (15 in humans and 2 in mice). Overall human and mice have similar arrangements of their MHC genes but with the main difference being that in mice MHC I genes are separated by class II and III genes. Image derived from Nardo et al, 2016, Front. Neurol [103].

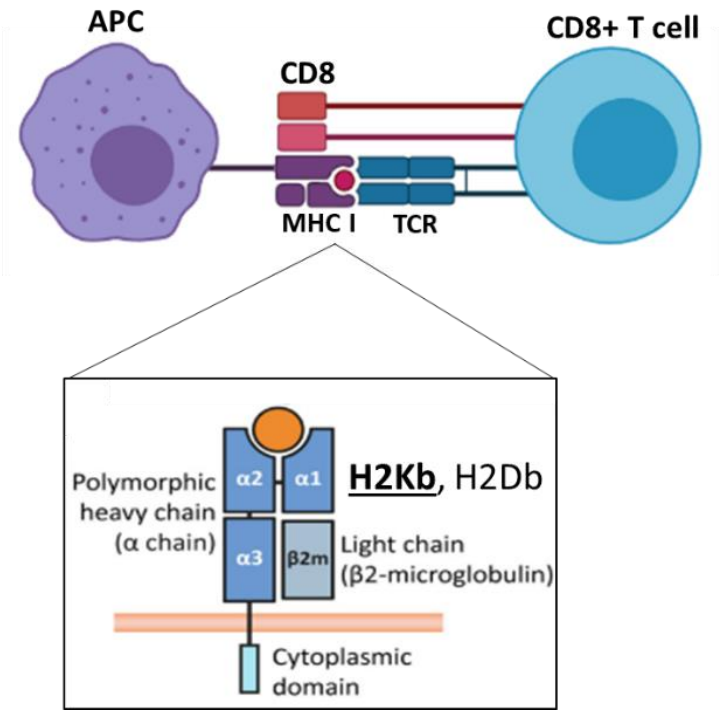

Figure 1.5. MHC Class I Antigen Presentation. MHC class I molecules are brought to the cell surface of any nucleated cell where they present antigen peptides to $CD8^+$ T cells. These peptides are usually derived from intracellular proteins. MHC I molecules are heterodimers consisting of an alpha heavy chain bound to a smaller protein subunit called β2-microglobulin (β2m). The alpha chain is highly polymorphic and allows for presentation of numerous peptides on different isoforms such as H2Kb and H2Db. Image generated using BioRender.

Table 1.1. Key Cellular Players In NASH.

Cell Type	Cellular Markers	Type of Immunity	Express MHC Class I	Function in NASH
Neutrophil	Ly6G	Innate	Yes	Promote inflammation and macrophage recruitment [17]
Kupffer Cell	CLEC4F, TIM4	Innate	Yes	Play a large role in liver homeostasis and are reduced during NASH [35, 37]
Monocyte	Ly6c, CD11b	Innate	Yes	Cytokine secretion and can differentiate into macrophages [39-41]
Monocyte-derived macrophage	Ly6c, CD11b, F4/80, CD64	Innate	Yes	Promote hepatic stellate cell activation and fibrosis. Can partially replace embryonically derived KC's that are lost during NASH [39-41].
Macrophage	CD11b, F4/80, CD64	Innate	Yes	Can differentiate into pro-inflammatory macrophages increasing inflammation during NASH [34, 38].
Dendritic Cell	CD11c, CD103, XCR1	Innate	Yes	Protective and pathogenic functions in NASH involved with inflammation and fibrosis [44, 45].
CD8 T cell	CD8, TCRb	Adaptive	Yes	Are increased and activated in the liver during NASH. They can activate hepatic stellate cells, recruit other immune cells, and secrete pro-inflammatory cytokines during NASH [18]
B cells	CD19, CD20	Adaptive	Yes	Associated with high levels of inflammation and fibrosis in NASH. Increased hepatic B cells in association with increased levels of IgG against oxidative stress antigens [49].
Stellate Cells	α-SMA	N/A	Yes	Can become activated by Macrophages or CD8 T cells under NASH conditions where they release their stored lipid droplets and secrete pro-fibrotic factors [85, 86].
Hepatocytes	Albumin	N/A	Yes	Become enlarged with large lipid droplets during NASH exhibiting hepatocyte ballooning, lobular inflammation, and apoptotic bodies. Are ultimately damaged and can die under NASH conditions [104-107].

CHAPTER 2: MHC Class I Characterization in NASH

Modified from publication: Adams, V.R., Collins L.B., Williams T.I, Holmes J., Hess P., Atkins H.M., Scheidemantle G., Liu X., Lodge M., Johnson A.J., Kennedy A. *Frontiers in Immunology*, **2023**, *Vol 14*, https://www.frontiersin.org/articles/10.3389/fimmu.2023.1302006

2.1 Introduction

In NASH activated $CD8^+$ T cells are elevated and are key players in driving fibrosis and inflammation. However, limited studies have evaluated mechanisms of $CD8^+$ T cell activation in NASH. MHC I antigen presentation is an important factor for priming $CD8^+$ T cell responses to infection and disease. In humans, human leukocyte antigen (HLA) regions are encoded by the MHC complex located on chromosome 6p21 [108]. This region is highly polymorphic containing a variety of genes that encode for molecules involved in immune responses [109]. Genome-wide associate studies have identified single nucleotide polymorphisms in the HLA region which contribute to various liver diseases such as NAFLD [110-112]. In humans, limited studies have addressed the impact of MHC Class I in regulating NAFLD associated pathologies. Human HLA class I alleles such as HLA*B27 are associated with advanced steatosis, while alleles HLA*C4, HLA*A31 and HLA*C6 correlate with NASH and advanced fibrosis [113, 114]. Although these studies highlight the importance of different MHC I isoforms in NASH development, additional studies are required to understand its impact on antigen presentation and $CD8^+$ T cell activation.

Other studies have evaluated the impact of major histocompatibility complex II molecules (MHC II) role in NASH as these molecules can also present antigens but to $CD4^+$ T cells [115]. However, MHC II knockout studies with mice on high fat diet showed no protective effects on liver inflammation or lipid accumulation. Additionally, MHC II KO mice treatment with carbon-tetra-chloride- (CCl4-) to induce hepatic cirrhosis were not protected from fibrosis

with no significant changes between the WT gene expression and histological staining for fibrosis [115]. This data suggests that the MHC II pathway is not involved in NASH development [115].

Although some work has been done to identify MHC I alleles associated with NAFLD pathologies in humans, additional studies are required to address their functional impacts on antigen presentation, cell specific expression of MHC I, and $CD8^+$ T cell activation [113, 114]. Non-specifically targeting $CD8^+$ T cells for therapy can be difficult as they are also required for the clearance of pathogens and malignant cells. Therefore, developing therapies to target key molecular pathways or factors such as MHC I molecules or antigen peptides involved in NASH-associated $CD8^+$ T cell activation is key. Our studies aim to determine how MHC I expression is altered in antigen presenting cells under NASH conditions. We hypothesize that myeloid cells will have increased MHC I expression and are the main antigen presenting cells in the liver during NASH. We propose to evaluate MHC I isoforms H2Kb and H2Db in myeloid cells and B cells during NASH using flow cytometry.

2.2 Materials and Methods

2.2.1 Animal Models

Male 5-wk-old C57BL/6J and low-density lipoprotein receptor knockout (LDLRKO) mice were originally purchased from Jackson Laboratories (Bar Harbor, ME) and further propagated in our colony. *LDLRKO NASH model*. Male 6-wk-old *LDLRKO* mice were fed chow or western diet (WD, 42 Kcal% fat with 0.2% added cholesterol, TD.22137; Harlan Laboratories) for 12 weeks. *Taconic Amylin NASH Model*. C57BL/6NTac (Tac) male mice were purchased from Taconic Biosciences on chow or amylin diet (AMLN, 40 kcal% fat, 20 kcal%

fructose and 2% cholesterol, Diet # D09100310i, Research Diets) remaining on diet for a total of 28 weeks. *WT Amylin NASH Model*. Male 6-wk-old C57BL/6J (WT) mice were fed chow or amylin diet (40 kcal% fat, 20 kcal% fructose and 2% cholesterol, Diet # D09100310i, Research Diets) for 28 weeks.

All Mice were housed with ad libitum access to food and water on a 12-hour light/dark cycle. Mice were sacrificed between the ages of 15-34 weeks. All animal procedures were approved by the Institutional Animal Care and Use Committee (IACUC) at North Carolina State University under protocol 21-502-B.

2.2.2 Immune Cell Isolation from Liver

Mice were anesthetized and perfused through the heart with 1X PBS. Mouse livers were collected and minced in RPMI, 1 mg/ml Collagenase IV, 2 mg/ml Collagenase II, 1 mg/ml Protease, and 0.01 mg/ml DNase and incubated at 37°C for 25 min shaking. The cell suspension was filtered through a 100-μm filter with wash buffer and centrifuged at 443 xg for 6 min at 4°C. Supernatant was discarded and the pellet washed and centrifuged at 443 xg for 6 min at 4°C. The pellet was re-suspended in 33% Percoll and centrifuged at 850 xg for 15 min at 4°C with minimum break and accelerator. The pellet was resuspended in wash buffer and centrifuged at 300 xg for 5 min at 4°C and the supernatant discarded. The pellet was resuspended in ACK lysing buffer and incubated at room temperature for 5 min. After incubating, wash buffer was added and centrifuged at 300 xg for 5 min at 4°C. The supernatant was discarded and the pellet resuspended in FACS buffer filtered through a cell strainer cap tube and prepared for cell culture or flow cytometry.

2.2.3 Flow Cytometry

Isolated cells from the liver were incubated with Fc block followed by incubation with fluorophore conjugated antibodies on ice in FACS buffer for the following panels: T cell panel: CD8a (PE-Cy7, 1:200, BD Biosciences), TCRβ (APC-Cy7, 1:200, BD Biosciences), CD44 (A700, 1:200, BD Biosciences), and CD62L (APC, 1:200, BD Biosciences). Macrophage Panel: F4/80 (A700, 1:200, Biolegend), CD64 (PE, 1:200, BD Biosciences), CD11b (FITC, 1:200, BD Biosciences), Ly6c (PerCP-Cy5.5, 1:200, BD Biosciences), H2Kb (APC-eFluor780, 1:200, ThermoFisher), and H2Db (PE-Cy7, 1:200, BD Biosciences). B Cell Panel: CD19 (APC, 1:200, BioLegend), H2Kb (APC-eFluor780, 1:200, ThermoFisher), H2Db (PE-Cy7, 1:200, BD Biosciences), and MHC II (PerCP-Cy5.5, 1:200, BD Biosciences). After incubation samples were washed twice with FACS buffer. Flow data was acquired on a Becton Dickinson LSRII machine in the NCSU flow Cytometry Core. All data was analyzed using FlowJo software v10.8. Flow gating strategies are provided (Figure 1.7).

2.2.4 Western Analysis

A 50 mg piece of frozen liver was homogenized in 0.5 ml of RIPA buffer (150 mM Sodium Chloride, 1% Triton X-100, 0.5% Sodium Deoxycholate, 0.1% SDS, 50 mM Tris, and 1 mM EDTA) containing 1X protease and phosphatase inhibitor cocktail (Halt). Samples were centrifuged for 15 min at 12,000 rpm at 4°C. Supernatants were aspirated and protein quantified using Pierce BCA protein assay according to manufacturer's instructions. Proteins were separated by SDS-PAGE and transferred to activated PVDF membranes. Membranes were blocked with OneBlock blocking buffer (Prometheus, Genessee Scientific) for 1 hr at room temperature shaking. Membranes were then probed with antibodies H2Kb (BioXCell) or H2Db

(Santa Cruz) at 4°C shaking overnight. All blots were probed for β-actin (Cell Signaling Technology) 1 hr at room temperature. After blocking membranes were washed three times for 5 min in 1X PBS with 0.1% Tween-20 at room temperature. After washing membranes were incubated with Licor secondary antibodies goat anti-rabbit IRDye 800CW and goat anti-mouse IRDye 680RD at 1:10,000 dilutions with 0.1% Tween-20 for 1 hr at room temperature protected from light. Blots were washed again as described previously and imaged on Odyssey Infrared Imaging System. Band intensity quantification was obtained using Image Studio Lite version 5.2 software.

2.3 Results

2.3.1 $CD8^+$ T cells are Increased and Activated in NASH

Our previous work has shown increased activated $CD8^+$ T cells in the LDLRKO obese/hyperlipidemia mouse model of NASH. We have shown that $CD8^+$ T cells play a key role in regulating inflammation and fibrosis through CD8 antibody depletion and adoptive transfer studies [81]. We demonstrate that activated $CD8^+$ T cells are significantly increased in obese mouse models of NASH using low density lipoprotein receptor knockout mice (LDLRKO) on western diet (WD) **(Fig. 2.1A-B)** and Taconic mice on amylin diet (Tac NASH) (**Fig. 2.1C-D).**

2.3.2 NASH Mice Have Increased H2Kb and H2Db in Myeloid Cells

Because $CD8^+$ T cells are class I restricted, we evaluated the expression of MHC I isoforms, H2Kb and H2Db, under NASH conditions. In mice classical Ia genes H2Kb and H2Db are responsible for encoding the peptide binding cleft of the alpha-1 and alpha-2 subunits of the MHC I molecules. This determines what peptides and $CD8^+$ T cells will bind to the MHC I

molecule. Total liver protein analysis revealed H2KB protein expression was significantly upregulated during NASH with increasing trends for H2DB expression **(Fig. 2.2A-B).** We used flow cytometry analysis to determine if NASH impacts myeloid specific expression of H2Kb and H2Db in WT mice fed amylin diet for 28 weeks. Macrophages and recruited monocytes are elevated in NASH and crucial to inflammation, fibrosis, and immune cell activation in chronic liver diseases [36]. In $CD11b^+$ myeloid cells, overall H2Kb expression was significantly increased compared to H2Db expression. Additionally, H2Kb expression was significantly increased in NASH compared to chow **(Fig. 2.2C).**

Our studies confirmed increased monocytes ($Ly6c^+$ $CD11b^+$), monocyte derived macrophages ($Ly6c^+CD11b^+F480^+CD64^+$), and macrophage populations ($Ly6c^-$ $CD11b^+F480^+CD64^+$) in our WT NASH model **(Fig. 2.2 D, G, J).** Additionally, H2Kb and H2Db were significantly increased in the myeloid cell populations in NASH compared to chow controls **(Fig. 2.2 E-F, H-I, K-L).** These findings were consistent across Tac NASH **(Fig. 2.3A-I)** and LDLRKO NASH models **(Fig. 2.4A-F).** In summary, H2Kb and H2Db are increased in myeloid cells in NASH livers. However, it remains unknown how changes in the expression of H2Kb or H2Db impact NASH progression or $CD8^+$ T cell activation.

2.3.3 H2Kb and H2Db Expression Does Not Change in NASH $CD19^+$ B Cells

Studies have shown that B cell deficiency protects mice against liver fibrosis and inflammation in diet induced NASH models [52, 116]. Studies also suggest that the gut microbiome can promote NASH progression through activation of intrahepatic B cells through microbial factors [116]. However, MHC II is often upregulated in patients with NASH preceding $CD8^+$ T cell infiltration into the liver [52]. It is known that B cells can activate $CD8^+$ T cells

though IgA-FcR signaling. However, the impact of NASH on B cell MHC I expression and antigen presentation has not been evaluated.

We examined MHC I expression on hepatic $CD19^+$ B cells and found no significant differences in H2Kb or H2Db in livers of normal and NASH mice **(Fig. 2.5).** This suggests that B cells may not play a role in MHC I antigen presentation and promote NASH primarily through other methods such as the IgA-FcR signaling. However, other subsets of B cells were not evaluated and differences may be seen depending on their tissue localization.

2.4 Discussion

In the present study, we demonstrate that MHC I expression is significantly upregulated in NASH. We have shown in three obese mouse models of NASH that MHC I isoforms H2Kb and H2Db are upregulated in myeloid cells under NASH conditions. Our data suggests this increase in H2Kb expression is cell specific as we have shown $CD19^+$ B cell MHC I expression was not affected by NASH. It remains to be determined if H2Kb expression alters antigen presentation capabilities and how this may impact $CD8^+$ T cell activation in NASH.

Hepatic inflammation has been linked to bone marrow derived monocyte infiltration into the liver driving NAFLD progression. Monocyte recruitment to the liver has been shown to be mediated by the CCR2 chemokine receptor. Inhibiting CCR2 in a mouse model of NASH showed reductions in steatosis, inflammation, and fibrosis [36, 81, 117]. Monocytes can further differentiate into monocyte-derived macrophages where they can release pro-inflammatory cytokines promoting further inflammation [81, 117, 118]. Macrophages are also key players involved in fibrosis development during NASH [119-122]. A recent transcriptomic study characterized macrophage subsets in NASH identifying increased pro-fibrotic and M2 macrophage subsets significantly correlated with degree of fibrosis in human patients [123]. This

data in conjunction with ours suggests that myeloid cells have a key role in fibrosis in NASH potentially through H2Kb antigen presentation.

Recently MHC I molecules have been found to not only be required for $CD8^+$ T cell activation, but also required for the generation of innate immune cell memory [124]. Pre-stimulated innate immune cells were shown to demonstrate stronger responses after being previously exposed to an antigen through epigenetic modifications displaying memory-like behaviors called trained immunity. Studies have shown strong evidence to support memory-like behaviors in innate cells such as macrophages through these epigenetic changes. Myeloid cells pre-stimulated with an antigen were found to have faster and more vigorous responses when responding to the same antigen, becoming more effective antigen presenting cells boosting $CD8^+$ T cell activation [125, 126]. This could provide a potential mechanism for altered H2Kb expression in myeloid cells and aid in antigen presentation capabilities.

Although much work has been done evaluating myeloid cell activation in NASH, little work has been done evaluating H2Kb expression and antigen presentation in NASH. Our data suggests that myeloid cells could be regulating $CD8^+$ T cell activation through increased H2Kb expression and antigen presentation to regulate fibrosis. However, more work needs to be done to evaluate if increased myeloid cell H2Kb expression is linked to increased antigen presentation capabilities and alterations in $CD8^+$ T cell activation.

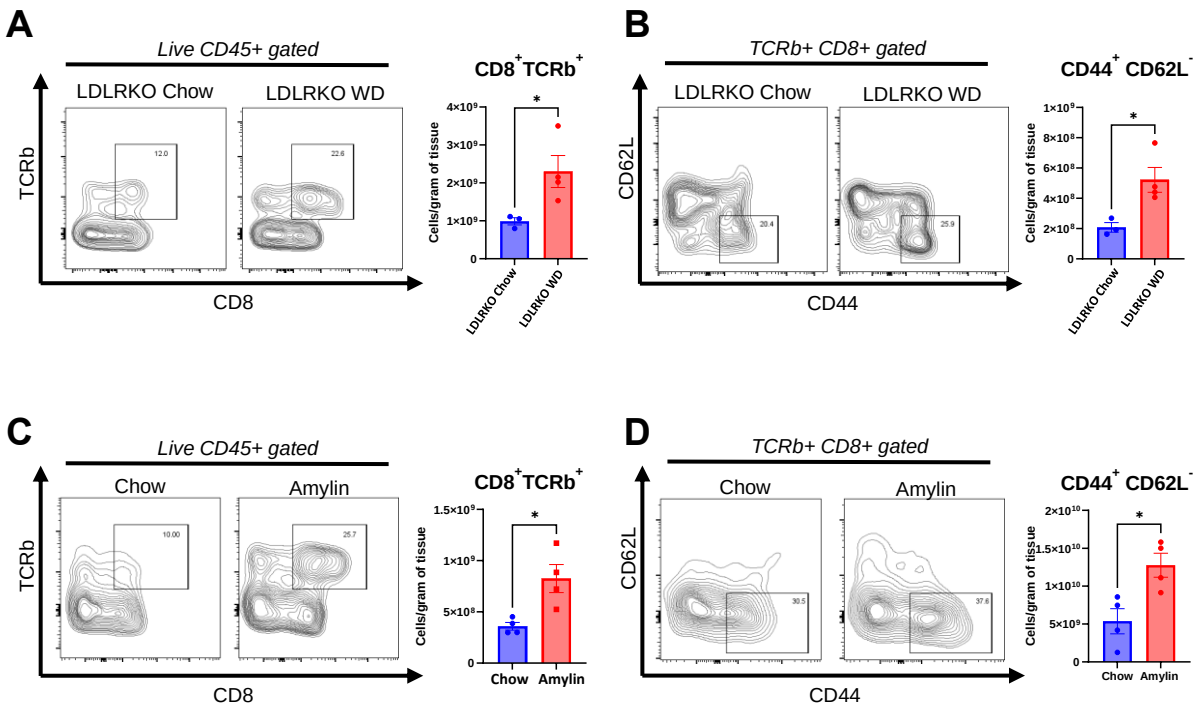

Figure 2.1. CD8$^+$ T cells are upregulated in NASH. LDLRKO mice on chow or WD for 12 wks (n=3-4 mice per group, 2 replicate studies). Taconic mice on chow or amylin diet for 28 wks (n=5 mice per group, 2 replicate studies). Representative flow plots and analysis of *CD8$^+$TCRb$^+$* cells **(A)** and activation **(B)** in the LDLRKO model. Representative flow plots and analysis of *CD8$^+$TCRb$^+$* cells **(C)** and activation **(D)** in the WT model. Data shown as the mean ± SEM. Two-tailed unpaired Student's t-tests was performed and considered statistically significant for $P<0.05$ (*).

Figure 2.2. H2Kb is upregulated in myeloid cells in NASH. WT mice were fed chow or amylin diet for 28 wks (n=5 per group) in two replicate cohorts. **(A)** Total liver protein of H2KB and H2DB. **(B)** Quantification of protein expression normalized to b-actin. (C) H2Kb and H2Db expression on $CD11b^+$ cells. **(D)** Flow analysis of monocytes (*$Ly6c^+CD11b^+$)* and monocyte H2Kb **(E)** and H2Db **(F)** expression. **(G)** Flow analysis of monocyte derived macrophages (*$Ly6c^+CD11b^+CD64^+F4/80^+$*) monocyte derived macrophage H2Kb **(H)** and H2Db **(I)** expression. **(J)** Flow analysis of macrophages (*$Ly6^-CD11b^+CD64^+F4/80^+$)* and macrophage H2Kb **(K)** and H2Db **(L)** expression. Data shown as the mean ± SEM. Two-tailed unpaired Student's t-tests and determined significant by $P<0.05$ (*), $P<0.01$ (**), $P<0.001$(***), and $P<0.0001$(****),

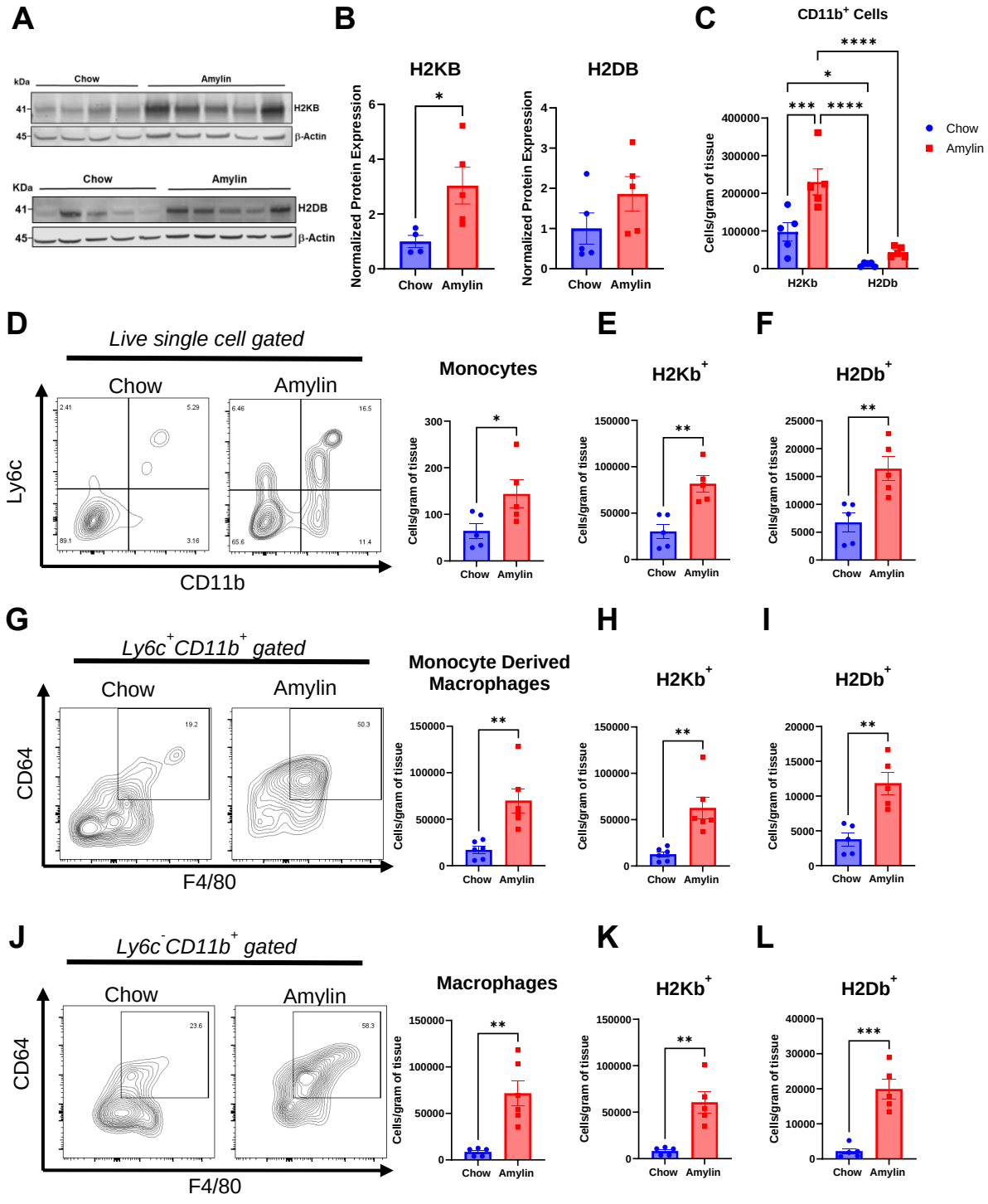
A
kDa
Chow
Amylin
41
45
H2KB
β-Actin
KDa
H2DB
B
H2KB
H2DB
Normalized Protein Expression
Chow
Amylin
C
CD11b+ Cells
Cells/gram of tissue
H2Kb
H2Db
D
Live single cell gated
Ly6c
CD11b
Monocytes
E
H2Kb+
F
H2Db+
G
Ly6c+CD11b+ gated
CD64
F4/80
Monocyte Derived Macrophages
H
I
J
Ly6c-CD11b+ gated
Macrophages
K
L

Figure 2.3. Taconic NASH mice have increased H2Kb and H2Db in myeloid cells.

Taconic mice on chow or amylin diet for 28 wks (n=4 mice per group, 2 replicate cohorts). Flow analysis of monocytes (*Ly6c*$^{+}$*CD11b*$^{+}$) **(A),** monocyte H2Kb expression **(B)**, and monocyte H2Db expression **(C)**. Flow analysis of monocyte derived macrophages (*Ly6c*$^{+}$*CD11b*$^{+}$ *CD64*$^{+}$*F480*$^{+}$) **(D),** monocyte derived macrophage H2Kb expression **(E)**, and monocyte derived macrophage H2Db expression **(F)**. Flow analysis of macrophages (*Ly6c*$^{-}$*CD11b*$^{+}$*CD64*$^{+}$*F480*$^{+}$) **(G),** macrophages H2Kb expression **(H)**, and macrophages H2Db expression **(I)**. Data shown as the mean ± SEM. Two-tailed unpaired Student's t-tests was performed and considered statistically significant for $P<0.05$ (*), $P<0.01$ (**), and $P<0.001$(***).

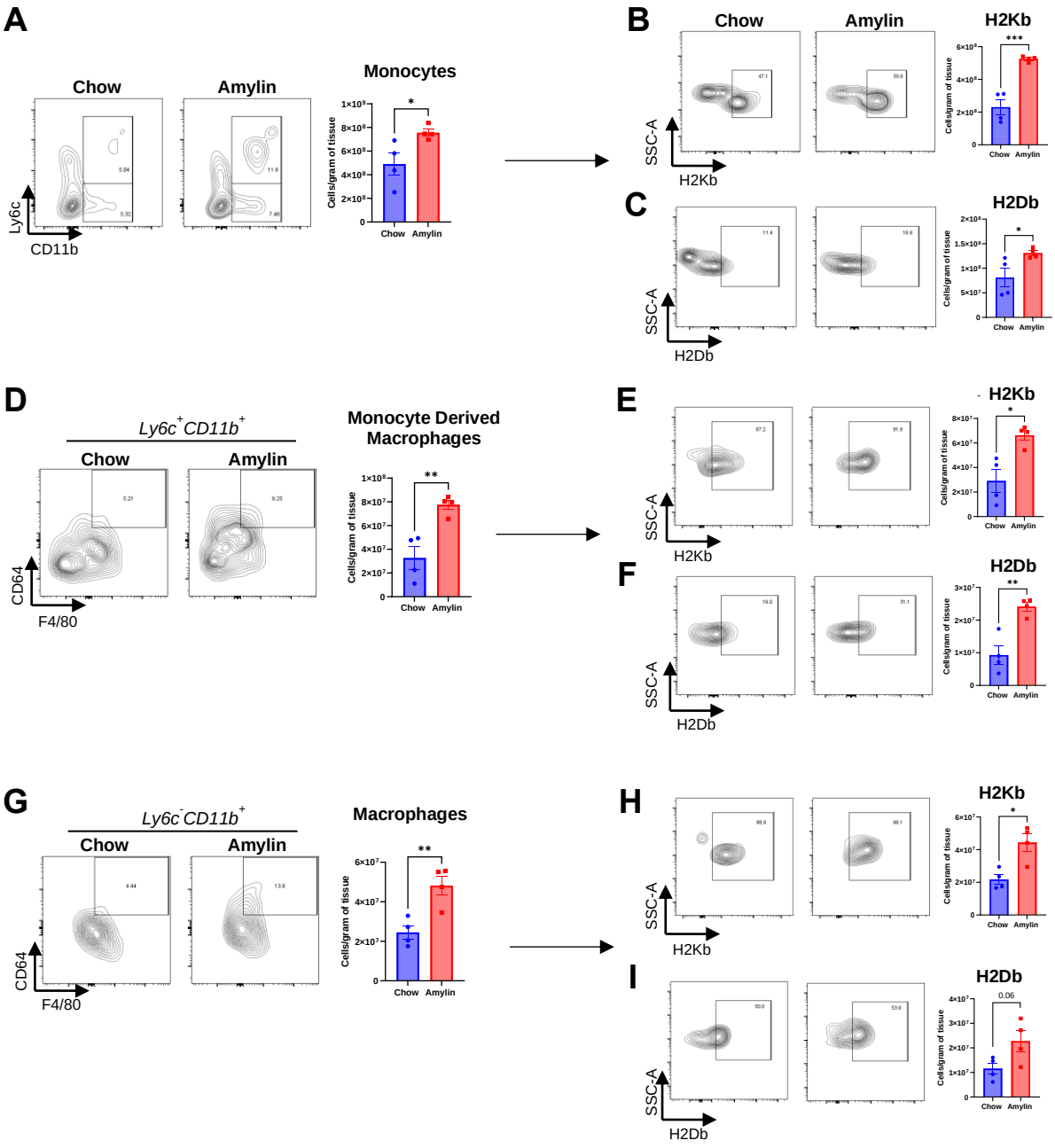
A
Chow
Amylin
Ly6c
CD11b
Monocytes
Cells/gram of tissue
Chow
Amylin
B
Chow
Amylin
H2Kb
SSC-A
H2Kb
Cells/gram of tissue
C
H2Db
SSC-A
H2Db
D
Ly6c+CD11b+
Chow
Amylin
CD64
F4/80
Monocyte Derived Macrophages
E
H2Kb
F
H2Db
G
Ly6c-CD11b+
Macrophages
H
I

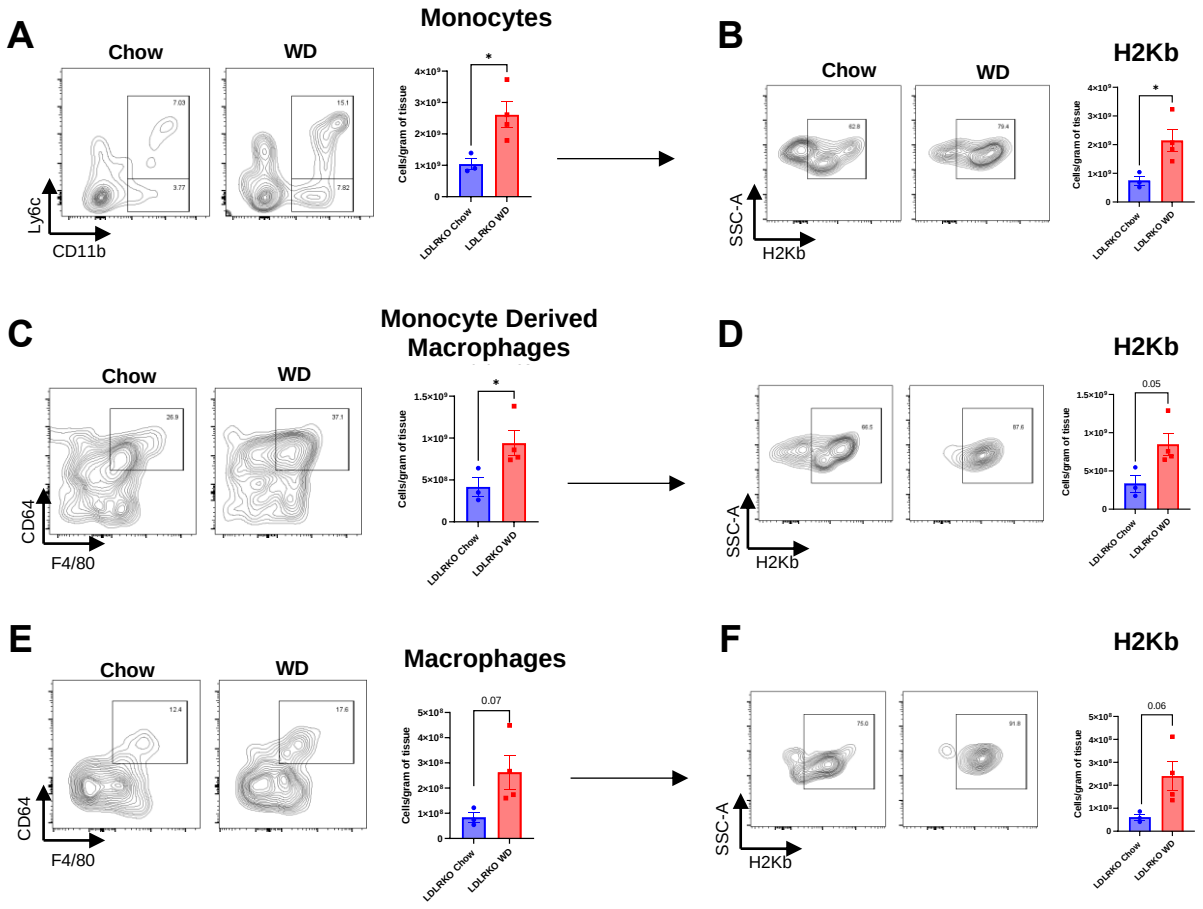

Figure 2.4. LDLRKO NASH mice have increased H2Kb in myeloid cells. LDLRKO mice on chow or WD for 12 wks (n = 3-4 mice per group, 1 cohort). Flow analysis of monocytes (*Ly6c*$^{+}$*CD11b*$^{+}$) **(A)** and monocyte H2Kb expression **(B)**. Flow analysis of monocyte derived macrophages (*Ly6c*$^{+}$*CD11b*$^{+}$*CD64*$^{+}$*F480*$^{+}$) **(C)** and monocyte derived macrophage H2Kb expression **(D)**. Flow analysis of macrophages (*Ly6c*$^{-}$*CD11b*$^{+}$*CD64*$^{+}$*F480*$^{+}$) **(E)** and macrophages H2Kb expression **(F).** Data shown as the mean ± SEM. Two-tailed unpaired Student's t-tests was performed and considered statistically significant for P<0.05 (*).

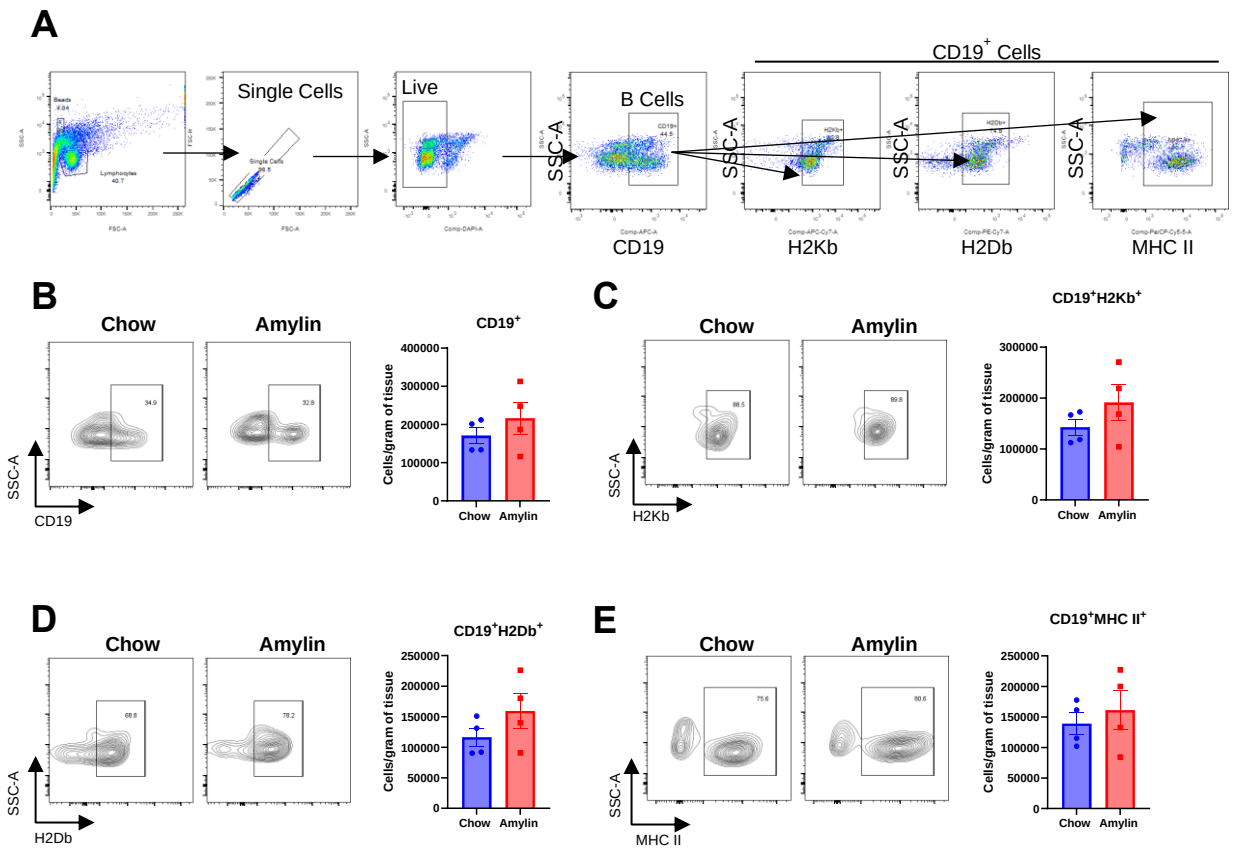

Figure 2.5. H2Kb and H2Db expression does not change in NASH CD19$^+$ B cells. Immune cells isolated from livers of Taconic chow or amylin mice on diet for 28 wks (n=4 mice per group). **(A)** Representative flow gating strategy. Flow analysis for CD19$^+$ B cells **(B)** and B cell H2Kb expression **(C)**, H2Db expression **(D)**, and MHC II expression **(E)**. Data shown as the mean ± SEM. Two-tailed unpaired Student's t-tests was performed.

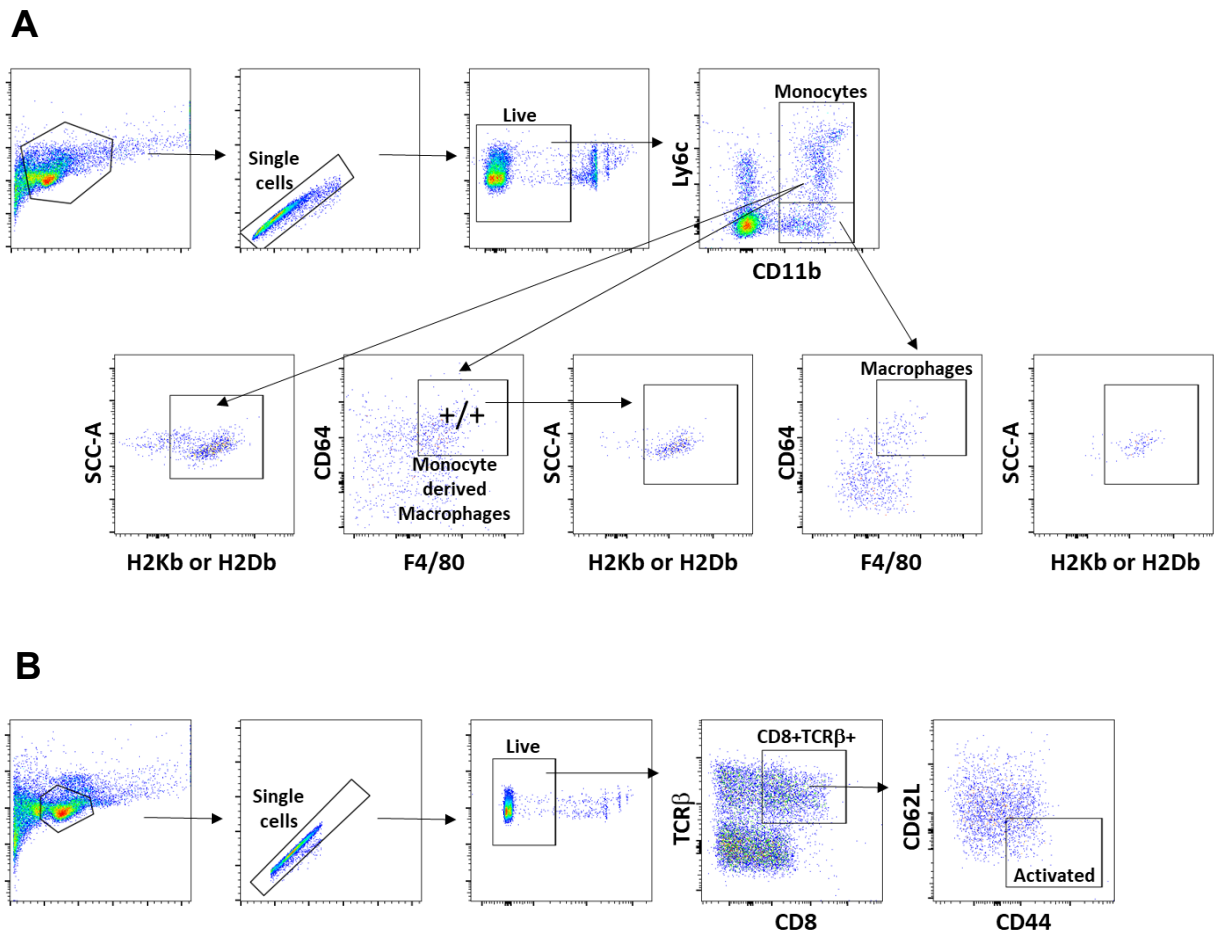

Figure 2.6. Flow cytometry gating strategies. (A) Myeloid cell flow gating strategies. **(B)** T cell flow gating strategies.

CHAPTER 3: $CD8^+$ T Cells Are Dependent on Antigen Presentation in NASH

Modified from publication: Adams, V.R., Collins L.B., Williams T.I, Holmes J., Hess P., Atkins H.M., Scheidemantle G., Liu X., Lodge M., Johnson A.J., Kennedy A. *Frontiers in Immunology*, **2023**, *Vol 14*, https://www.frontiersin.org/articles/10.3389/fimmu.2023.1302006

3.1 Introduction

$CD8^+$ T cells are key players in NASH promoting inflammation and fibrosis in both humans and mice [21]. Limited work has determined how $CD8^+$ T cells become activated during NASH and identifying mechanisms that regulate this process could identify key therapeutic targets. Antigen presentation is an important mechanism for $CD8^+$ T cell activation. However, this mechanism has not been evaluated in NASH directly or in a cell specific manner. Previous studies targeting MHC I antigen presentation have shown protection against NASH. Tap1 deficient mice, which lack the ability to load antigens onto MHC I molecules, were shown to be protected against induced NASH [127]. In contrast to this, an independent study characterized a resident memory subset of $CD8^+$ T cells that are autoreactive to hepatocytes that act in an antigen independent manner [56]. These authors also propose that intestinal B cells are responsible for T cell activation outside of MHC I and through IgA [128]. In both humans and mice, NASH-induced B and T cell infiltration positively correlate with the presence of antibodies targeting antigens derived from oxidative stress [129]. Rag1 knockout mice, which lack mature B and T cells, were also shown to be protected from high fructose induced hepatic steatosis [130]. Further evaluation is required to identify the contribution of specific antigen presenting cells and peptides that drive in $CD8^+$ T cell activation in NASH.

In the present study, we address how MHC I expression impacts NASH development. We hypothesize H2Kb antigen presentation by myeloid cells drives $CD8^+$ T cell activation, inflammation, and fibrosis. To evaluate antigen presentation in NASH, we will utilize mice that lack MHC I, H2Kb expression only, and H2Kb knockout in myeloid cells. These mice will be

placed on amylin diet and compared to WT mice that develop a NASH phenotype. Flow cytometry will be used to determine changes in $CD8^+$ T cell activation. Changes in inflammation and fibrosis will be determined by liver Sirius Red staining and total liver gene expression for markers of inflammation and fibrosis.

3.2 Materials and Methods

3.2.1 Animal Models

Male 5-wk-old C57BL/6J mice were originally purchased from Jackson Laboratories (Bar Harbor, ME) and further propagated in our colony. C57BL/6J mice were used to generate MHC I-deficient mice that lack endogenous H2Db and H2Kb (MHC I KO). Transgenic Kb mice were generated by introducing the H2Kb transgene (Kb LoxP) into MHC I KO mice developed by the Mayo Clinic Transgenic Mouse Core (Rochester, MN). Kb mice were then crossed with MHC I deficient mice expressing Cre recombinase under the LysM promoter (LysM Kb KO, myeloid cell specific). This cross generated a conditional knockout of Kb in myeloid cells. All Mouse genotypes were confirmed through flow cytometry. MHC I KO, Kb, and LysM Kb KO mice were donated from Dr. Aaron Johnson and further propagated in our colony [131]. *MHC I KO, Kb, and LysM Kb KO Studies.* 6-wk-old male mice from WT, MHC I KO, Kb, LysM Kb KO were fed chow or amylin diet (40 kcal% fat, 20 kcal% fructose and 2% cholesterol, Diet # D09100310i, Research Diets) for 28 weeks.

All Mice were housed with ad libitum access to food and water on a 12-hour light/dark cycle. Mice were sacrificed between the ages of 15-34 weeks. Tissues were snap-frozen and stored in -80°C freezer. All animal procedures were approved by the Institutional Animal Care and Use Committee (IACUC) at North Carolina State University under protocol 21-502-B.

3.2.2 Immune Cell Isolation from Liver

Mice were anesthetized and perfused through the heart with 1X PBS. Mouse livers were collected and minced in RPMI, 1 mg/ml Collagenase IV, 2 mg/ml Collagenase II, 1 mg/ml Protease, and 0.01 mg/ml DNase and incubated at 37°C for 25 min shaking. The cell suspension was filtered through a 100-µm filter with wash buffer and centrifuged at 443 xg for 6 min at 4°C. Supernatant was discarded and the pellet washed and centrifuged at 443 xg for 6 min at 4°C. The pellet was resuspended in 33% Percoll and centrifuged at 850 xg for 15 min at 4°C with minimum break and accelerator. The pellet was resuspended in wash buffer and centrifuged at 300 xg for 5 min at 4°C and the supernatant discarded. The pellet was resuspended in ACK lysing buffer and incubated at room temperature for 5 min. After incubating, wash buffer was added and centrifuged at 300 xg for 5 min at 4°C. The pellet was resuspended in FACS buffer filtered through a cell strainer cap tube and prepared for cell culture or flow cytometry.

3.2.3 Immune Cell Isolation from Spleen

Mouse spleens were isolated and strained through a 100-µm filter with FACS buffer and centrifuged at 500 xg for 5 min at 4°C. Pellets were washed with FACS and centrifuged at 500 xg for 5 min at 4°C. Pellets were resuspended in ACK Lysing Buffer and incubated for 5 mins. After incubation, FACS buffer was added and centrifuged at 500 xg for 5 min at 4°C. Pellets were resuspended in 1ml FACS buffer and filtered through a cell strainer. Cells were centrifuged at 500 xg for 5 min at 4°C and resuspended in FACS buffer and prepared for T cell assays.

3.2.4 T Cell Functional Assays

Stimulated wells were initially coated with IgG (clone RTK2758, BioLegend) and incubated at room temperature for 3 hr. Stimulated wells were washed twice with PBS and

coated with 1 µg/ml anti-CD3 (clone 145-2C11, Bio-Rad) and 1 µg/ml anti-CD28 (clone E18, Bio-Rad) overnight at 4°C. Plates were washed twice with PBS prior to plating cells. Unstimulated samples were not cultured with CD3 or CD28 and supplemented only with IL-2. Immune cells from WT, MHC I KO, and Kb chow mice were isolated from livers or spleens of chow mice as described previously. $CD8^+$ T cells were magnetically sorted using a $CD8^+$ T cell isolation kit (Miltenyi Biotec). $CD8^+$ T cells were stained with cell trace violet (Life Technologies) according to manufacturer's instructions. $CD8^+$ T cells were plated in 6 well plates with $1.5x10^5$ cells/well in 2 ml of RPMI medium (Corning) supplemented with 10% FBS, L-glutamine (400 mM), penicillin (100 U/ml), streptomycin (100 µg/ml), 2-mercaptoethanol (50 µM), and IL-2 (100 ng). T cells were plated under stimulated (CD3/CD28) or unstimulated conditions and cultured at 37°C for 3 days and harvested for flow cytometry. Cells were stained using the following panel: CD8a (PE-Cy7, 1:200, BD Biosciences), TCRβ (APC-Cy7, 1:200, BD Biosciences), CD44 (A700, 1:200, BD Biosciences), CD62L (APC, 1:200, BD Biosciences), Cell Trace Violet (3mM working concentration, ThermoFisher) and Propidium Iodide (PI, 1:10,000, ThermoFisher). Data was acquired on the Becton Dickinson LSRII machine in the NCSU flow Cytometry Core. All data was analyzed using FlowJo software v10.8.

3.2.5 Flow Cytometry

Isolated cells from the liver or spleen were incubated with Fc block followed by incubation with fluorophore conjugated antibodies on ice in FACS buffer for the following panels: Genotyping Panel: CD11b (FITC, 1:200, BD Biosciences), H2Kb (APC-eFluor780, 1:200, ThermoFisher), and H2Db (PE-Cy7, 1:200, BD Biosciences). NK T cell panel: NK1.1 (PE, 1:100, BD Biosciences), TCRβ (APC-Cy7, 1:200, BD Biosciences), CD8a (PE-Cy7, 1:200, BD Biosciences), and CD4 (AF488, 1:200, BD Biosciences). T cell panel: CD8a (PE-Cy7,

1:200, BD Biosciences), TCRβ (APC-Cy7, 1:200, BD Biosciences), CD44 (A700, 1:200, BD Biosciences), and CD62L (APC, 1:200, BD Biosciences). After incubation samples were washed twice with FACS buffer. Flow data was acquired on a Becton Dickinson LSRII machine in the NCSU flow Cytometry Core. All data was analyzed using FlowJo software v10.8.

3.2.6 Analysis of Lipid Species by LC-MS/MS

Liver lipids were analyzed using LC-MS/MS workflow on an Orbitrap Exploris 480 mass spectrometer with a HESI probe operating in positive/negative switching mode. Data was collected in data-dependent acquisition mode [132].

3.2.7 Liver Tissue Histology Staining

Paraffin-embedded sections from mouse livers were used for Hematoxylin and eosin (H&E) and Sirius red staining [81]. Whole slide images were captured on BioTek Cytation 5 at 10X magnification.

3.2.8 RNA Isolation and Real Time PCR

For RNA isolation, 25 mg of frozen liver tissue was homogenized in Tri-Reagent (Fisher) and extracted using Direct-zol RNA MiniPrep kit (Genesee) according to manufacturer's instructions. cDNA was synthesized on a BioRad iQ5 thermocycler using qScript cDNA supermix (QuantaBio) according to manufacturer's instructions. Real-time RT-PCR analysis was performed using PerfeCTa qPCR FastMix II (QuantaBio) and TaqMan assay (ThermoFisher) on a 7500 fast Dx thermocycler. Relative gene expression was normalized to 18s expression and determined using the delta-delta CT method. All sample reactions performed in duplicate. List of qPCR primers can be found in **table 3.1**.

3.2.9 Statistical Analysis

GraphPad Prism 10.0.2 software was used for all statistical analyses. Two-tailed unpaired Student's t-tests were performed for two group comparisons. Two-way ANOVA was performed for genotype versus diet followed by T test comparisons. All data is presented as the mean ± SEM. Data was considered statistically significant for $P<0.05$ (*), $P<0.01$ (**), $P<0.001$(***), and $P<0.0001$(****).

3.3 Results

3.3.1 Altered MHC I Expression Does Not Impair CD8$^+$ T Cell Function

Given that H2Kb had higher overall expression in myeloid cells compared to H2Db, we then investigated the impacts of H2Kb on the activation of CD8$^+$ T cells in NASH. To probe the function of H2Kb in NASH, we used three genetically modified mouse models: mice lacking H2Kb and H2Db (MHC I KO), expressing only H2Kb and no H2Db (Kb), and conditional Kb knockout in myeloid cells (LysM Kb KO) **(Fig. 3.1A).** By flow analysis, H2Kb and H2Db were not detected in the livers of MHC I KO mice. H2Kb was only detected with no H2Db expression in the Kb mouse model, and the LysM Kb KO mouse model was deficient in H2Kb on CD11b$^+$ cells **(Fig. 3.1B-D).**

Because MHC I disruption can impact CD8$^+$ T cell homeostasis we evaluated changes in TCRb$^+$CD8$^+$ T cells in WT, MHC I KO, Kb, and LysM Kb KO chow mice. Interestingly, no significant changes were identified in the number of liver CD8$^+$ T cells between the WT and MHC I KO, Kb, or LysM Kb KO mice. However, MHC I KO mice demonstrated significant reductions in both spleen and blood CD8$^+$ T cell numbers **(Fig. 3.2A)** [133]. We next evaluated if MHC I deletion impacts CD8$^+$ T cell function in both the spleen and liver. Isolated splenic or

liver $CD8^+$ T cells were cultured under unstimulated or stimulated conditions with CD3/CD28 to confirm functionality in the MHC I KO genotype. Using flow cytometry, we identified less splenic $CD8^+$ T cells in the MHC I KO model and no differences between WT and Kb $CD8^+$ T cells. Both MHC I KO and Kb $CD8^+$ T cells responded to stimulation with increased activation (*$CD44^+$, $CD62L^-$*) and proliferation comparable to WT $CD8^+$ T cells **(Fig.3.2B-E).** Liver $CD8^+$ T cells in the MHC I KO mice did not to respond to CD3/CD28 stimulus to the same extent as WT mice with less total $CD8^+$ $TCR\beta^+$ cells present under stimulated conditions. However, MHC I KO $CD8^+$ T cells were still able to response to stimulus with increased activation and proliferation **(Fig. 3.2F-H).** Previous studies have evaluated the impact of Kb deletion in myeloid cells on $CD8^+$ T cell development. These studies reported no significant changes in the proportion of $CD8^+$ T cells or changes in the TCR repertoire diversity [131]. This data shows that $CD8^+$ T cells are still functional under MHC I deficient conditions and phenotypic changes in these models are due to changes in antigen presentation.

3.3.2 Natural Killer T Cells Are Not Impacted Under MHC I Deficient Conditions

Since MHC I also can directly impact NK T cell numbers, we sought to determine if our mouse models have altered NK cell populations. Many early studies indicated that NK cell responses were induced by the absence of MHC I expression on target cells. This idea was described by the missing-self hypothesis stating that host cells that express MHC I are protected from NK cells, and cells that do not express this molecule are targeted for cell death [134]. This is supported by work done showing that virally infected cells and cancer cells that have decreased MHC I expression are more susceptible to NK-cell death [134]. However, additional studies were done to evaluate this mechanism and found that in Tap1 and beta-2-microgolbin

(b2m) deficient mice NK cells were tolerant to the missing MHC I expression and retain normal functions [135, 136].

To determine if altered MHC I expression impacts NK1.1^{+} and NK T cells, immune cells from livers of chow WT, MHC I KO, Kb, and LysM Kb KO mice were evaluated. Flow cytometry analysis revealed no significant differences in *NK1.1^{+}TCRβ^{-}* and *NK1.1^{+}TCRβ^{+}* cells between WT and MHC I KO, Kb, and LysM Kb KO mice **(Fig. 3.3A-C).** Additionally, no significant changes were detected in *NK1.1^{+}TCRβ^{+}* subsets for *CD4^{+}* and *CD4^{-}CD8^{-}* subsets **(Fig. 3.3D-E).** This data further supports that these models are suitable for evaluating antigen presentation in mice.

3.3.3 MHC I Expression Does Not Regulate Lipid Accumulation During NASH

After confirming CD8^{+} and NK T cell functionality under altered MHC I conditions, we probed the function of H2Kb during NASH progression. After 28 weeks, amylin diet significantly increased body weight and epididymal fat in WT, MHC I KO, Kb, and LysM Kb KO mice **(Fig. 3.4A-B).** MHC I KO mice on amylin diet behaved most similar to WT with increased body weight and liver weights **(Fig. 3.4B-C).** Interestingly, Kb and LysM amylin fed mice had reduced liver weights compared to WT amylin fed mice and no changes in body weight in the Kb amylin fed mice **(Fig. 3.4B-C).** However, Kb mice on amylin diet had a more advanced NASH phenotype with the formation of cancer-like nodules in the liver **(Fig. 3.4D).**

To further understand how MHC I impacts NASH pathology, liver tissue sections were stained with H&E. WT amylin mice demonstrated diffuse lipid accumulation and minimal lymphatic inflammation compared to chow controls. However, no significant changes were detected between WT, MHC I KO, and LysM Kb KO mice on amylin diet. In contrast, Kb amylin fed mice displayed hepatocyte necrosis and oval cell hyperplasia **(Fig. 3.5A**, **Table 3.2).**

To examine hepatic steatosis, we performed mass spectrometry analysis of lipid species in the liver. We found total liver triglycerides and diglycerides were significantly upregulated with amylin diet and not impacted by genotype **(Fig. 3.5B).**

3.3.4 MHC I KO and LysM Kb KO prevent CD8$^+$ T cell activation in NASH

During NASH CD8$^+$ T cells are activated and can promote further immune cell recruitment into the liver. To evaluate if MHC I expression impacts CD8$^+$ T cell activation in NASH, we used WT, MHC I KO, Kb, and LysM Kb KO mice on amylin diet for 28 weeks. Notably, we found MHC I KO and LysM Kb KO mice were protected against NASH induced increases in hepatic gene expression of immune cell markers *Cd8* and *Cd11b.*Whereas Kb mice responded similar to WT mice on amylin diet with increased expression of both markers. Interestingly, F4/80 gene expression was not impacted by MHC I expression **(Fig. 3.6A).** Next, we determined how the loss of MHC I, H2Kb expression only, and H2Kb expression in myeloid cells impacts hepatic CD8$^+$ T cell activation during NASH development. Flow cytometry analysis demonstrated that MHC I KO and LysM Kb KO mice were protected from hepatic CD8$^+$ T cell activation compared to WT and Kb amylin mice **(Fig. 3.6B-C).**

This data supports that H2Kb antigen presentation on myeloid cells could be an important mechanism for CD8$^+$ T cell activation in NASH.

3.3.5 MHC I KO and LysM Kb KO are protective against NASH

We next evaluated the impact of MHC I function on hepatic inflammation and fibrosis, key hallmarks of the NASH pathology. In the absence of H2Kb and H2Db, mice were protected from diet induced increases of inflammatory genes *Tnf, Il1b and Il10* and compared to WT

amylin mice. However, Kb and LysM Kb KO mice demonstrated significant increases in *Tnf* with amylin diet. MHC I KO and Kb mice had significant reductions in Il10 expression while LysM Kb KO mice increased with amylin diet **(Fig. 3.7A).** Interestingly, MHC I KO and LysM Kb KO mice were protected from diet induced fibrosis with significant reductions in Sirius red staining compared to WT and Kb amylin mice. Kb amylin mice demonstrated significantly increased collagen deposition compared to WT amylin mice. **(Fig. 3.7B).** In correlation with Sirius red staining, MHC I KO and LysM Kb KO mice showed significant reductions in hepatic gene expression of fibrotic markers *Col1a1* and *Tgfβ* in contrast to the significant increases in WT and Kb mice on amylin **(Fig. 3.7C).**

Our findings suggest that H2Kb and H2Db are necessary for NASH induced $CD8^+$ T cell activation, inflammation, and fibrosis but do not regulate hepatic lipid accumulation. Additionally, H2Kb expression in the absence of H2Db leads to advanced NASH fibrosis. Meanwhile, H2Kb specific knockout in myeloid cells reduced fibrosis but not NASH associated inflammation **(Table 3.3).**

3.4 Discussion

Here we demonstrated that MHC I KO, Kb, and LysM Kb KO mice are valid models to evaluate antigen presentation in NASH. We have shown that these models do not impair $CD8^+$ T cell function or NK T cell numbers. MHC I expression was not found to regulate lipid accumulation during NASH as all genotypes increased body and adipose tissue weights on amylin diet similar to WT mice. This is further supported by increases in liver triglyceride and diglyceride species in mice on amylin diet regardless of genotype. However, our data shows that MHC I expression is important for regulating inflammation, fibrosis, and $CD8^+$ T cell activation

in NASH. Myeloid cell H2Kb expression was found to be important for $CD8^+$ T cell activation and fibrosis but not inflammation. Taken together this data suggests that myeloid cell antigen presentation could have potential therapeutic implications for NASH.

Our data shows that MHC I expression does not regulate hepatic steatosis. However, the liver plays an essential role in lipid metabolism which has many complex processes that regulate synthesis, export, and redistribution of fatty acids to other tissues [137]. During steatosis lipids are dysregulated and accumulate as lipid droplets in hepatocytes. Some studies have suggested that certain lipid species such as cholesterol can be pro-inflammatory and may contribute to the progression from steatosis to NASH [104-107]. This lipotoxicity can damage or kill hepatocytes through apoptosis, necrosis, or pyroptosis. Pyroptosis cell death can lead to the release of danger associated molecular patterns (DAMPs) which can lead to the release of pro-inflammatory cytokines and chemokines [138, 139]. These signals can attract other immune cells, in particular activated macrophages [140]. Hepatocyte lipotoxicity could provide an alternative mechanism for macrophage recruitment outside of MHC I expression as our data showed F4/80 expression increased with amylin diet regardless of MHC I expression. However, further work is required to fully elucidate how specific lipids impact immune cell activation directly and indirectly to progress NASH.

Our data demonstrates that MHC I deficiency and H2Kb deficiency in myeloid cells can protect against liver fibrosis and $CD8^+$ T cell activation in NASH. With the advancement of single cell RNA sequence, studies have identified multiple subsets of $CD8^+$ T cells in human and mouse models of NAFLD [141]. In contrast to our findings, a recent study argues that $CD8^+$ T cells are activated through B cell stimulation through the IgA-FcR signaling in a choline deficient high fat (CD-HFD) model [56, 128]. The pathogenic $CD8^+$ T cell subset in this NASH

model was classified as auto-aggressive towards hepatocytes. This subset is characterized by expressing high levels of CXCR6, cytotoxicity (granzyme), and exhaustion marker PD-1. However, the hepatic $CD8^+$ T cells were discovered to act in an antigen-independent manner relying on IL-15 driven transcriptional reprogramming and metabolic signals acetate and ATP for activation [56]. This study also showed that *in vitro* blocking of MHC I with an MHC I antibody is ineffective at preventing NASH $CD8^+$ T cell activation by intestinal B cells [128]. However, previous work has shown that in a methionine and choline deficient high fat diet (MCD) model of NASH, $CD8^+$ T cells did not regulate hepatic inflammation, fibrosis, or stellate cell activation [81]. Alternatively, β2m KO studies have shown that when using the CD-HFD model mice were protected from $CD8^+$ T cell activation, inflammation, and fibrosis. However, this model does not account for just MHC I antigen presentation as β2m is also present on CD1, Qa-1, and neonatal Fc receptor (FcRn) receptors impacting more than just $CD8^+$ T cells [77]. Differences in choline content of the NASH diets may contribute to the factors that regulate $CD8^+$ T cell activation and function. $CD8^+$ T cells function may be altered under choline deficient conditions as activation of the T cell receptor (TCR) through antigen presentation upregulates components of their cholinergic system [142]. Therefore, targeting MHC I with an antibody may be ineffective as these molecules are typically bound with peptides when presented at the cell surface which could prevent the binding of blocking antibodies. Further studies are necessary to clarify the mechanisms of $CD8^+$ T cell activation across various dietary models of NASH. Alternative methods are also needed to better target MHC I molecules bound to specific NASH peptides.

Comparable to our findings, in a mouse model of cerebral malaria deficiency of H2Kb and H2Db led to reductions in $CD8^+$ T cell activation resulting in improved survival [143]. Using

the Kb and LysM Kb KO mouse models our data demonstrates that H2Kb on myeloid cells is required for regulating $CD8^+$ T cell activation and fibrosis in NASH. Interestingly, studies are beginning to highlight the distinct roles of H2Kb and H2Db in priming $CD8^+$ T cells and disease progression [144]. In the context of Theiler's murine encephalomyelitis virus (TMEV) infection, H2Db, but not H2Kb, controls the development of brain atrophy [145, 146]. In addition, $CD8^+$ T cell activation through an H2Db restricted TMEV-derived peptide contributes to brain atrophy [145]. In lymphocytic choriomeningitis virus (LCMV) mouse models, deficiency of H2Db led to more severe liver pathology, increased hepatocyte apoptosis, and increased H2Kb restricted cytotoxic $CD8^+$ T cell numbers compared to WT and H2Kb KO mice [147]. These studies in conjunction with our data, suggest that antigen presentation by different MHC I isoforms is important in regulating the type of $CD8^+$ T cell responses and are important factors in infection and chronic disease progression.

In the present study we demonstrated the importance of MHC I expression in regulating inflammation, fibrosis, and $CD8^+$ T cell activation in NASH. This data suggests that H2Kb antigen presentation is an important mechanism driving NASH progression. Myeloid cell H2Kb expression was specifically found to regulate $CD8^+$ T cell activation and fibrosis identifying myeloid cells as the potential antigen presenting cell in NASH. Future studies are required to identify the specific myeloid cell and antigen responsible for T cell activation. Additionally, inflammation was not found to be regulated by myeloid cell H2Kb expression suggesting the role of other cells or processes involved in regulating inflammation.

Table 3.1. List of qPCR primers.

Reagent or resource	Source	Identifier
Tri Reagent	Fisher Scientific	Cat# NC9330796
Direct-zol RNA MiniPrep	Genesee Scientific	Cat# 11-331
qScript cDNA Supermix	QuantaBio	Cat# 95048
PerfeCTa qPCR FastMix II, Low ROX	QuantaBio	Cat# 95120-12
CD8a Taqman Assay	ThermoFisher Scientific	Cat# 4331182; Mm01188922_m1
Itgam (CD11b) Taqman Assay	ThermoFisher Scientific	Cat# 4331182; Mm00434455_m1
Adgre1 (F480) Taqman Assay	ThermoFisher Scientific	Cat# 4331182; Mm00802529_m1
Tnf Taqman Assay	ThermoFisher Scientific	Cat# 4351370; Mm99999068_m1
IL-1b Taqman Assay	ThermoFisher Scientific	Cat# 4331182; Mm00434228_m1
IL-10 Taqman Assay	ThermoFisher Scientific	Cat# 4351370; Mm01288386_m1
Col1a1 Taqman Assay	ThermoFisher Scientific	Cat# 4331182; Mm00801666_g1
Tgfb Taqman Assay	ThermoFisher Scientific	Cat# 4331182; Mm01178820_m1

A

Genetic Models	
Genotype	**MHC I Expression**
WT (C57BL/6J)	MHC I fully expressed (Kb and Db)
MHC I KO	H2Kb and H2Db KO
KbLoxP	H2Kb expression only
LysM Kb KO	Myeloid cell Kb KO, on Kb only background

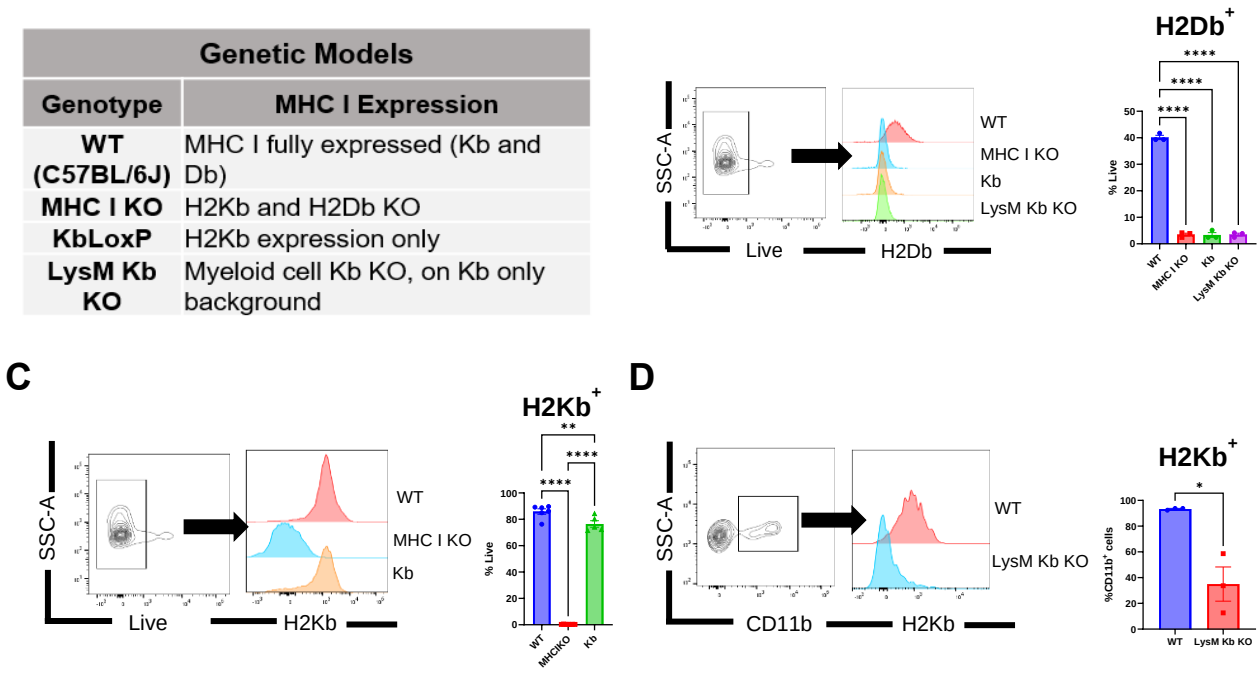

Figure 3.1. Efficient H2Kb and H2Db knockout in MHC I KO, Kb transgenic mice, and Kb KO in myeloid cells. WT, MHC I KO, Kb, LysM Kb KO chow mice (n=5-7 per group, three cohorts). **(A)** Genetic mouse model descriptions. Representative flow plots of isolated liver cells gated for: **(B)** total $H2Db^+$ cells, **(C)** total $H2Kb^+$ cells., and **(D)** $CD11b^+$ cells $H2Kb^+$ expression Data shown as the mean ± SEM. Two-tailed unpaired Student's t-tests for data with two groups and Two-way ANOVA was performed for more than two and was considered statistically significant for P<0.05 (*), P<0.01 (**), P<0.001(***), and P<0.0001(****).

Figure 3.2. Functional spleen and liver $CD8^+$ T cells in MHC I KO and Kb transgenic mice. WT, MHC I KO, and Kb, chow mice (n=5-7 per group, three cohorts). **(A)** Flow cytometry data for $CD8^+TCRb^+$ cells in WT, MHC I KO, and Kb chow mouse livers or spleens. T cell activation assay with sorted $CD8^+$ spleen or liver T cells under stimulated and unstimulated conditions from WT, MHC I KO, or Kb chow mice harvested after 3 days (n=4-5). **(B)** T cell activation flow gating strategy. Flow cytometry analysis of splenic $CD8^+TCRb^+$ cells **(C),** activation ($CD44^+$, $CD62L^-$) **(D),** and proliferation **(E).** Flow cytometry analysis of liver $CD8^+TCRb^+$ cells **(F),** activation ($CD44^+$, $CD62L^-$) **(G),** and proliferation **(H).** Data shown as the mean ± SEM. Two-tailed unpaired Student's t-tests for data with two groups and Two-way ANOVA was performed for more than two and was considered statistically significant for $P<0.05$ (*), $P<0.01$ (**), $P<0.001$(***), and $P<0.0001$(****).

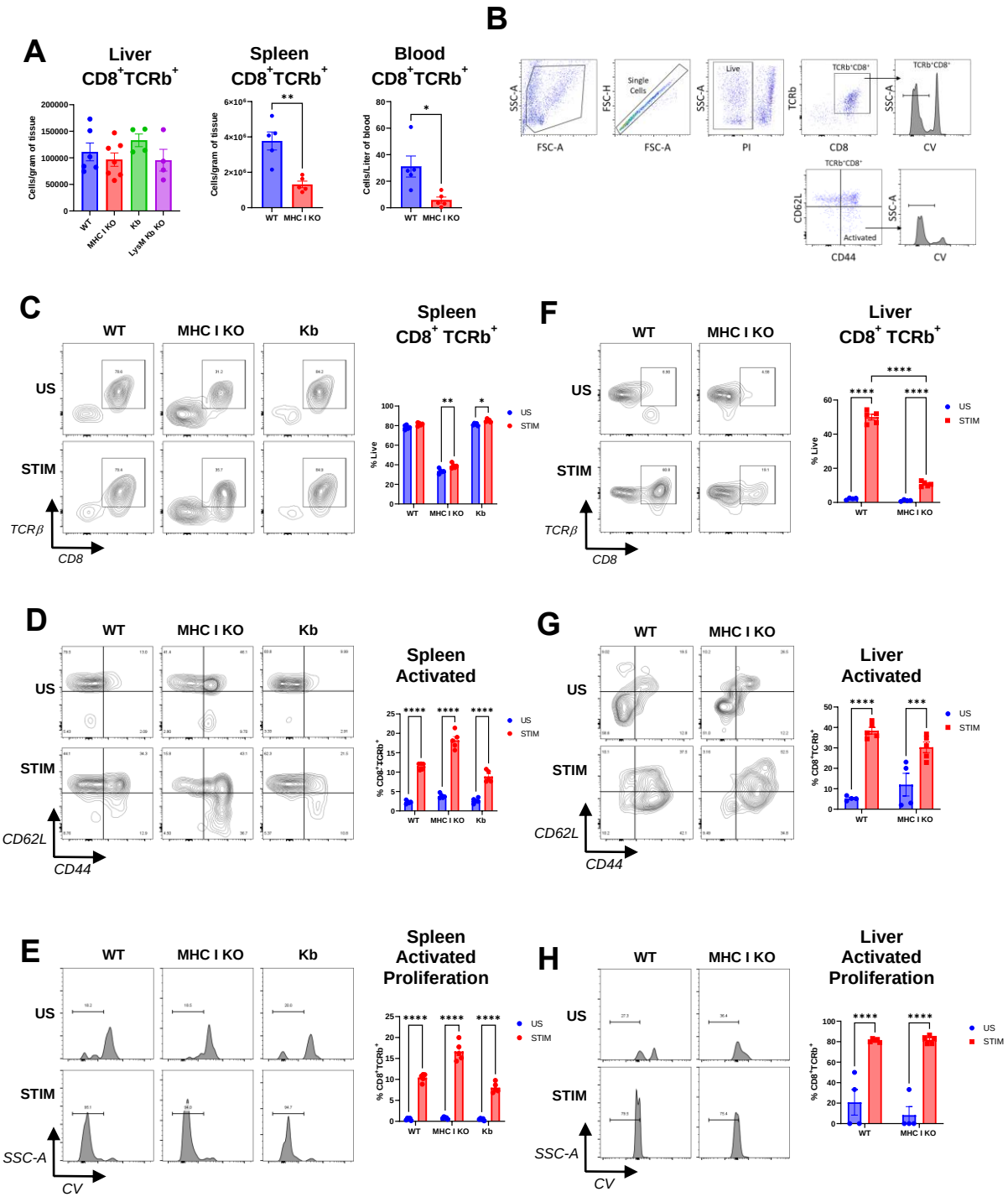
A
Liver
CD8+TCRb+
Cells/gram of tissue
WT
MHC I KO
Kb
Lys/M Kb KO
Spleen
CD8+TCRb+
Cells/gram of tissue
WT
MHC I KO
Blood
CD8+TCRb+
Cells/Liter of blood
WT
MHC I KO
B
SSC-A
FSC-A
FSC-H
Single Cells
Live
PI
TCRb
CD8
CV
CD62L
CD44
Activated
C
WT
MHC I KO
Kb
US
STIM
TCRβ
CD8
Spleen
CD8+ TCRb+
% Live
F
Liver
CD8+ TCRb+
D
Spleen
Activated
CD62L
CD44
G
Liver
Activated
E
Spleen
Activated
Proliferation
SSC-A
CV
H
Liver
Activated
Proliferation

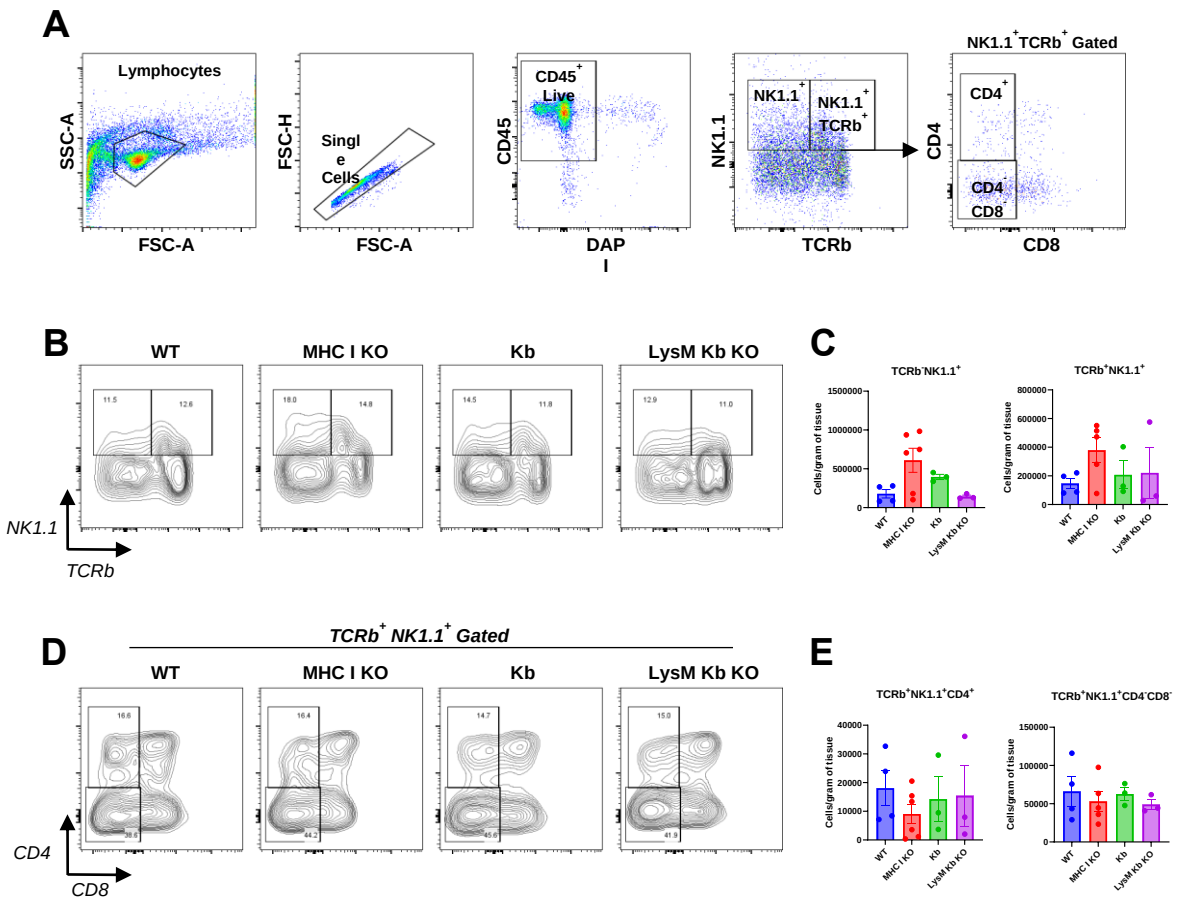

Figure 3.3. Natural Killer T cells are not impacted in livers of MHC I KO, Kb, or LysM Kb KO mice. Female WT, MHC I KO, Kb, and LysM Kb KO chow mice (n=3-6 per group). **(A)** Representative flow gating strategy for NK T cells. **(B-C)** Flow analysis of *NK1.1*$^{+}$ *TCRb*$^{+}$ and *NK1.1*$^{+}$ *TCRb*$^{-}$ cells. **(D-E)** Flow analysis of *CD4*$^{+}$ *or CD4*$^{-}$*CD8*$^{-}$ expression in *NK1.1*$^{+}$ *TCRb*$^{+}$ cells. Data shown as the mean ± SEM. One-Way ANOVA was performed.

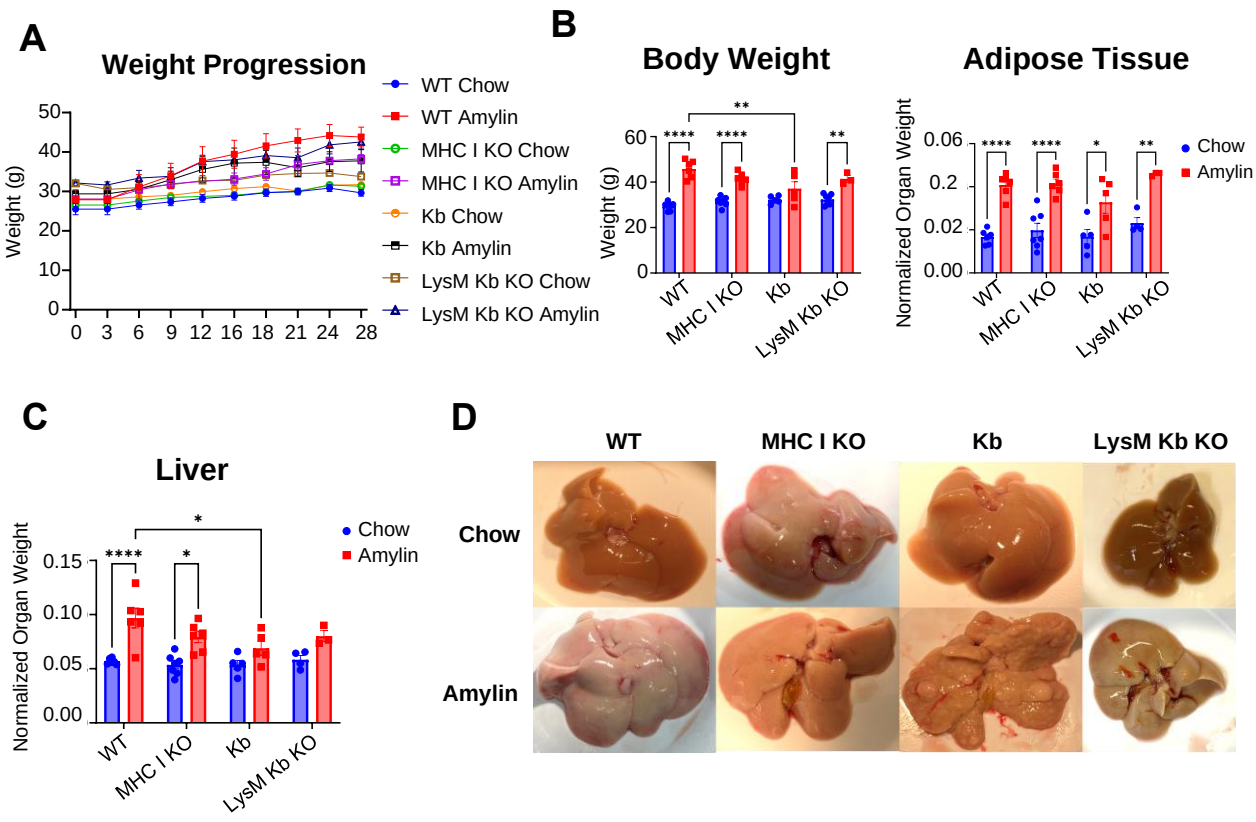

Figure 3.4. MHC I expression does not regulate lipid accumulation during NASH. WT, MHC I KO, Kb or LysM Kb KO mice were on diet for 28 wks (n=3-7 per group) in two replicate cohorts. **(A)** Weight progression over time. **(B)** Body weight and adipose tissue weights. **(C)** Total liver weights. **(D)** Gross representative liver pathology. Data shown as the mean ± SEM. Two-way ANOVA were performed and determined significant by P<0.05 (*), P<0.01 (**), P<0.001(***), and P<0.0001(****).

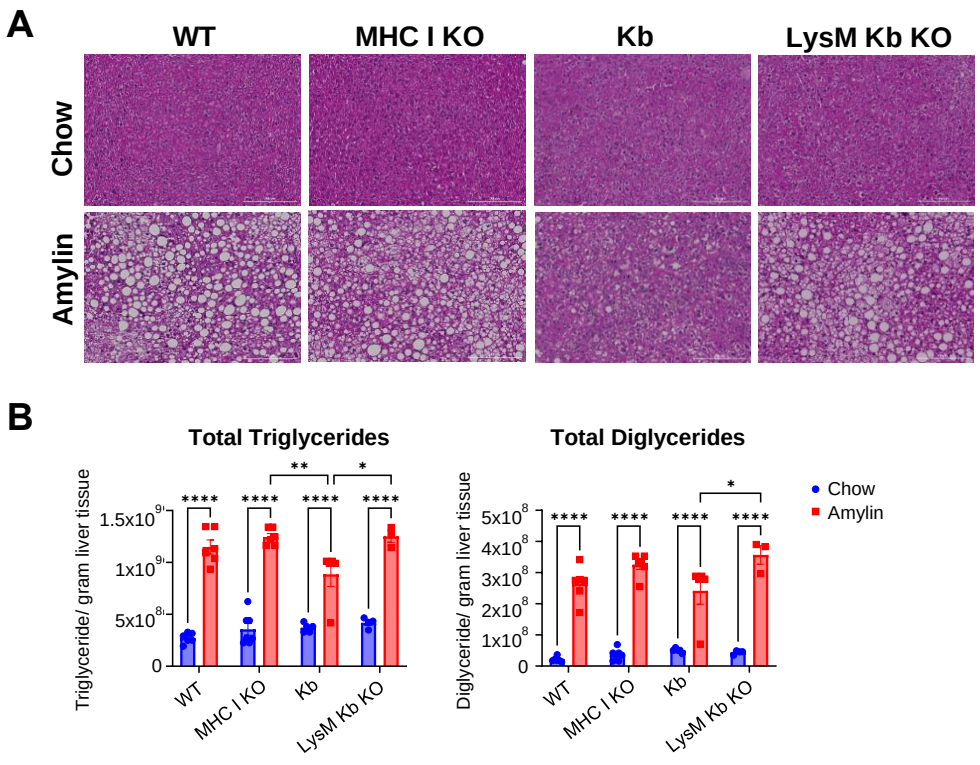

Figure 3.5. MHC I expression does not impact Triglyceride or Diglyceride liver accumulation during NASH. WT, MHC I KO, Kb or LysM Kb KO mice were on diet for 28 wks (n=3-7 per group) in two replicate cohorts. **(A)** Representative images of H&E staining of mouse liver sections. **(B)** Quantification of liver triglyceride and diglyceride lipid species detected by LC-MS/MS analysis. Data shown as the mean ± SEM. Two-way ANOVA were performed and determined significant by P<0.05 (*), P<0.01 (**), P<0.001(***), and P<0.0001(****).

Table 3.1. H&E Pathology Scoring.

H&E Pathology Scoring						
Sample ID	**Hepatocyte Necrosis**	**Oval Cell Hyperplasia**	**Lipid Accumulation**	**Lipid Vacuole Size**	**Glycogen**	**Comments**
WT Chow-1	0	0	0	N/A	1	NSL
WT Chow-2	0	0	0	N/A	1	NSL
WT Chow-3	0	0	0	N/A	1	NSL
WT Chow-4	0	0	0	N/A	1	NSL
WT Amylin-1	0	0	0	N/A	1	NSL
WT Amylin-2	0	0	5	Mixed	N/A	Diffuse lipid accumulation, some minimal lymphocytic inflammation
WT Amylin-3	0	0	5	Mixed	N/A	Diffuse lipid accumulation, some minimal lymphocytic inflammation
WT Amylin-4	0	0	5	Mixed	N/A	Diffuse lipid accumulation, some minimal lymphocytic inflammation
WT Amylin-5	0	0	5	Mixed	N/A	Diffuse lipid accumulation, some minimal lymphocytic inflammation
WT Amylin-6	2	4	4	Macro	N/A	Multifocal yellow pigment in hepatocytes (presumed bile)
MHC I KO Chow-1	0	0	0	N/A	0	NSL
MHC I KO Chow-2	0	0	0	N/A	0	NSL
MHC I KO Chow-3	0	0	0	N/A	0	NSL
MHC I KO Chow-4	0	0	0	N/A	0	NSL
MHC I KO Amylin-1	0	0	4	Mixed	N/A	Diffuse lipid accumulation, some minimal lymphocytic inflammation
MHC I KO Amylin-2	0	0	4	Mixed	N/A	Diffuse lipid accumulation, some minimal lymphocytic inflammation
MHC I KO Amylin-3	0	0	4	Mixed	N/A	Diffuse lipid accumulation, some minimal lymphocytic inflammation
MHC I KO Amylin-4	1	0	5	Mixed	N/A	Diffuse lipid accumulation, some minimal neutrophilic and mononuclear inflammation
Kb Chow-1	0	0	0	N/A	1	Diffuse moderate glycogen accumulation
Kb Chow-2	1	0	0	N/A	1	Diffuse mild glycogen accumulation, neutrophilic inflammation associated with the focus of hepatocyte necrosis
Kb Chow-3	1	0	0	N/A	1	Diffuse mild glycogen accumulation, neutrophilic inflammation associated with the focus of hepatocyte necrosis

Table 3.1 (Continued).

Kb Amylin-1	2	1	2	Macro	0	Rare clusters of lymphocytes,and macrophages few neutrophils; multifocal yellow pigment in hepatocytes (presumed bile)
Kb Amylin-2	0	0	5	Mixed	N/A	Diffuse lipid accumulation, some minimal lymphocytic inflammation
Kb Amylin-3	2	4	0	N/A	N/A	Multifocal yellow pigment in hepatocytes (presumed bile)
LysM Kb KO Chow-1	0	0	0	N/A	0	NSL
LysM Kb KO Chow-2	1	0	0	N/A	0	Rare foci of neutrophilic/lymphocytic and histiocytic inflammation
LysM Kb KO Chow-3	3	0	0	N/A	0	Lymphocytes, plasma cells and histiocytes with surrounding hepatocyte degeneration
LysM Kb KO Chow-4	1	0	0	N/A	0	Rare clusters of lymphocytes, and histocytes with surrounding hepatocyte degeneration (hepatitis)
LysM Kb KO Amylin-1	0	0	5	Mixed	N/A	Diffuse lipid accumulation
LysM Kb KO Amylin-2	0	0	4	Micro	1	
LysM Kb KO Amylin-3	0	0	4	Mixed	1	
LysM Kb KO Amylin-4	0	0	4	Mixed	0	

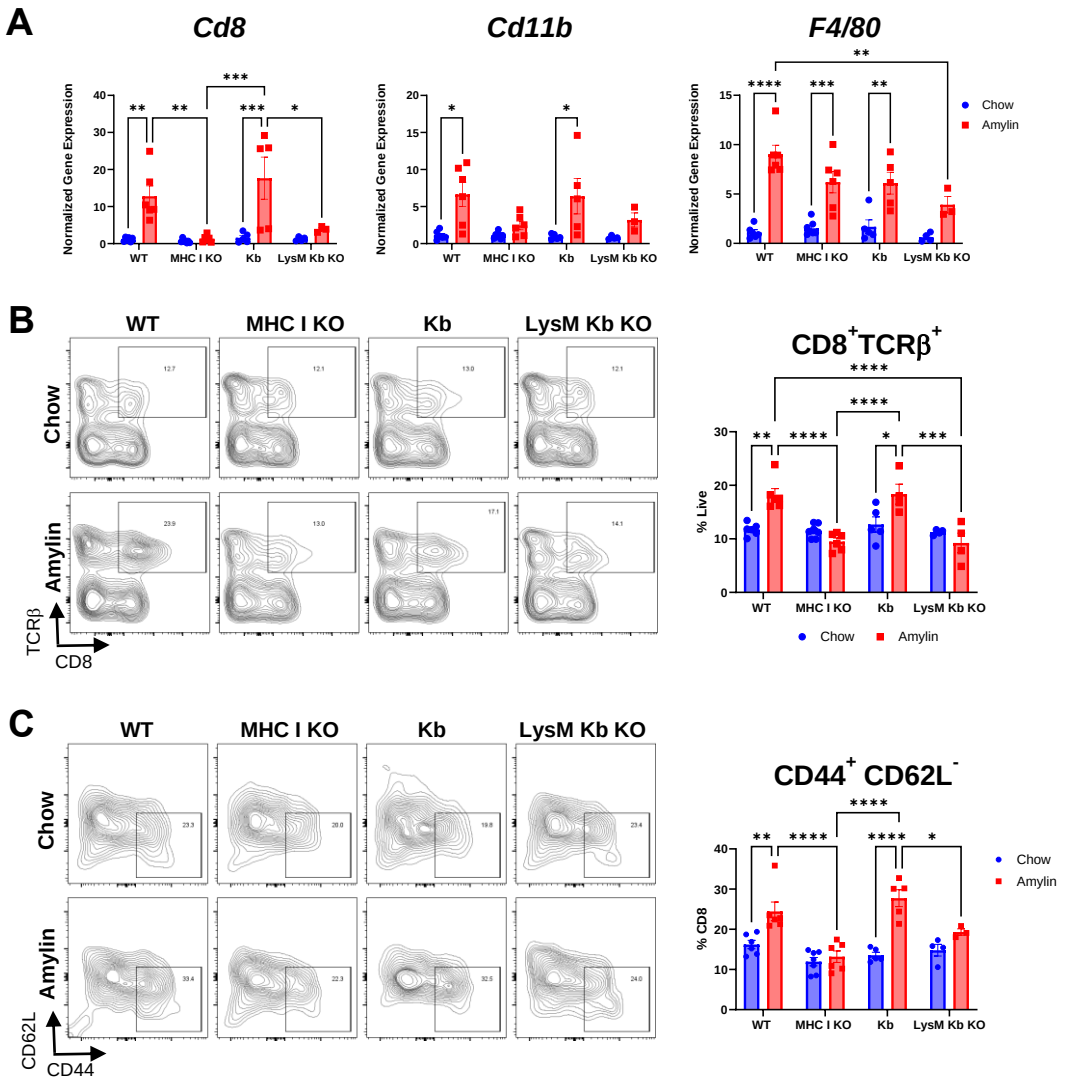

Figure 3.6. MHC I KO and LysM Kb KO prevent CD8$^+$ T cell activation in NASH. WT, MHC I KO, Kb or LysM Kb KO mice were on diet for 28 wks (n=3-7 per group) in two replicate cohorts. **(A)** Hepatic gene expression for immune cell markers. Flow analysis of *Tcrb*$^+$*CD8*$^+$ T cells **(B)** and activation (*CD44*$^+$*CD62L*$^-$*)* **(C).** Data shown as the mean ± SEM. Two-way ANOVA were performed and determined significant by P<0.05 (*), P<0.01 (**), P<0.001(***), and P<0.0001(****).

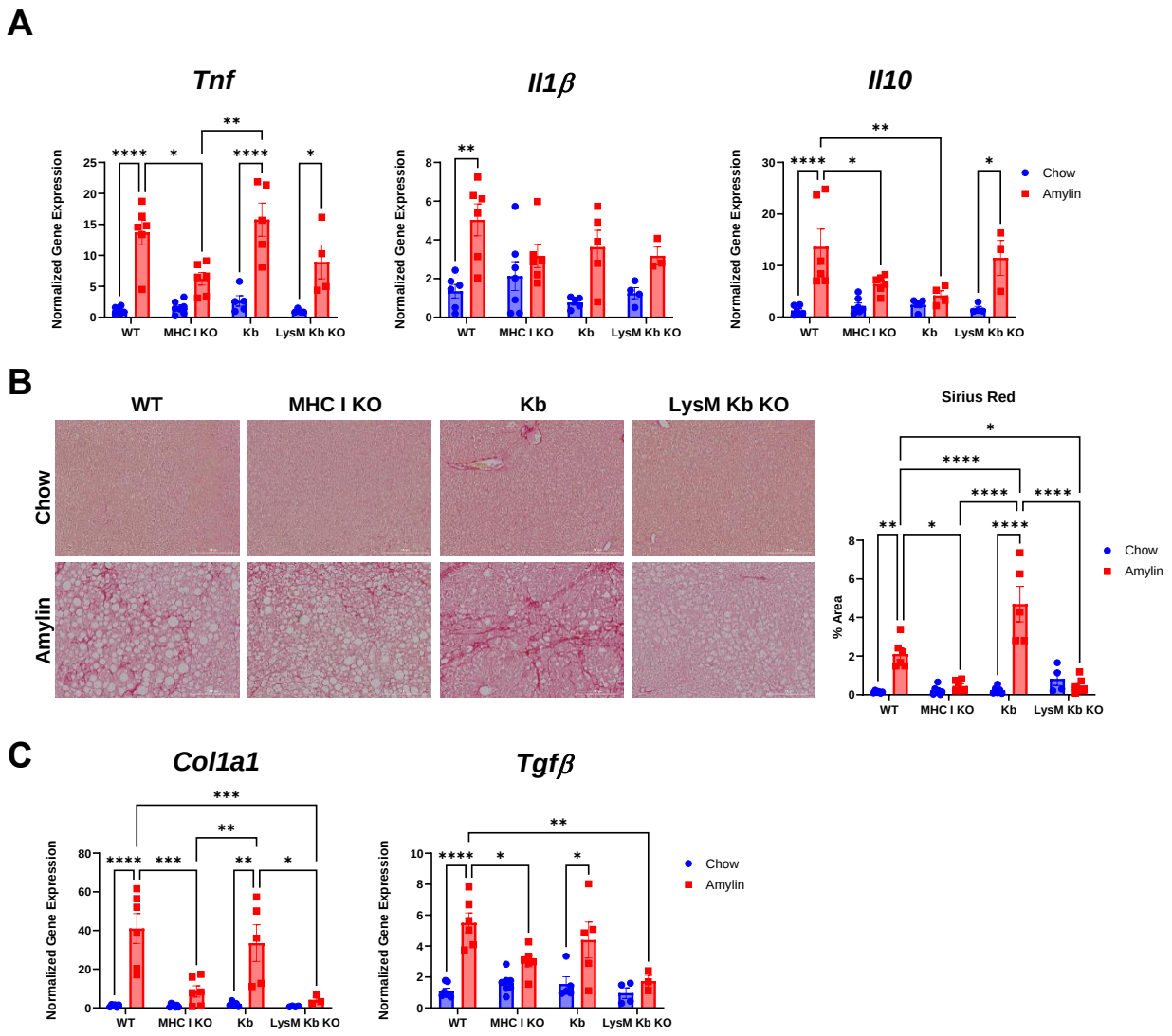

Figure 3.7. MHC I KO and LysM Kb KO are protective against NASH. WT, MHC I KO, Kb, or LysM Kb KO mice were on diet for 28 wks (n=3-7 per group, in two replicate cohorts). **(A-B)** Hepatic gene expression. **(C)** Representative figures of Sirius red staining of mouse liver sections and quantification. **(D)** Quantification of liver triglyceride and diglyceride lipid species detected by LC-MS/MS analysis. Data shown as the mean ± SEM. Two-way ANOVA were performed and determined significant by P<0.05 (*), P<0.01 (**), P<0.001(***), and P<0.0001(****).

Table 3.3. Impact of MHC I Expression on NASH Development

Genotype	MHC I Expression	Liver Phenotype	Body Weight	Liver weight	Adipose Tissue Weight	CD8 T cell Infiltration and Activation	Inflammation	Fibrosis
WT (C57BL/6J)	Endogenous MHC I fully expressed (Kb and Db)	Diffuse lipid accumulation	++++	++++	++++	++++	++++	++++
MHC I KO	H2Kb and H2Db Knockout	Diffuse lipid accumulation	++++	++++	++++	+	++	+
KbLoxP	Transgenic H2Kb expression only	Diffuse lipid accumulation and development of cancer-like nodules	+++	++++	++++	++++	++++	+++++
LysM Kb KO	Myeloid cell Kb KO, on Kb only background	Diffuse lipid accumulation	++++	++++	++++	+	++++	+

CHAPTER 4: Unique NASH Peptide Ncf2 Activates NASH CD8$^+$ T Cells

Modified from publication: Adams, V.R., Collins L.B., Williams T.I, Holmes J., Hess P., Atkins H.M., Scheidemantle G., Liu X., Lodge M., Johnson A.J., Kennedy A. *Frontiers in Immunology*, **2023**, *Vol 14*, https://www.frontiersin.org/articles/10.3389/fimmu.2023.1302006

4.1 Introduction

Our studies have shown that antigen presentation is an important factor for CD8$^+$ T cell activation in NASH. Knocking out MHC I was shown to prevent CD8$^+$ T cell activation and protect against NASH-associated inflammation and fibrosis. However, it is unknown what specific antigen peptides these CD8$^+$ T cells are responding to or what cells are presenting them.

Recent studies have highlighted the complexity of the MHC I immunopeptidome and its relevance to CD8$^+$ T cell activation under disease conditions. The immunopeptidome is shaped by protein translation and degradation [94, 95]. Under disease conditions these processes can be altered and lead to the development of immunogenic peptides [95]. Various studies have identified tumor-associated MHC I peptides that can be recognized by CD8$^+$ T cells [148-152]. Inflammatory cytokines can also alter the immunopeptidome leading to the generation of new peptides that can be recognized by CD8$^+$ T cells in both type 1 diabetes and healthy individuals [153]. Under obese conditions, it was found that visceral adipose tissue (VAT) was able to generate unique immunogenic peptides. These peptides were able to induce pro-inflammatory responses from CD8$^+$ T cells. VAT CD8$^+$ T cells also had a restricted TCR repertoire indicating T cell expansion of antigen specific T cells under obese conditions [96, 154-156]. However, it remains to be determined whether NASH alters the liver MHC I immunopeptidome and generates peptides that can drive CD8$^+$ T cell activation.

In NASH both pathogenic and beneficial CD8$^+$ T cell populations have been identified [56, 77, 157-159]. It was previously thought that NASH was irreversible. However, recent studies have shown that resolution of liver fibrosis is possible and is mediated by a subset of

TRM $CD8^+$ T cells in mice [88]. This subset is responsible for fibrosis resolution expressing cell surface markers CXCR6 and CD69. These cells operate in a CCR5-dependent chemoattractant manner relying on IL-15 and target activated HSC cells for apoptosis [88]. TRMs during fibrosis resolution and NASH were found to have enriched TCR clonotypes suggesting a role of antigens in regulating $CD8^+$ TRM T cell responses in resolution. However, it remains to be determined what peptide may be driving pathogenic $CD8^+$ T cell activation in NASH and which subset may be more responsive to antigen stimulation. We hypothesize that pathogenic $CD8^+$ T cell activation in NASH is driven by unique H2Kb antigen peptides. The objective of this study is to determine if NASH conditions alter the H2Kb immunopeptidome in mice. Additionally, we aim to identify and test candidate peptides for $CD8^+$ T cell reactivity using LC-MS/MS and flow cytometry.

4.2 Materials and Methods

4.2.1 Animal Models

Male 5-wk-old C57BL/6J and low-density lipoprotein receptor knockout (LDLRKO) mice were originally purchased from Jackson Laboratories (Bar Harbor, ME) and further propagated in our colony. MHC I KO, Kb, and LysM Kb KO mice were generated as mentioned previously. *LDLRKO NASH model.* Male 6-wk-old *LDLRKO* mice were fed chow or western diet (WD, 42 Kcal% fat with 0.2% added cholesterol, TD.22137; Harlan Laboratories) for 12 weeks. *WT Sucrose WD NASH model.* Male 6-wk-old C57BL/6J wild type (WT) mice were fed chow or western diet (WD, 42 Kcal% fat with 0.2% added cholesterol, TD.22137; Harlan Laboratories) with 30% glucose/fructose water for 25 weeks. *Taconic Amylin NASH Model.* C57BL/6NTac (Tac) male mice were purchased from Taconic Biosciences on chow or amylin

diet (AMLN, 40 kcal% fat, 20 kcal% fructose and 2% cholesterol, Diet # D09100310i, Research Diets) remaining on diet for a total of 28 weeks. *MHC I KO, Kb, and LysM Kb KO Studies.* 6-wk-old male mice from WT, MHC I KO, Kb, LysM Kb KO were fed chow or amylin diet (40 kcal% fat, 20 kcal% fructose and 2% cholesterol, Diet # D09100310i, Research Diets) for 28 weeks.

All Mice were housed with ad libitum access to food and water on a 12-hour light/dark cycle. Mice were sacrificed between the ages of 15-34 weeks. Tissues were snap-frozen and stored in -80°C freezer. All animal procedures were approved by the Institutional Animal Care and Use Committee (IACUC) at North Carolina State University under protocol 21-502-B.

4.2.2 Isolation of H2Kb Peptides from Liver

Liver lysates were prepared following Kowalewski's methods with some modifications [160]. Livers were isolated and pooled together 5 Control or 5 NASH age matched mice or isolated individually and immediately minced in one volume of 2x solubilization buffer (1X PBS, 12% CHAPS, protease inhibitor mini tablet (Pierce), and PhosSTOP inhibitor tablet (Roche). Lysates were then manually homogenized and rinsed in 1X solubilization buffer and stirred for 1 hr at 4°C. Lysates were sonicated with 120w of ultrasonic power and 30% pulse length for 3 min on ice and then stirred for 1 hr at 4°C. Lysates were then centrifuged at 2,000 x g for 20 min. Supernatants were collected and subjected to ultracentrifugation at 150,000 x g for 70 min at 4°C. Supernatants were collected and filtered through a 0.22 µm pore syringe filter.

Column preparation was modified from methods by Chen and colleagues [156]. 1 ml HiTrap NHS-activated HP immunoaffinity columns (Cytiva) were prepared based on the following steps. Briefly, a drop of ice-cold 1 mM HCl was added to the top of the column and 6

ml of ice-cold 1 mM HCl was added to the column at a flow rate not exceeding 1 ml/min. For antibody coupling 10 ml of 1 mg/ml anti-H2Kb mAb (Clone:Y3, BioXCell) antibody in antibody coupling buffer (0.2 M of NaHCO3, 0.25 M NaCl, pH 8.3) was circulated at a flow rate of 1 ml/min for 4 hr at 4°C with a peristalsis pump. To deactivate any excess active groups, the column was injected with 3 x 2 ml buffer A (0.5 M ethanolamine, 0.25 M NaCl, pH 8.3) and 3 x 2 ml buffer B (0.1 M sodium acetate, 0.25 M NaCl, pH 4) alternatively with a syringe not exceeding 1 ml/min. After the column was left to rest at room temperature for 30 min, alternate washes of 3 x 2 ml buffer B and 3 x 2 ml buffer A were injected into the column. The prepared liver lysate was then continually circulated over the column overnight at a flow rate of 1 ml/min at 4°C. Columns were then washed with the following buffers: 15 ml of wash buffer 1 (50 mM Tris-HCl, pH 8, 75 mM NaCl, and 1% CHAPS), 15 ml of wash buffer 2 (50 mM Tris-HCl, pH 8, 75 mM NaCl in deionized H2O), 25 ml of wash buffer 3 (50 mM Tris-HCl, pH 8, 225 mM NaCl in deionized H2O), and 35 ml of wash buffer 4 (50 mM Tris-HCl, pH 8 in deionized H2O). H2Kb peptides were eluted in 6 ml of 10% acetic acid and filtered using a 3kDa ultrafiltration filter (Millipore) and frozen in -80°C. Frozen peptide elutes were lyophilized overnight and resuspended in 300 µL of 0.1% TFA. Peptide solutions were desalted using peptide desalting columns (Pierce) according to manufacturer's instructions.

4.2.3 Analysis of H2Kb Peptides by LC-MS/MS

Immunoaffinity H2Kb captured peptide solutions were analyzed by a discovery proteomics workflow using a hybrid quadrupole-orbitrap mass spectrometer (Thermo Scientific™ Orbitrap Exploris™ 480, Bremen Germany) incorporating an Easy-Spray™ nanoelectrospray source (Thermo Scientific™, San Jose) coupled to an Easy-nLC™ 1200 nano-liquid-chromatography system (Thermo Scientific™, San Jose). Mass spectrometry data were

acquired using non-targeted data-dependent acquisition (DDA) at top scan speed with a full experiment time of 3 seconds. Samples were injected in a random order. Commercially obtained, standardized bovine serum albumin (BSA) digest and HeLa digest were evaluated throughout the injection sequence to ensure proper nanoLC−MS/MS reproducibility. Proteins were identified by processing raw nanoLC/MS data with Proteome Discoverer 2.5 software (Thermo Scientific™, San Jose, CA) using a Mus musculus protein database obtained from Swiss-Prot (Taxon 10090 including sub-taxonomies; 17,090 sequences).

4.2.4 Western Analysis

Samples were prepared for western blot analysis as described previously. Membranes were probed with antibodies specific for Ncf2 (ThermoFisher) and β-actin (Cell Signaling Technology). Licor secondaries were used as described previously and imaged on the Odyssey Infrared Imaging System. Band intensity quantification was obtained using Image Studio Lite version 5.2 software.

4.2.5 RNA Isolation and Real Time PCR

RNA and RT-PCR was prepared as described previously. Relative gene expression was normalized to 18s expression and determined using the delta-delta CT method. All sample reactions were performed in duplicate.

4.2.6 Peptide Synthesis

Unique NASH H2Kb restricted peptides were synthesized at a crude purity from Peptide 2.0 Inc (Chantilly, VA). Synthetic peptides were used for functional assays and LC-MS/MS validation.

4.2.7 H2Kb Peptide Binding Assay

RMA-S cells were seeded into a 96 well plate at $1x10^5$ per well in 100 µL of media (RPMI with 10% FBS) and incubated at 27°C for 18 hrs. Following incubation cells were treated with 100 µM of vehicle control, Ova, Ncf2 peptide, or Gpnmb peptide (FVYVFHTL) and incubated at 37°C for 5 hrs. Cells were harvested for flow cytometry and incubated with Fc block for 5 min followed by a 30 min incubation with fluorophore conjugated antibodies on ice in FACS buffer for H2Kb (APC-eFluor780, 1:200, ThermoFisher) and Propidium Iodide (PI, 1:10,000, ThermoFisher). Data for this assay was acquired on a BD Accuri C6 machine. All data was analyzed using FlowJo software v10.8.

4.2.8 $CD8^+$ T Cell Activation Assay

CD3/CD28 stimulated wells were prepared as previously described. Unstimulated samples were not cultured with CD3 or CD28 and supplemented only with IL-2. Immune cells were isolated from livers or spleens of NASH mice as described previously and $CD8^+$ T cells were magnetically sorted using a $CD8^+$ T cell isolation kit (Miltenyi Biotec). $CD8^+$ T cells were stained with cell trace violet (Life Technologies) according to manufacturer's instructions. RMA-S cells were treated with vehicle control, Ova, Ncf2 peptide, or Gpnmb peptide as described previously. $CD8^+$ T cells were plated at $5x10^4$ per well and co-cultured with $1x10^4$ of treated RMA-S cells per well in a total of 200 µL of RPMI medium (Corning) supplemented with 10% FBS, L-glutamine (400 mM), penicillin (100 U/ml), streptomycin (100 µg/ml), 2-mercaptoethanol (50 µM), and IL-2 (100 ng). Cells were cultured at 37°C and harvested after 3 and 5 days and prepared for flow cytometry using the $CD8^+$ T cell panel. Data for this assay was acquired on a Beckman Coulter CytoFLEX machine in the NCSU flow Cytometry Core. All data was analyzed using FlowJo software v10.8.

4.2.9 Cytokine Analysis

Media from T cell activation assays were collected and analyzed using a 9-plex mouse luminex discovery assay targeting RANTES, Granzyme B, IFN-gamma, Il-2, IL-4, IL-6, IL-10, IL-13 and TNF alpha on the Bio-Rad Bio-Plex 200 multiplex suspension array system in the Advanced Analytical Core at UNC Chapel Hill. Media was diluted to 1:5 using assay buffer.

4.2.10 Flow Cytometry

Cells were prepared for flow cytometry as previously mentioned. Cells were stained with the following panels: T cell activation panel: CD8a (PE-Cy7, 1:200, BD Biosciences), TCRβ (APC-Cy7, 1:200, BD Biosciences), CD44 (A700, 1:200, BD Biosciences), CD62L (APC, 1:200, BD Biosciences), Cell Trace Violet (3mM working concentration, ThermoFisher) and Propidium Iodide (PI, 1:10,000, ThermoFisher). T cell subsets and tetramer panel: CD8a (PE-Cy7, 1:200, BD Biosciences), TCRβ (APC-Cy7, 1:200, BD Biosciences), CD44 (A700, 1:200, BD Biosciences), CD62L (APC, 1:200, BD Biosciences), CXCR6 (FITC, 1:100, Biolegend), CCR7 (PerCP-Cy5.5, 1:100, Biolegend), and Ncf2 Tetramer (PE, 1:100, NIH Tetramer Core Facility). T cell subsets was acquired on the Becton Dickinson LSRII machine in the NCSU flow Cytometry Core. T cell activation assays were acquired on the Beckman Coulter CytoFLEX machine in the NCSU flow Cytometry Core. All data was analyzed using FlowJo software v10.8.

4.2.11 Statistical Analysis

GraphPad Prism 10.0.2 software was used for all statistical analyses. Two-tailed unpaired Student's t-tests were performed for two group comparisons. Two-way ANOVA was performed for genotype versus diet studies followed by multiple T test comparisons. All data is presented as

the mean ± SEM. Data was considered statistically significant for P<0.05 (*), P<0.01 (**), P<0.001(***), and P<0.0001(****).

4.3 Results

4.3.1 Unique H2Kb Peptides are Identified in NASH

Given H2Kb expression is important for $CD8^+$ T cell activation, we aimed to identify H2Kb restricted peptides in NASH. Peptides were isolated from livers of NASH mice using immunoaffinity chromatography in three different mouse models of NASH (LDLRKO, Tac, and WT) compared to chow controls **(Fig. 4.1A-C).** Using BioVenn filtering analysis, we identified unique NASH peptides in NASH mouse models by removing chow associated peptides **(Fig. 4.1D)**. NASH peptides demonstrated a preference for 8 amino acids in length **(Fig. 4.2A-C).** BioVenn filtering identified 59 NASH peptides found in all three mouse models of NASH **(Fig. 4.2D).** Pathway analysis of peptide related proteins revealed enrichment in pathways such as cellular response to stress, adaptive immune system, response to endoplasmic reticulum stress, and protein catabolic processes **(Fig. 4.2E).** Using NetMHCPan-4.1, all peptides were predicted to be strong H2Kb binders **(Table 4.1).**

4.3.2 Identification of Unique NASH Peptide Ncf2

Out of the 59 unique peptides found in all NASH models, the peptide VHYKYTVV (Ncf2 peptide) was identified and predicted to strongly bind to H2Kb with high specificity and not predicted to bind to any other MHC I isoforms **(Fig. 4.3A-B).** The Ncf2 peptide is associated with the p67phox protein, a critical subunit for NADPH oxidase activity **(Fig. 4.3C)** [161-163]. Additionally, Ncf2 protein and gene expression was significantly upregulated under NASH condition in both the Taconic and LDLRKO NASH models **(Fig. 4.3D-G).** Interestingly, MHC I

KO and LysM Kb KO mice showed reduced Ncf2 protein and gene expression compared to WT amylin mice. Additionally, Kb amylin behaved similar to WT amylin mice with increased Ncf2 expression **(Fig. 4.4A-D).** This data indicates that NASH upregulates Ncf2 expression and its expression can be regulated by MHC I expression.

4.3.3 Ncf2 Peptide Activates $CD8^+$ T Cells *in vitro*

Next, we determined the ability of the Ncf2 peptide to activate NASH $CD8^+$ T cells *in vitro*. To confirm Ncf2 predicted H2Kb binding, a peptide binding assay was performed using RMA-S cells **(Fig. 4.5A).** Cells were pulsed with a vehicle control containing no peptide (NP), a known H2Kb binding peptide ovalbumin (Ova), or the Ncf2 peptide. Flow cytometry analysis confirmed the peptides Ncf2 and Ova bind to H2Kb compared to NP control **(Fig. 4.5B).**

We then investigated whether Ncf2 could activate $CD8^+$ T cells isolated from NASH mice. Using the LDLRKO NASH model, hepatic $CD8^+$ T cells were isolated and co-cultured with RMA-S cells pulsed with NP, Ova, or Ncf2 and harvested for flow analysis at days 3 and 5. By day 3 samples treated with the Ncf2 peptide showed increased $CD8^+$ T cell activation ($CD44^+$ $CD62L^-$) and proliferation compared to both NP and Ova treated cells **(Fig. 4.5C-D).** To test for cytotoxicity, cytokines and cytotoxic granules from the media were evaluated and showed significant increases in IL-13, IFNγ, RANTES, and GRANZYME B by day 5 in Ncf2 treated cells compared to NP **(Fig. 4.5E).**

To test if Ncf2 reactive T cells were unique to the liver, splenic $CD8^+$ T cells from LDLRKO NASH mice were evaluated. By day 5 splenic $CD8^+$ T cells responded similar to hepatic $CD8^+$ T cells with increased activation and proliferation in response to the Ncf2 peptide **(Fig. 4.6A-B).** Splenic $CD8^+$ T cells activated by the Ncf2 peptide shared a similar cytokine

profile to hepatic $CD8^+$ T cells with significant increases in GRANZYME B and increasing trends in IFNγ and RANTES **(Fig. 4.6C).**

Comparable to the LDLRKO NASH model, hepatic and splenic $CD8^+$ T cells from the Tac NASH model also demonstrated significant increases in $CD8^+$ T cell activation and proliferation when exposed to the Ncf2 peptide compared to NP control **(Fig. 4.7A-D).** To rule out non-specific responses from stimulated conditions, splenic $CD8^+$ T cells from the Tac NASH model were evaluated for Ncf2 reactivity under unstimulated conditions. Under unstimulated conditions $CD8^+$ T cells were still able to respond to the Ncf2 peptide with increased activation and proliferation **(Fig.4.7E-F).** These results demonstrate that H2Kb restricted peptide Ncf2 can activate both hepatic and splenic $CD8^+$ T cells from NASH mice *in vitro* and with increased activation, proliferation, and cytotoxicity.

4.3.4 Ncf2 Reactive $CD8^+$ T Cells are Detected *in vivo*

To confirm $CD8^+$ T cell reactivity to the Ncf2 peptide, an H2Kb-Ncf2 tetramer was used to detect the presence of Ncf2 specific $CD8^+$ T cells *in vivo*. Immune cells were isolated from livers of Taconic chow or Amylin mice and stained for flow cytometry. Flow analysis confirmed increased $CD8^+$ T cells and activation in NASH. Additionally, $CD8^+$ T cell subsets were evaluated and identified significant increases in T cell effector memory (TEM, $CD62L^-$, $CD44^+$, $CCR7^-$, $CXCR6^-$) and T cell resident memory subsets (TRM, $CD62L^-$, $CD44^+$, $CCR7^-$, $CXCR6^+$) with no changes in T cell central memory cells (TCM, *CD6L2+*, $CD44^+$, $CCR7^+$) **(Fig. 4.8A-C).** TEM and TRM $CD8^+$ T cell subsets showed a significant increase in Ncf2 Tetramer signal compared to chow controls with no significant changes detected in TCMs **(Fig. 4.9A-D).** This data provides insight into which $CD8^+$ T cell subset may be responsible for driving NASH-associated inflammation and fibrosis in response to the Ncf2 peptide.

4.3.5 Ncf2 Peptide is Not Present During Fibrosis Resolution

A recent study has shown that tissue-resident memory (TRM) $CD8^+$ T cells play a key role in resolving fibrosis during resolution (RES). NASH RES can be established within 5 weeks of switching from a high fat high cholesterol diet to a chow diet. At 5 weeks of resolution $CD8^+$ T cells remain elevated, but mice show reductions in inflammation and fibrosis [141]. Utilizing this model concept, we investigated if the expression of peptide Ncf2 is altered during RES at 5 weeks when $CD8^+$ T cells are still elevated **(Fig. 4.10A).** As seen in previous studies, RES mice had significantly reduced body weight, liver weight, and adipose tissue compared to NASH mice after 5 weeks of resolution **(Fig. 4.10B-D)** [141]. Hepatic gene expression in RES mice showed significant reductions in inflammation (*Tnf* and *Il10)* and fibrosis (*Col1a1)* compared to NASH mice **(Fig. 4.10E).** Additionally, gene expression for immune cell markers *Cd8* and *Cd11b* remained elevated during resolution whereas *F4/80* expression was significantly reduced compared to NASH mice **(Fig. 4.10F).** Next, we used mass spectrometry to evaluate if the Ncf2 peptide is present during resolution. Interestingly, the Ncf2 peptide was only present under NASH conditions **(Fig. 4.11A).** Ncf2 hepatic protein and gene expression was also reduced during resolution compared to NASH mice **(Fig. 4.11B-C).** These results indicate that the Ncf2 peptide may be necessary for *in vivo* pathogenic $CD8^+$ T cell activation in NASH and the presence of the peptide is dependent on dietary signals.

4.4 Discussion

In the current study we examined the hepatic immunopeptidome, which consists of all antigens bound to H2Kb in normal and NASH mouse livers. We identified 59 unique H2Kb dependent antigens in NASH livers with peptides deriving from proteins associated with

pathways such as tight junctions and cellular stress. Of these NASH peptides, we identified a $CD8^+$ T cell reactive Ncf2 peptide. This Ncf2 peptide increased activation, proliferation, and cytokine production in NASH hepatic and splenic $CD8^+$ T cell *in vitro*. Additionally, using an H2Kb-Ncf2 tetramer, Ncf2 reactive hepatic $CD8^+$ T cells were increased in NASH mice specifically in TRM and TEM memory T cell subsets. Interestingly, under resolution conditions the Ncf2 peptide was not detected suggesting peptide presentation depends on diet-related factors. This data provides insights into the mechanisms for $CD8^+$ T cell activation in NASH identifying the Ncf2 protein or peptide as a potential therapeutic target.

Our findings further support the role of oxidative stress in the pathogenesis of NASH [40]. Oxidative stress in the liver is especially detrimental as it can play a role in cellular dysfunction, injury, and even cell death [164-166]. NADPH oxidases are membrane bound enzymatic complexes that are responsible for generating cytoplasmic ROS [42]. Interestingly, our studies identified unique NASH peptide Ncf2 which is associated with the cytosolic protein subunit p67phox/NCF2 of the NOX2 NADPH oxidase complex. The NOX2 isoform consists of a complex of proteins containing a RAC1 subunit, one membrane regulatory subunit (P22phox/CYBA), a catalytic subunit (gp91phox), and three cytosolic subunits (P67phox/NCF2, p40phox/NCF4, and p47phox/NCF1) [42, 43]. Previous studies have shown that the NOX2 isoform is increased in NASH with reports that it reduces high fat diet (HFD) induced steatosis and insulin resistance [44] and ROS and fibrosis in CCl4-induced liver fibrosis [42]. In a lupus mouse model, knockdown of NCF2 reduces splenic $CD8^+$ T cells [46]. NADPH oxidase superoxide production in dendritic cells is also linked to the formation of highly reactive γ-ketoaldehydes that rapidly react with self-proteins to form isolevuglandins serve as neoantigens

in hypertension and obesity [45]. However, the function of the NCF2 protein and peptide generation during NASH progression remains to be investigated.

Our data shows that the Ncf2 peptide can activate NASH $CD8^+$ T cells. In agreement to our findings, analysis of the TCR repertoires of hepatic memory $CD8^+$ T cells during NASH demonstrated less diversity indicating possible antigen regulation [141]. In high fat fed mice, hepatic $CD8^+$ T cells share distinct clonotypes in their TCR repertoires with $CD8^+$ T cells from adipose tissue [96]. Additionally, we previously highlighted myeloid cells as potential antigen presenting cells in NASH as H2Kb KO in myeloid cells lead to a reduction in fibrosis. Notably, the p67phox/NCF2 protein associated with the Ncf2 peptide is expressed by monocytes and macrophages, as well as hepatocytes and dendritic cells, suggesting myeloid cells could be presenting the Ncf2 peptide during NASH. Alternatively, cross presentation by dendritic cells may also provide a mechanism for antigen presentation. Upon examination of dendritic subsets, classical dendritic cells (cDC1) were found to be elevated and drive liver injury and $CD8^+$ T cell activation [167]. Similarly, adipose tissue dendritic cells are linked to metabolic dysfunction, were depletion of conventional dendritic cells prevents HFD model induced inflammation [168]. Further work is required to confirm what cell type is producing the Ncf2 peptide and presenting it under NASH conditions.

Figure 4.1 Liver H2Kb peptide characterization reveals unique NASH peptides. Taconic mice on chow or amylin diet for 28 wks (n=5 mice per group, 2 replicate cohorts). LDLRKO mice on chow or WD for 12 wks (n=3-4 mice per group, 2 replicate cohorts). WT mice on chow or WD and sucrose water for 25 wks (n=5 mice per group, 1 cohort). **(A)** NASH mouse model descriptions. **(B)** H2Kb immunoaffinity chromatography peptide isolation overview. **(C)** Peptide analysis workflow. **(D)** BioVenn filtering analysis for Taconic, LDLRKO, and WT mouse models chow vs NASH.

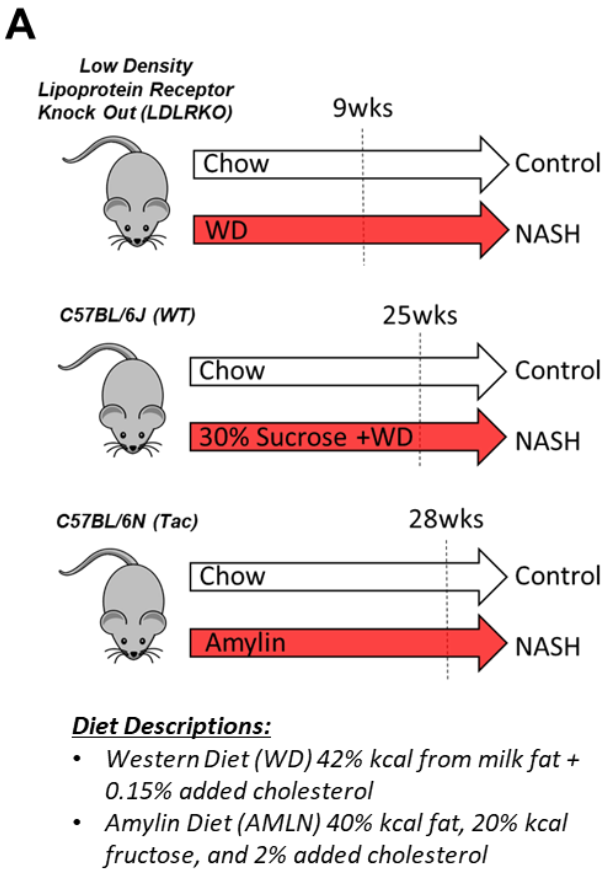
A
Low Density Lipoprotein Receptor Knock Out (LDLRKO)
9wks
Chow
Control
WD
NASH
C57BL/6J (WT)
25wks
Chow
Control
30% Sucrose +WD
NASH
C57BL/6N (Tac)
28wks
Chow
Control
Amylin
NASH
Diet Descriptions:
Western Diet (WD) 42% kcal from milk fat + 0.15% added cholesterol
Amylin Diet (AMLN) 40% kcal fat, 20% kcal fructose, and 2% added cholesterol

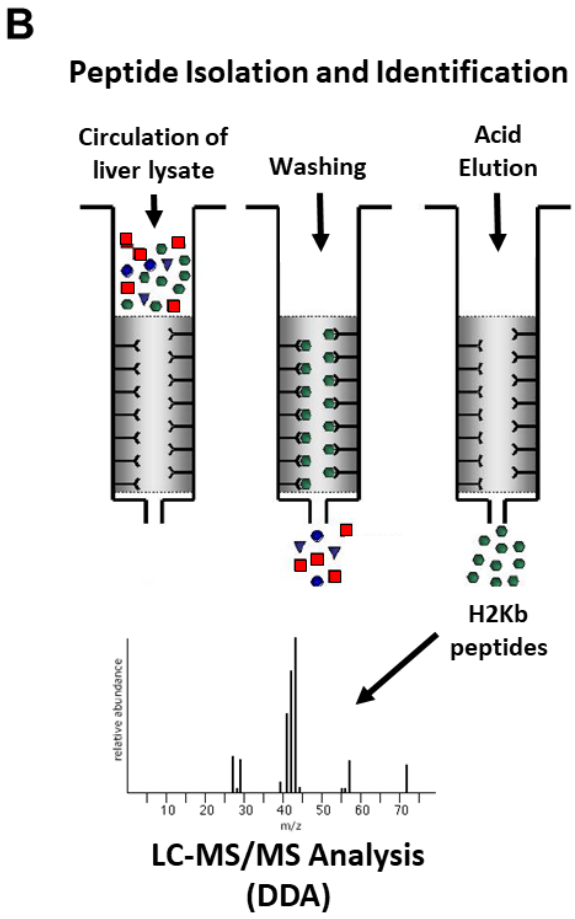
B
Peptide Isolation and Identification
Circulation of liver lysate
Washing
Acid Elution
H2Kb peptides
relative abundance
10
20
30
40
50
60
70
m/z
LC-MS/MS Analysis (DDA)

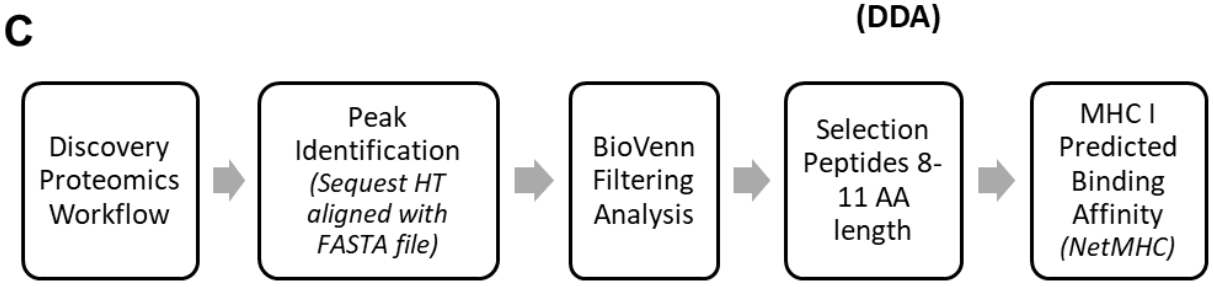
C
Discovery Proteomics Workflow
Peak Identification (Sequest HT aligned with FASTA file)
BioVenn Filtering Analysis
Selection Peptides 8-11 AA length
MHC I Predicted Binding Affinity (NetMHC)

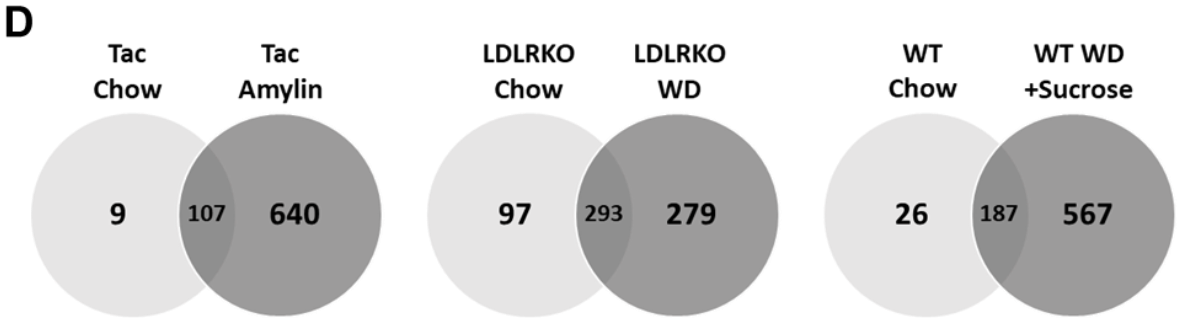
D
Tac Chow
Tac Amylin
9
107
640
LDLRKO Chow
LDLRKO WD
97
293
279
WT Chow
WT WD +Sucrose
26
187
567

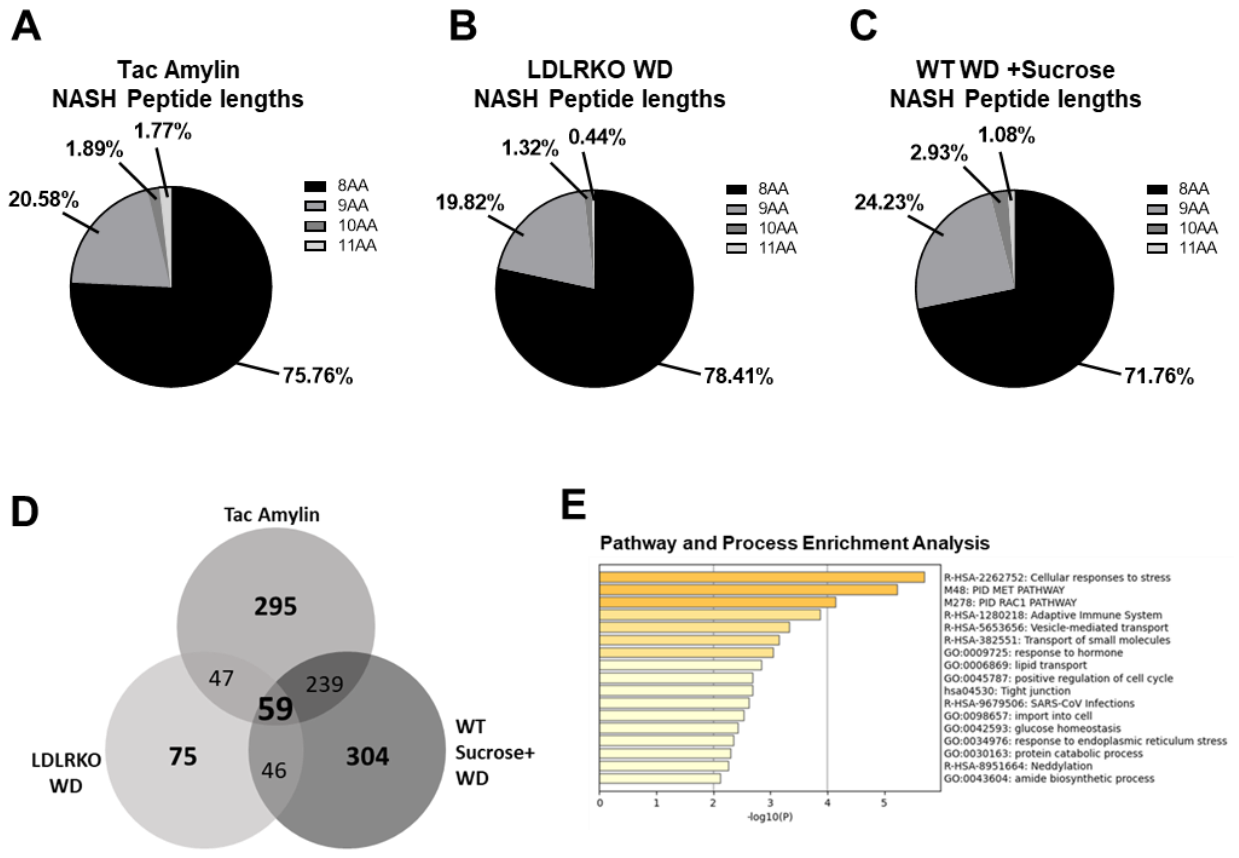

Figure 4.2 Unique NASH peptides show preference for 8 amino acid peptides. Taconic mice on chow or amylin diet for 28 wks (n=5 mice per group, 2 replicate cohorts). LDLRKO mice on chow or WD for 12 wks (n=3-4 mice per group, 2 replicate cohorts). WT mice on chow or WD and sucrose water for 25 wks (n=5 mice per group, 1 cohort). Pie chart of the percentage of peptides with different amino acid lengths from **(A)** Tac NASH model, **(B)** LDLRKO NASH model, and **(C)** WT WD and Sucrose NASH model. **(D)** BioVenn filtering analysis for 3 NASH mouse models for shared NASH only peptides between models. **(E)** Bar graph of enriched terms across input gene lists, colored by p-values using Metascape.

Table 4.1. Top 59 NASH peptides MS/MS data and H2Kb predicted binding affinity.

Table S1

Sequence	Length	Charge	MH+ [Da]	ΔM [ppm]	RT [min]	Proteins	Protein Accessions	Sequest q-value	H2Kb binding Affinity(nM)
AALIYGKL	8	2	848.52402	-0.7	25.4304	1	Q9DC23	0.0070	47.49
AAYSYFRL	8	2	990.50434	0.1	29.6579	1	Q8R4U0	0.0070	2.83
AGPSRTVGL	9	2	857.48394	-0.29	18.168	1	Q64521	0.0037	860.84
AQYRFIYM	8	2	1107.52918	0.92	25.2868	2	P35235, P35235-2	0.0078	9.12
ATYSYKEAL	9	2	1045.52005	0.01	21.026	1	Q8R349	0.0037	29.22
AVHEFQNL	8	2	957.47886	-0.82	21.0445	1	Q8VCB3	0.0420	16.64
EAYRFTGL	8	2	956.48361	1.43	26.3243	2	Q8K015, Q8K015-2	0.0037	16.66
EIVSFQHL	8	2	972.51491	-0.59	27.935	1	Q8R502	0.0037	452.69
EPPVYANL	8	2	902.46181	0.71	29.7156	1	P05627	0.0037	4414.99
HVYYFAHL	8	2	1049.52033	1.38	25.9122	1	Q80SU7	0.0037	3.27
IFYYVQKL	8	2	1073.60299	-0.61	29.4592	1	Q69ZR2	0.0037	42.01
INLNYKDL	8	2	992.54112	-1.29	26.4768	1	Q9CY50	0.0490	49.34
INQIYEARV	9	2	1105.60003	-0.45	21.8794	1	Q8K2H4	0.0037	136.61
IPPEYRHL	8	2	1024.55744	-0.38	18.0785	7	P51125-4, P51125-7, P51125-6, P51125-5, P51125-1, P51125-3, P51125-2	0.0037	845.23
ISLDYQHL	8	2	988.50982	-0.81	27.4757	1	Q5SYL3	0.0057	7.82
ITFIFKSL	8	2	968.58153	0.76	34.9107	1	Q9JLN9	0.0044	3.3
KNIRFFLM	8	2	1018.58663	0.02	25.7934	6	Q80TF4-2, Q80TF4-5, Q80TF4-4, Q80TF4, Q80TF4-3, Q6ZPT1	0.0037	14.07
KNVTFHGI	8	2	915.50468	-0.12	18.1704	1	P19096	0.0037	89.31
KNYDFAQV	8	2	984.47852	-0.45	22.3666	3	Q8BGF7-2, Q8BGF7, Q8BGF7-3	0.0057	7.09
KSLEIRTL	8	2	959.58841	-0.68	19.3302	4	Q61301-2, Q61301-3, P26231, Q61301	0.0037	417.45
KTLEHINAI	9	2	1038.59422	-0.29	18.3673	1	P16301	0.0400	809.08
KVLEFERV	8	2	1019.58841	-0.64	21.0608	1	Q8CEC6	0.0037	136.24
QVVQFNRL	8	2	1003.56834	-1.39	24.1097	1	O88653	0.0037	62.22
RAFLFNKV	8	2	994.58326	-1.19	23.9096	1	P62700	0.0037	16.16
RSYNMPSL	8	2	967.46658	-0.8	23.6594	2	Q91ZV0, Q8R311	0.0037	31.18
SAARFFQL	8	2	939.50468	0.72	29.9437	1	Q9QY30	0.0037	10.13
SALIYSNL	8	2	880.47746	-0.06	32.1398	1	O55013	0.0037	4.45
SALKYYQL	8	2	985.53531	-0.79	25.0987	2	Q62PU9-1, Q62PU9-3	0.0037	10.19
SEYRYTLL	8	2	1044.53604	-0.45	27.2462	1	Q9D1Q6	0.0037	49.3
SGPDLSTAL	9	2	860.43599	-0.25	28.9577	1	Q91VS7	0.0340	1268.48
SNPEFRQL	8	2	990.50032	-0.34	20.6513	1	Q3UWM4	0.0078	50.52
SSAEFHSL	8	2	877.40502	-0.08	19.4898	1	Q61810-1	0.0037	16.85
SSVLYSRV	8	2	910.49926	-0.2	20.196	1	Q8CGC7	0.0037	14.48
SSYRFVQNV	9	2	1099.55308	0.39	22.4486	1	P42128	0.0044	4.2
STFVYNTM	8	2	978.42371	0.42	24.1463	1	Q8CFB4	0.0037	6.13
SVYTHSYL	8	2	969.46762	0.83	21.5721	5	Q3TZX8-3, Q3TZX8-2, Q8K0L2-2, Q8K0L2, Q3TZX8-1	0.0037	5.74
TILFTKV	8	2	934.59718	-1.27	31.8743	2	Q8K2V6-2, Q8K2V6-1	0.0044	43.16
TNISFTNM	8	2	943.41896	0.3	24.212	1	Q9CYY7	0.0240	10.67
TNVLFNHL	8	2	957.51524	-0.57	27.9848	1	Q9D706	0.0037	16.43
TTYRFPEL	8	2	1026.52547	0.2	29.1235	2	Q8K440, Q8K440-2	0.0096	3.08
TVPELTQQM	9	2	1062.51359	0.12	22.6054	6	Q7TMM9, Q9D6F9, Q9ERD7, P68372, Q9CWF2, Q922F4	0.0044	3132.55
VFYEREVQM	9	2	1200.57177	0.35	24.5077	1	Q80SY3	0.0037	95.16
VGYRQPLV	8	2	931.53598	-0.76	21.0133	1	P97370	0.0046	137.01
VHYKYTVV	8	2	1008.55129	-0.22	18.6048	1	O70145	0.0037	40.94
VIFNYKGKNV	10	3	1181.66772	-0.38	19.3954	1	P14211	0.0037	424.81
VITNFSARI	9	2	1020.58366	0.61	25.3305	2	Q3UVL4-1, Q3UVL4-2	0.0037	48.12
VIVRFLTV	8	2	946.60841	-1.32	32.6811	1	P62245	0.0044	19.64
VMYRVIQV	8	2	1007.57065	0.02	26.3151	1	Q61069	0.0037	32.58
VNLVFEKI	8	2	961.57169	-0.82	30.0931	4	Q6AW69-4, Q6AW69-5, Q6AW69-1, Q6AW69-3	0.0037	51.25
VNRVFDKL	8	2	990.57309	-0.72	20.0245	1	P28076	0.0037	50.28
VNSIFQHL	8	2	957.51524	0.07	28.0498	1	Q80SU7	0.0037	16.64
VNVCYKEL	8	2	967.49173	0.27	28.3798	1	Q8BKT7	0.0037	33.28
VNYPRKIGA	9	2	1017.58399	-0.86	17.0715	1	O35488	0.0037	475.37
VQYEMRTL	8	2	1055.51901	-1.08	18.5278	1	Q80ZK0	0.0037	27.17
VSTKFEHL	8	2	960.51491	-0.03	17.972	1	B2RXC1	0.0037	27.81
VSYWFDQRF	9	2	1247.58438	0.3	34.0188	1	P54751	0.0037	15.32
VTITFKNM	8	2	953.51246	0.1	25.2831	2	Q8R4Y4, Q8R4Y4-2	0.0037	8.71
VVAEFGRI	8	2	890.50943	0.36	24.6606	1	Q8BXC6	0.0120	79.83
VVYIYRQI	8	2	1053.60914	1.19	25.6224	7	Q62417-3, Q62417-5, Q62417-2, Q62417-4, Q62417, Q62417-7, Q62417-6	0.0300	6.35

Figure 4.3. Ncf2 characterization. (A) LC-MS/MS MS2 Ncf2 spectrum. **(B)** NetMHC predicted binding affinities for Ncf2 peptide to MHC I isoforms. **(C)** NADPH Oxidase 2 activated protein complex. Total liver Ncf2 protein in Taconic NASH model **(D)** and LDLRKO NASH model **(E)**. Total liver Ncf2 gene expression in Taconic NASH model **(F)** and LDLRKO NASH model **(G)**. Data shown as the mean ± SEM. Two-tailed unpaired Student's t-tests were performed for two group comparisons. Data was considered statistically significant for $P<0.01$ (**), $P<0.001$(***), and $P<0.0001$(****).

A

Ncf2 MS2 Spectra

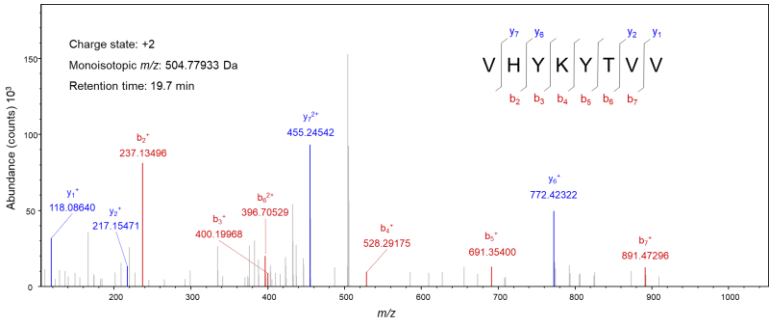

B

NetMHC Predicted Binding Affinity (Ncf2)			
Isoform	Affinity (nM)	Rank	Bind Level
H2Kb	**18.64**	**0.06**	**SB**
H2Db	29901.88	14	NB
H2Dd	27940.6	9.5	NB
H2Kd	8755.49	5	NB
H2Kk	28994.51	19	NB
H2Ld	37520.91	20	NB

C

NADPH Oxidase (NOX2)

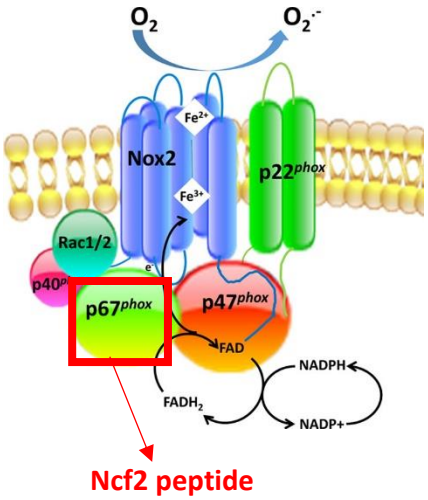

D

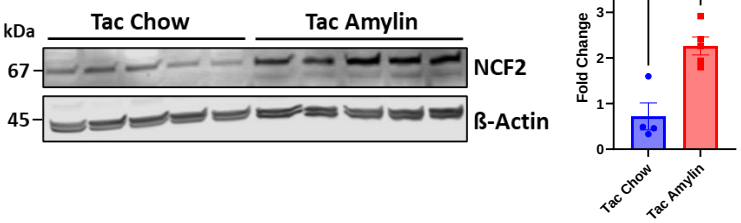

E

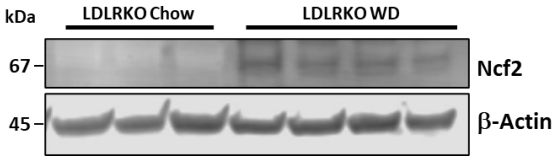

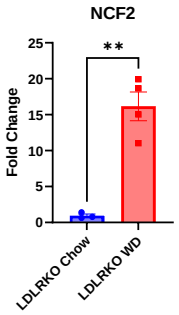

F

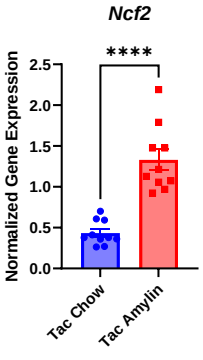

G

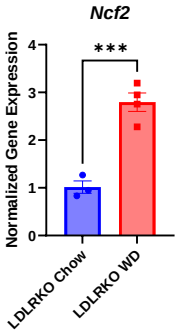

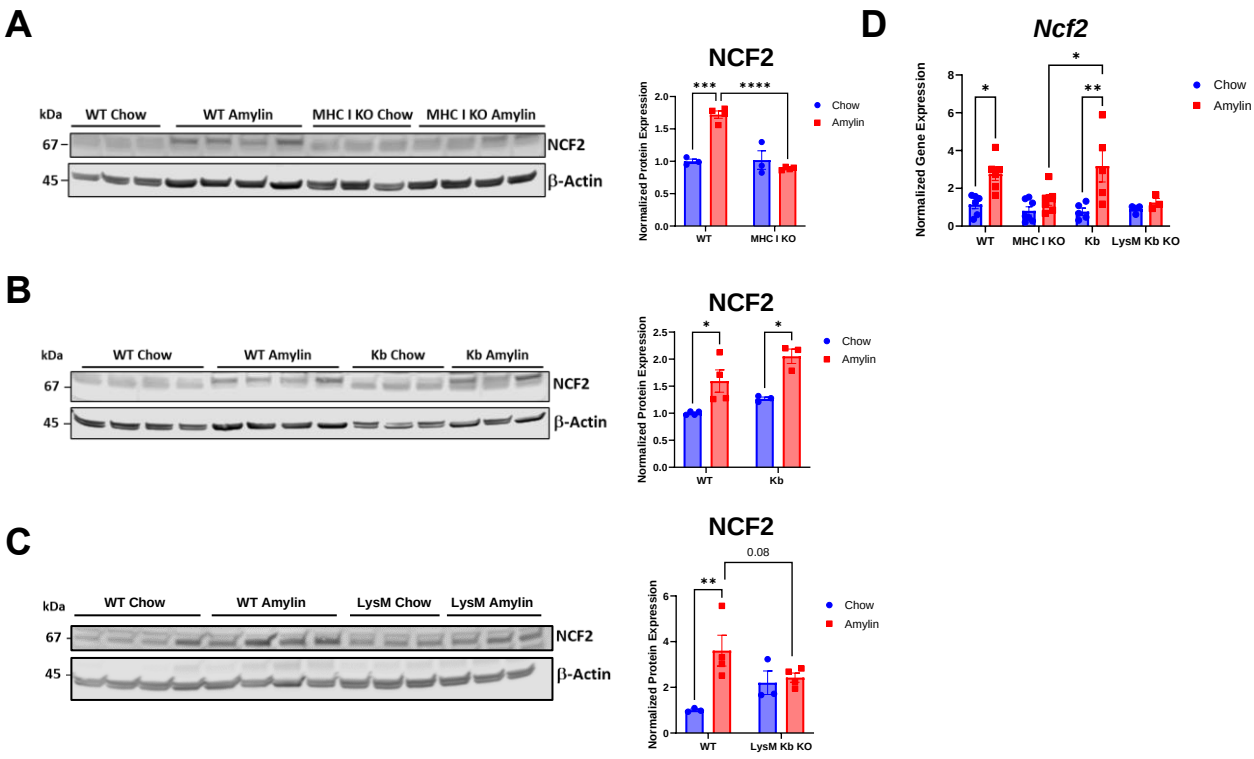

Figure 4.4 Ncf2 is regulated by H2Kb expression. WT, MHC I KO, Kb, or LysM Kb KO mice on chow or amylin diet (n= 3-7 mice per group, 2 replicate cohorts). Total liver Ncf2 protein **(A-C)** and gene expression **(D)** in WT, MHC I KO, Kb, and LysM Kb KO mice. Data shown as the mean ± SEM. Two-way ANOVA was performed for multiple genotypes versus diet studies. Data was considered statistically significant for P<0.05 (*), P<0.01 (**), P<0.001(***), and P<0.0001(****).

Figure 4.5 Ncf2 peptide activates hepatic LDLRKO NASH CD8$^+$ T cells. Hepatic CD8$^+$ T cells were isolated from LDLRKO NASH mice (2 combined NASH livers per cohort, 4 replicate cohorts, n=3 technical replicates per study). **(A)** Peptide binding assay schematic. **(B)** Flow cytometry analysis of H2Kb expression to determine binding with NP, Ova, or Ncf2 peptide pulsed RMA-S cells (n=4 technical replicates, 3 replicate studies). T cell activation assay of hepatic CD8$^+$ T cells co-cultured with NP, Ova, or Ncf2 peptide pulsed RMA-S cells. Cells were harvested on day 3 for flow cytometry analysis of CD8$^+$ T cells (*CD8$^+$TCRb$^+$)* and gated for **(C)** activation (*CD44$^+$ CD62L$^-$*) and **(D)** proliferation. **(E)** Cytokine analysis of media from day 5 of the T cell activation assay. Data shown as the mean ± SEM. Two-way ANOVA was performed for groups more than 2 and was considered statistically significant for P<0.05 (*), P<0.01 (**), P<0.001(***), and P<0.0001(****).

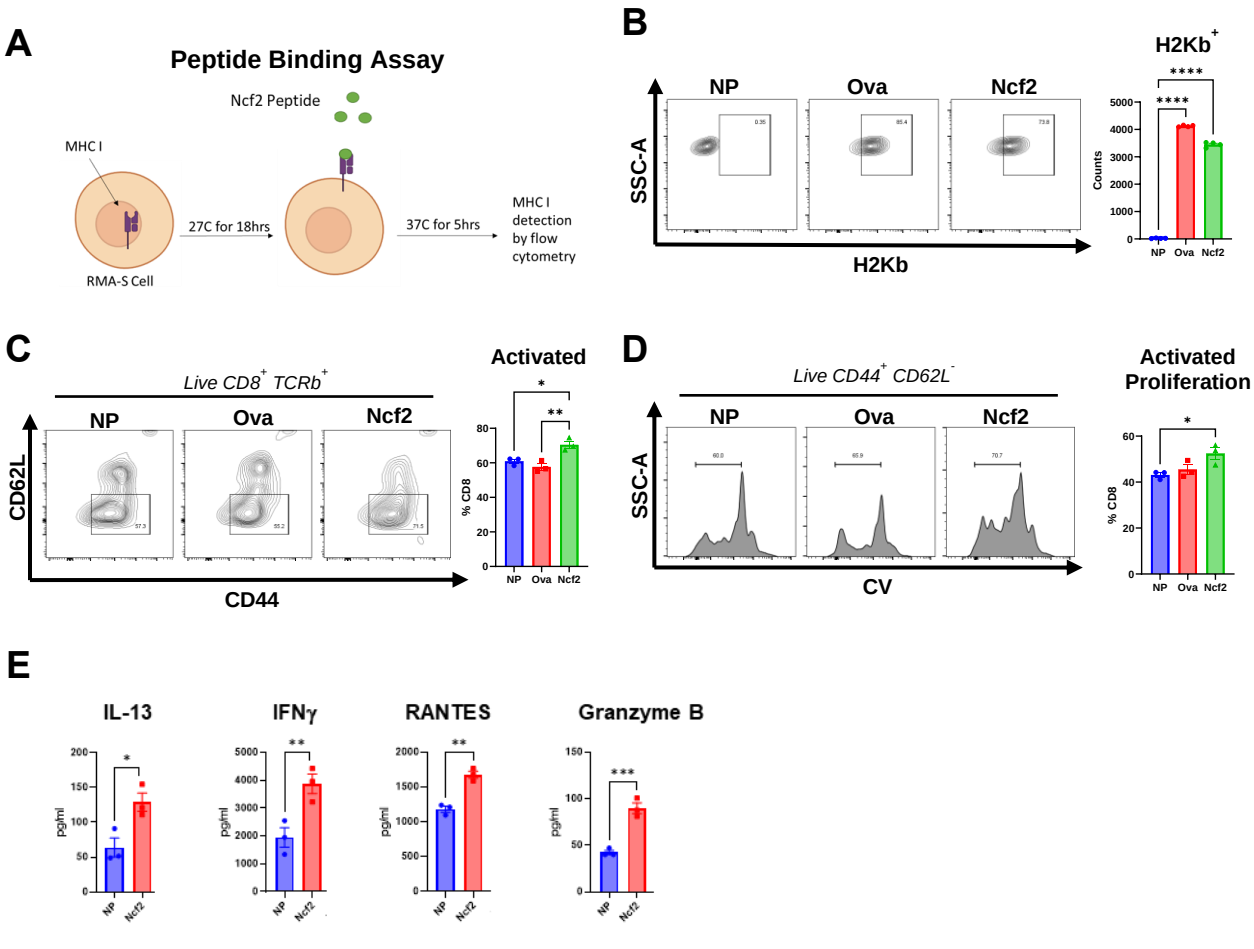
A
Peptide Binding Assay
Ncf2 Peptide
MHC I
RMA-S Cell
27C for 18hrs
37C for 5hrs
MHC I detection by flow cytometry
B
NP
Ova
Ncf2
SSC-A
H2Kb
H2Kb+
Counts
****
****
C
Live CD8+ TCRb+
NP
Ova
Ncf2
CD62L
CD44
Activated
% CD8
*
**
D
Live CD44+ CD62L-
NP
Ova
Ncf2
SSC-A
CV
Activated Proliferation
% CD8
*
E
IL-13
IFNγ
RANTES
Granzyme B
pg/ml
NP
Ncf2

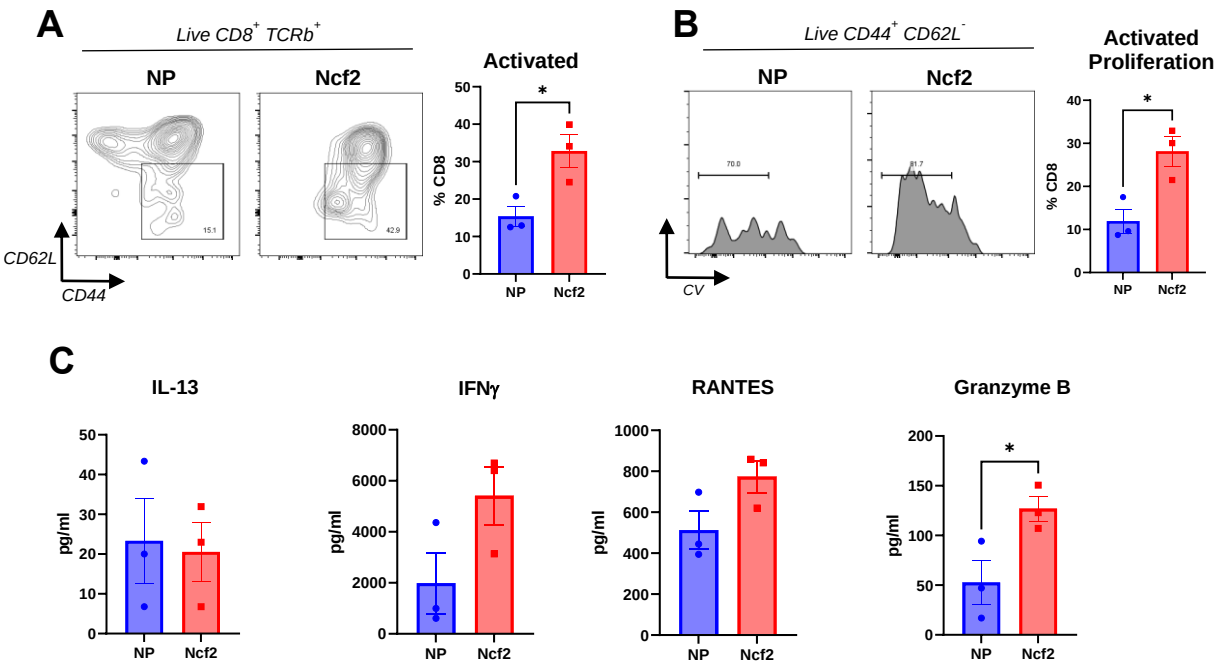

Figure 4.6 Ncf2 peptide activates splenic LDLRKO NASH CD8+ T cells. $CD8^+$ T cells were isolated from spleens of LDLRKO NASH mice (n = 2 mice combined per trial) done in 3-4 replicate studies and cocultured with NP, Ova, or Ncf2 pulsed RMA-S cells. Flow analysis of splenic $CD8^+$ T cell activation (A) and proliferation (B) after 5 days incubation with peptide pulsed RMA-S cells. (C) Cytokine analysis of media after day 5 of incubation. Data shown as the mean ± SEM. Two-tailed unpaired Student's t-tests was performed for data sets with 2 groups and was considered statistically significant for $P<0.05$ (*).

Figure 4.7 Ncf2 activates hepatic and splenic Taconic NASH CD8$^+$ T cells. CD8$^+$ T cells were isolated from livers or spleens of Tac NASH mice (n = 2 mice combined per trial) done in 3-4 replicate studies and cocultured with NP, Ova, or Ncf2 pulsed RMA-S cells. Flow analysis of hepatic CD8$^+$ T cell activation **(A)** and proliferation **(B)** after 3 days incubation with peptide pulsed RMA-S cells under stimulated (CD3/CD28) conditions. Flow analysis of splenic CD8$^+$ T cell activation **(C)** and proliferation **(D)** after 5 days incubation with peptide pulsed RMA-S cells under stimulated conditions. Flow analysis of splenic CD8$^+$ T cell activation **(E)** and proliferation **(F)** after 5 days incubation with peptide pulsed RMA-S cells under unstimulated conditions supplemented with 100ng/ml IL-2. Data shown as the mean ± SEM. Two-tailed unpaired Student's t-tests was performed for data sets with 2 groups and Two-way ANOVA was performed for groups more than 2 and was considered statistically significant for $P<0.05$ (*) and $P<0.01$ (**).

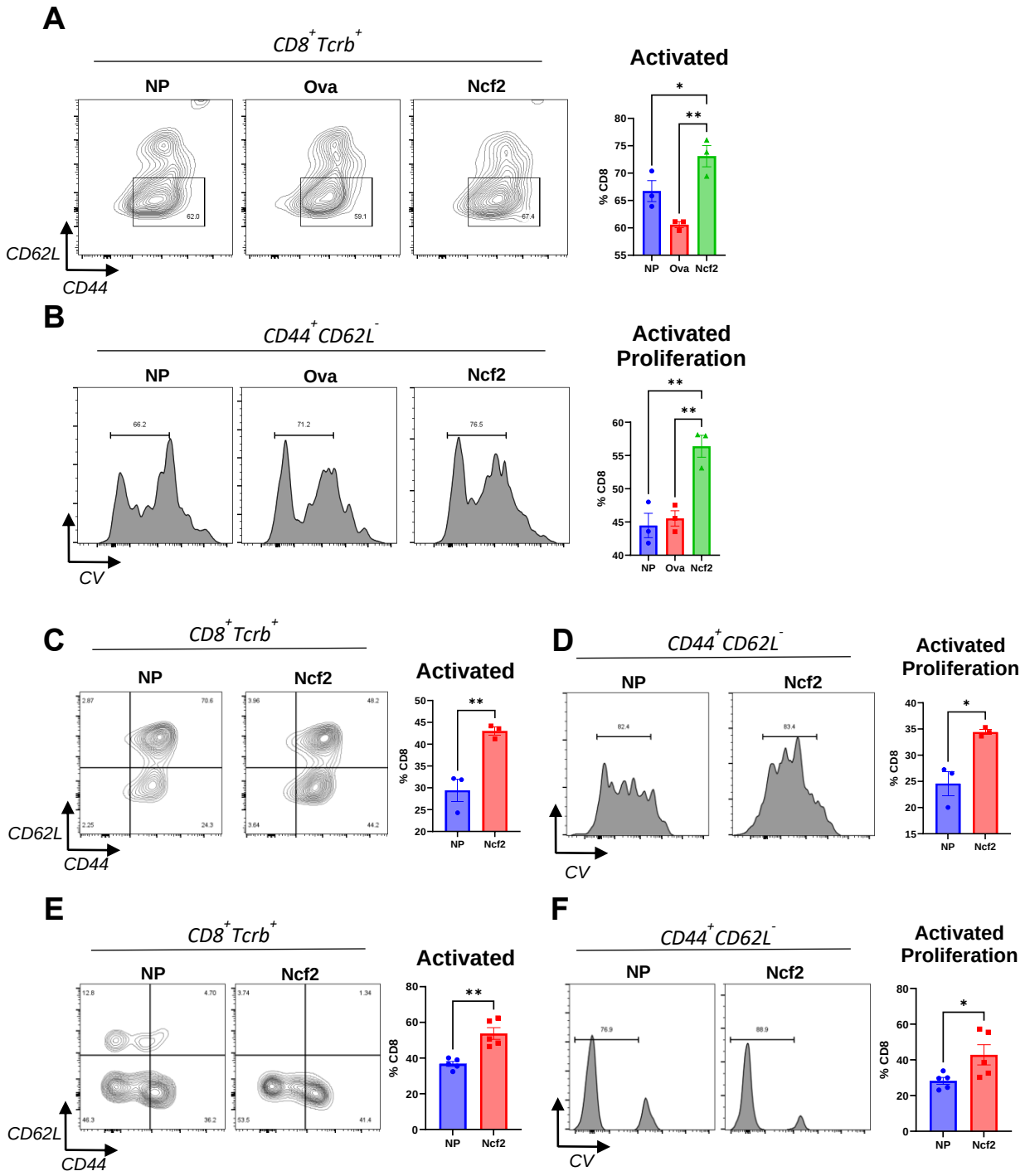
A
CD8+Tcrb+
NP
Ova
Ncf2
CD62L
CD44
Activated
% CD8
NP Ova Ncf2
B
CD44+CD62L-
CV
Activated Proliferation
C
D
E
F

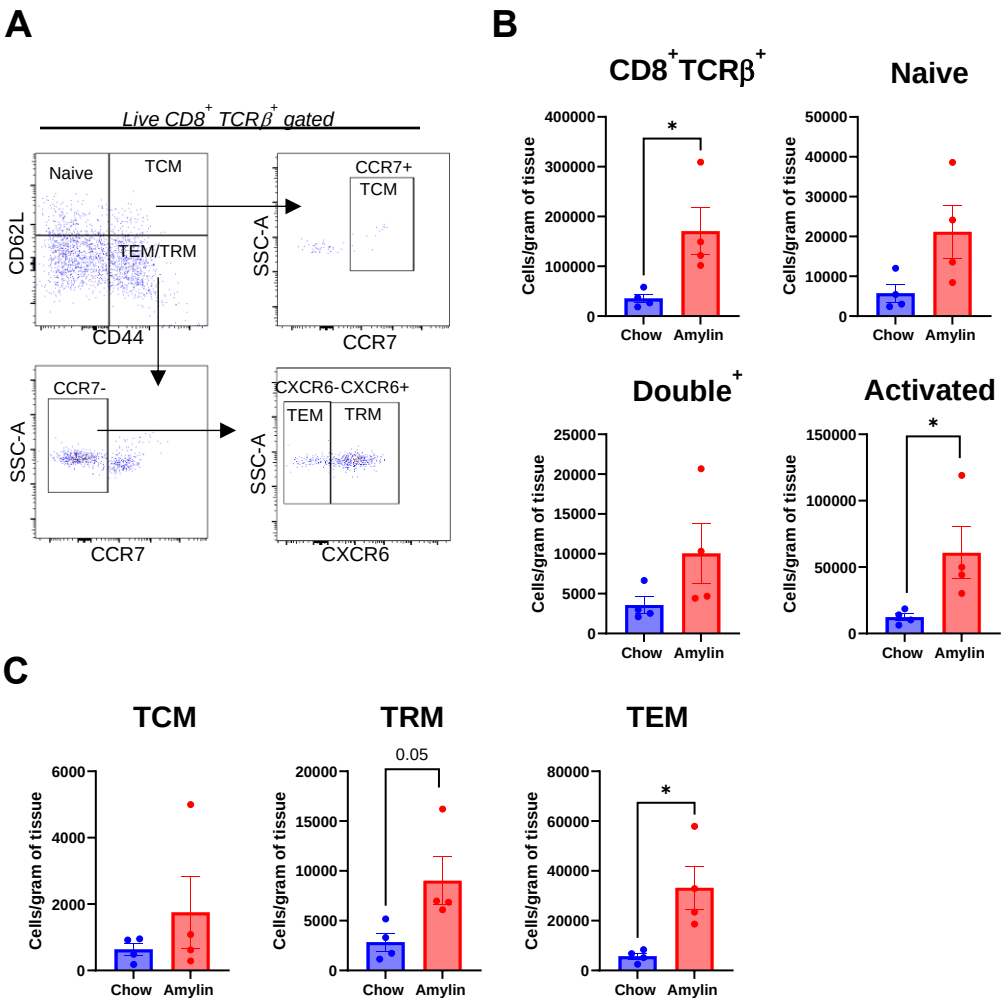

Figure 4.8 CD8$^+$ T cell resident and effector memory subsets are increased in NASH. Tac NASH mice were fed chow or amylin diet for 28 wks (n=4 per group). **(A)** Flow cytometry CD8$^+$ T cell subsets gating strategy from CD8$^+$Tcrb$^+$ liver lymphocytes. **(B)** Quantification of flow cytometry CD8$^+$Tcrb$^+$ and activation states: Naïve (*CD44$^-$CD62L$^+$*), Double+ (*CD44$^+$CD62L$^+$*), and activated (*CD44$^+$CD62L$^-$*). (C) Quantification of flow cytometry data for CD8$^+$ T cell memory subsets (*CD44$^+$CD62L$^-$)*: Central (*TCM*, *CCR7$^+$CXCR6$^-$*), Resident (*TRM*, *CCR7$^-$CXCR6$^+$*), and Effector (*TEM*, *CCR7$^-$CXCR6$^-$*). Data shown as the mean ± SEM. Two-tailed unpaired Student's t-tests was performed and considered statistically significant for P<0.05 (*).

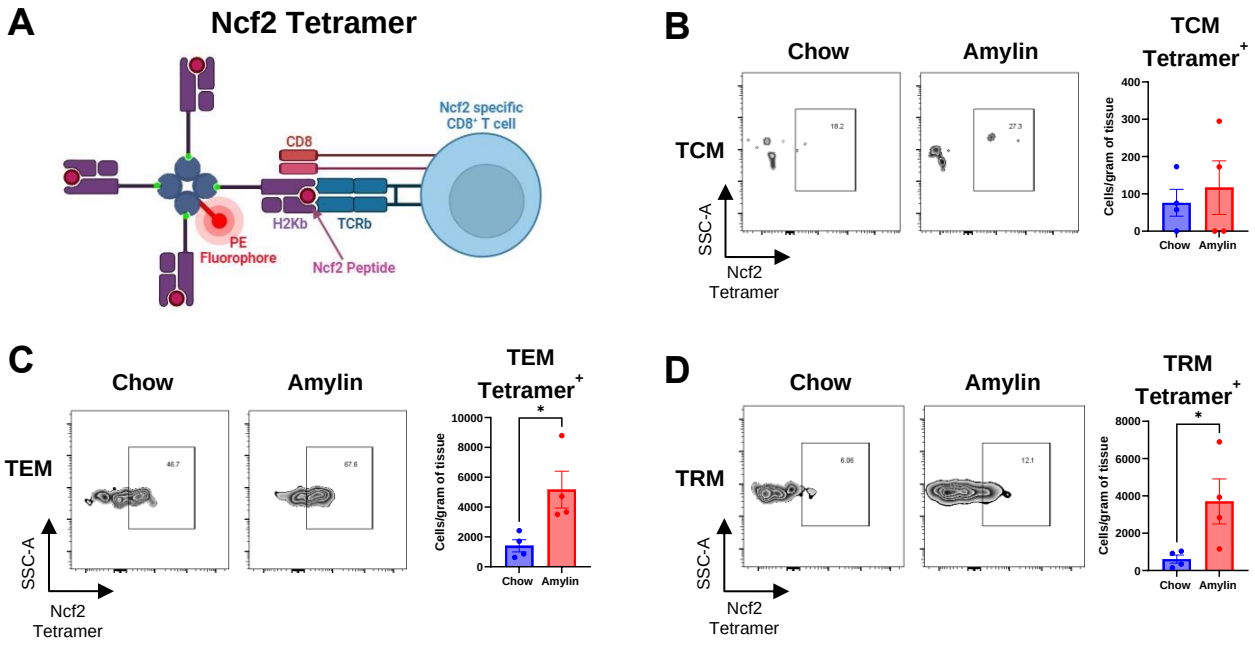

Figure 4.9 Ncf2 reactive CD8$^+$ T cells are detected in vivo. Tac NASH mice were fed chow or amylin diet for 28 wks (n=4 per group). **(A)** H2Kb-Ncf2 tetramer schematic. Representative Ncf2 Tetramer positive flow cytometry plots and quantification from liver CD8$^+$ T cell subsets: **(B)** TCM, **(C)** TEM, and **(D)** TRM populations. Data shown as the mean ± SEM. Two-tailed unpaired Student's t-tests was performed and considered statistically significant for $P<0.05$ (*).

Figure 4.10 Fibrosis and inflammation are reduced during NASH resolution. Tac NASH mice were fed chow or amylin diet for 33 wks. Tac RES mice were fed amylin diet for 28 wks and then switched to chow diet for 5 wks (n=4, 2 replicate cohorts). **(A)** Resolution study schematic. **(B)** Body weight progression. **(C)** Total liver weight. **(D)** Epididymal adipose tissue weight. **(E-F)** Hepatic gene expression. Data shown as the mean ± SEM. Two-way ANOVA was performed and considered statistically significant for $P<0.05$ (*), $P<0.01$ (**), and $P<0.001$(***).

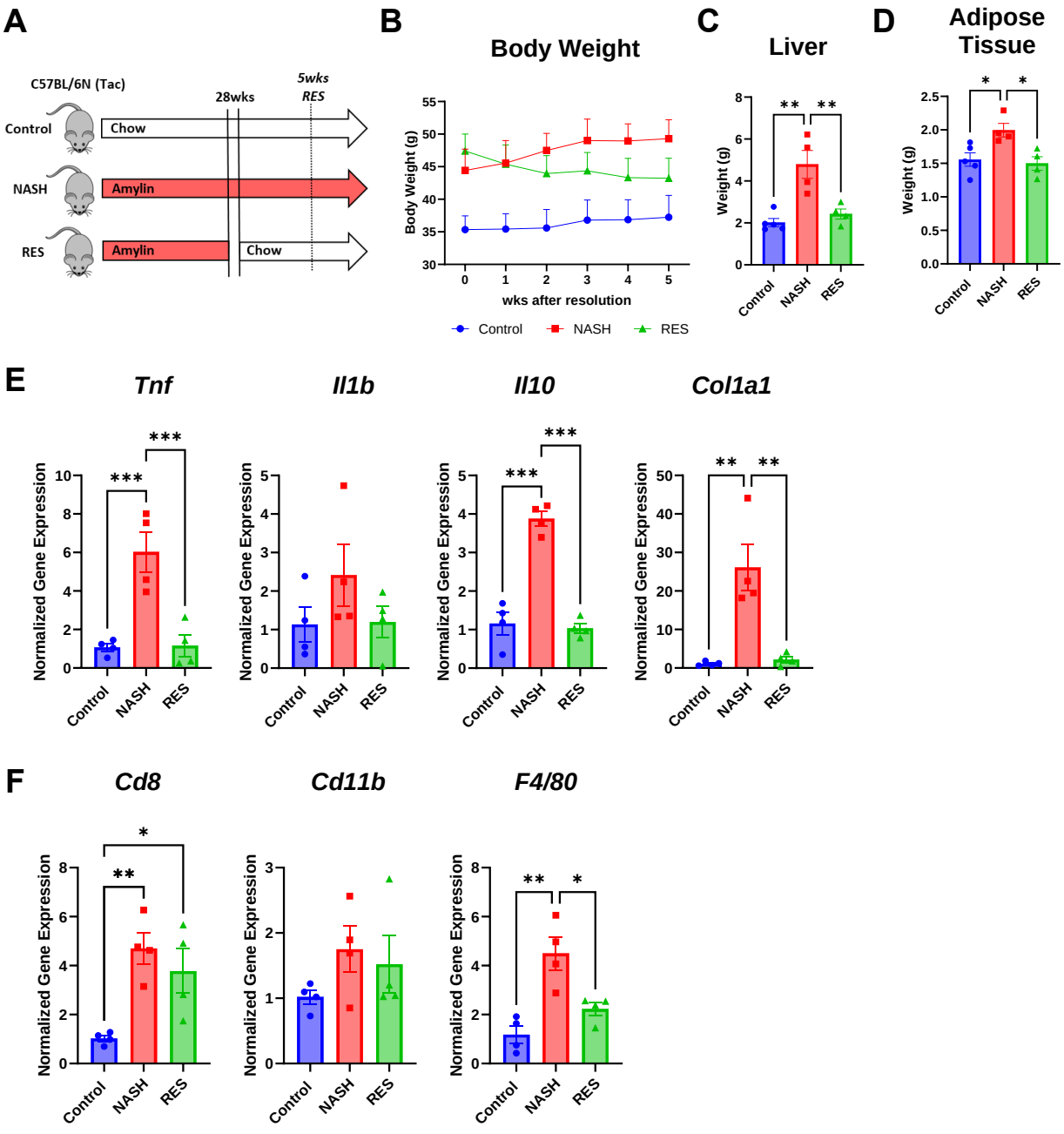
A
C57BL/6N (Tac)
28wks
5wks
RES
Control
Chow
NASH
Amylin
RES
Amylin
Chow
B
Body Weight
Body Weight (g)
wks after resolution
Control
NASH
RES
C
Liver
Weight (g)
Control
NASH
RES
D
Adipose Tissue
Weight (g)
Control
NASH
RES
E
Tnf
Il1b
Il10
Col1a1
Normalized Gene Expression
Control
NASH
RES
F
Cd8
Cd11b
F4/80
Normalized Gene Expression
Control
NASH
RES

A

LC-MS/MS Detection												
Ncf2 peptide	Control 1	Control 2	Control 3	Control 4	NASH 1	NASH 2	NASH 3	NASH 4	RES 1	RES 2	RES 3	RES 4
VHYKYTVV	Not Found	Not Found	Not Found	Not Found	Low	Low	High	Low	Not Found	Not Found	Not Found	Not Found

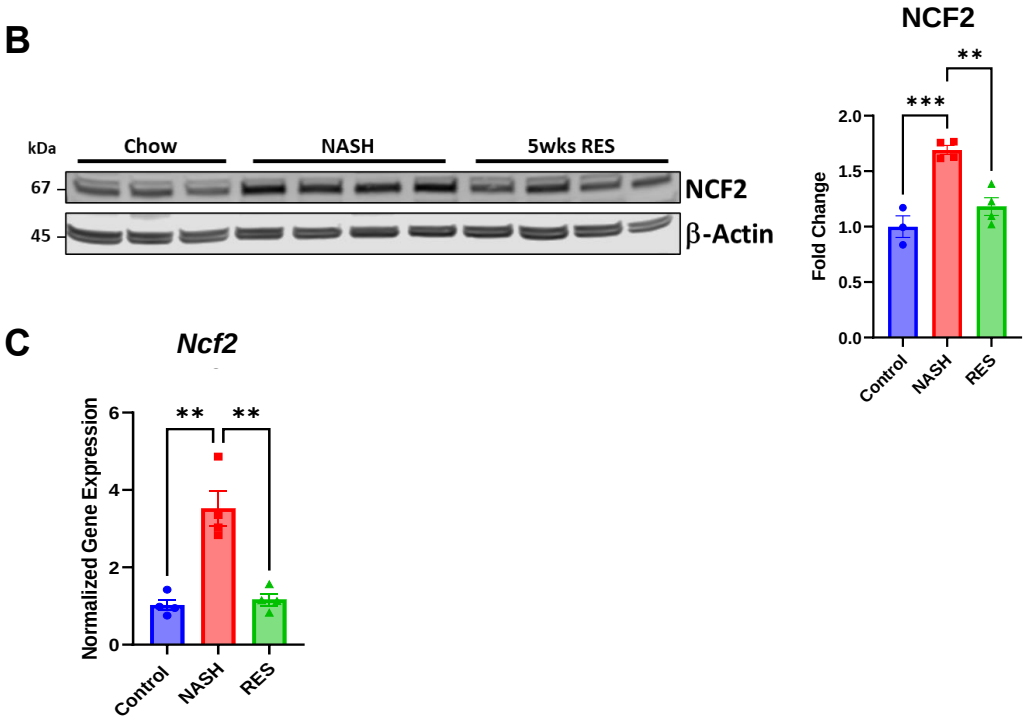

Figure 4.11 Ncf2 peptide is not found during NASH resolution. Tac NASH mice were fed chow or amylin diet for 33 wks. Tac RES mice were fed amylin diet for 28 wks and then switched to chow diet for 5 wks (n=4, 2 replicate cohorts). **(A)** LC-MS/MS detection of Ncf2 peptide from total livers of individual mice from control (chow), NASH (Amylin), or RES (n=4). Total liver Ncf2 protein (B) and gene (C) expression. Data shown as the mean ± SEM. Two-way ANOVA was performed and considered statistically significant for $P<0.01$ (**) and $P<0.001$(***).

CHAPTER 5: Development of MHC Class I Blocking Peptides to target NASH Associated CD8 T Cell Activation

In preparation: Adams V.R, Sarma S., Hall C.K., Kennedy A., 2024.

5.1 Introduction

Non-alcoholic fatty liver disease (NAFLD) is one of the most common liver diseases. NAFLD represents a spectrum of liver pathologies that can transition from simple hepatic steatosis to nonalcoholic steatohepatitis (NASH) [104]. This transition is a significant concern as NASH is characterized further by increased inflammation, fibrosis, and $CD8^+$ T cell activation, which can ultimately develop into hepatocellular carcinoma (HCC) [76-78, 80]. With no current FDA-approved treatments for NAFLD-related liver injuries, developing targeted therapeutic techniques is essential for preventing and treating this disease [9].

Previous work demonstrates that $CD8^+$ T cells drive hepatic inflammation and fibrosis in mice and humans [22-26]. Recent work has identified multiple mechanisms that activate $CD8^+$ T cells under NASH conditions. Metabolites, such as adenosine triphosphate (ATP) and acetate, have been implicated in the development of auto-aggressive hepatic $CD8^+$ T cells [56]. In addition, the cytokine IL-15 is associated with activation in mouse models of NASH [141]. Classically, antigens presented by the major histocompatibility complex (MHC) class I activate $CD8^+$ T cells. The antigens are peptides 8 to 9 amino acids in length and are collectively known as the MHC I immunopeptidome. The immunopeptidome is complex, contains both self and foreign immunogenic peptides, and is influenced heavily by protein translation and degradation. Metabolic diseases and infections can also alter the immunopeptidome. Antigens have been identified in diabetes, obesity, and other metabolic disorders and are essential in activating $CD8^+$ T cells. Recently, we identified a unique H2Kb immunopeptidome under NASH conditions that

contains the peptide Ncf2 (sequence: VHYKYTVV), which activates both hepatic and splenic NASH $CD8^+$ T cells *in vitro* [169-172]. This suggests that blocking H2Kb Ncf2 antigen presentation could provide a potential therapeutic benefit for treating NASH.

Blocking peptides have the potential to be a valuable tool for the treatment of chronic inflammatory and autoimmune diseases [173]. Blocking peptides are short amino acid sequences that, due to their small size, have the ability to interfere with protein-protein interactions. They are emerging as valuable molecules in the drug discovery and development pipeline because of their high potency, low toxicity, and modest manufacturing cost. Due to the identification of key peptides that activate NASH associated $CD8^+$ T cells, designing blocking peptides that disrupt MHC class I dependent antigen presentation to $CD8^+$ T cells may be an effective NASH therapy.

Blocking peptides can prevent T cell activation by either binding to the T cell receptor (TCR) to prevent its association with a specific antigen or by binding to the MHC class I receptor to prevent T cells from interacting with specific antigens. There are several different ways to design blocking peptides. One common approach is to use sequence-based methods to predict binding of peptides that have a high affinity for the MHC class I molecule of interest. Specific residues can be identified that are important for the activity of a targeted protein. An alternative to this approach is to computationally design peptides that bind specifically to the antigen and thereby block its activity. Here we use the *Pep*tide *B*inding *D*esign algorithm (PepBD). A Monte-Carlo search in peptide sequence and conformation space to discover peptides that bind with higher affinity and selectivity to a bio-molecular target than a known "reference ligand". The performance of the best peptide binders predicted by PepBD is evaluated *in-silico* by performing atomistic molecular dynamics (MD) simulations and calculating the binding free energy ($\Delta G_{binding}$) of the peptide:protein complex using the implicit-solvent

molecular mechanics/generalized Born surface area (MM/GBSA) approach with the variable internal dielectric constant model [174-178]. Using the PepBD algorithm, we developed blocking peptides that competitively inhibit the interaction between Ncf2 peptide and H2Kb to prevent $CD8^+$ T cell activation and ultimately possible effective anti-NASH therapeutic strategy.

5.2 Materials and Methods

5.2.1 Animal Models

LDLRKO NASH model. 5-wk-old male low-density lipoprotein receptor knockout (LDLRKO) mice were originally purchased from Jackson Laboratories (Bar Harbor, ME) and propagated further in our colony. 6-wk-old male LDLRKO mice were fed western diet (WD, 42 Kcal% fat with 0.2% added cholesterol, TD.22137; Harlan Laboratories) for 12 weeks. *Taconic Amylin NASH Model*. C57BL/6N (Tac) male mice were originally purchased from Taconic Biosciences on amylin diet (AMLN, 40 kcal% fat, 20 kcal% fructose and 2% cholesterol, Diet # D09100310i, Research Diets) for 28 weeks. Mice were housed on a 12-hour light/dark cycle with ad libitum food and water access. Mice were sacrificed between the 18-34 weeks of age. All animal procedures were approved by the Institutional Animal Care and Use Committee (IACUC) at North Carolina State University under protocol 21-502-B.

5.2.2 Isolation and identification of H2Kb Peptides from Liver

Peptides were isolated and identified using methods previously described [169].

5.2.3 Computational Peptide Design

*Pep*tide *B*inding *D*esign (PepBD) is a Monte-Carlo search algorithm that identifies peptide sequences that bind with higher affinity and specificity to a biomolecular target than a

known “reference ligand”. The starting input structure for the algorithm is a complex formed between the reference ligand (in this case Gpnmb) and the target protein of interest (in this case H2Kb). The design algorithm iterates through 10,000 evolution steps and generates variants to the original peptide that bind to H2Kb. Two kinds of moves: sequence change and conformation change moves are performed to generate peptide variants. After each move, the score (a measure of the peptide-target binding energy) for each trial peptide, is compared to that of the previous sequence/conformation and accepted or rejected using the Monte-Carlo Metropolis sampling technique. The best peptide variants, meaning those with the best “scores”, are evaluated in explicit-solvent atomistic molecular dynamics simulations to calculate the binding free energy, $\Delta G_{binding}$, of the peptide:H2Kb complex.

5.2.4 Atomistic Molecular Dynamics Simulation

Explicit-solvent atomistic MD simulations are carried out in the canonical (NVT) ensemble using the AMBER 18 package to examine the dynamics of the binding process between the peptide:H2Kb complexes. We carry out three independent simulations for each peptide:H2Kb complex. Each simulation starts with a 1000 step solvent minimization with restraint force = 500 kcal/mol. This is followed by a 2500 step unsconstrained energy minimization. The production simulations are performed for 100 ns. We solvated each peptide-receptor complex in a periodically truncated octahedral box containing a 12 Å buffer of TIP3P water ($\sim$ 22,700 water molecules) surrounding the complex in each direction. Particle Mesh Ewald (PME) summation is used to calculate the long-ranged electrostatic interactions with a cut-off radius of 8 Å and a 1×10^{-5} tolerance for the Ewald convergence to calculate the nonbonded interactions. Hierarchical clustering analysis is performed on the last 5 ns of the simulation trajectories to obtain the representative structure of the peptide:H2Kb complex. The

last 5 ns simulation trajectory of each peptide:H2Kb complex is evaluated to calculate the binding free energy by using the implicit-solvent molecular mechanics/generalized Born surface area (MM/GBSA) approach with the variable internal dielectric constant model. More details regarding our computational procedures and post-analysis of the atomistic MD simulations can be found in our previous work [174].

5.2.5 Peptide Synthesis

All peptides were synthesized at a crude purity from Peptide 2.0 Inc (Chantilly, VA). Synthetic peptides were used for peptide binding and T cell activation assays.

5.2.6 H2Kb Peptide Binding Assay

RMA-s cells were seeded into a 96 well plate at $1x10^5$ per well in 100 µL of media (RPMI with 10% FBS) and incubated at 27°C for 18 hrs. Following incubation cells were treated with 100 µM for each of the following peptides: no peptide vehicle control (NP), Ncf2 peptide, MHCP3, or MHCP5. Additionally, blocking peptides MHCP3 and MHCP5 were pre-treated for 1 hr before Ncf2 or in combination with the Ncf2 peptide to evaluate blocking potential. All peptide treatments were incubated at 37°C for 5 hrs and harvested for flow cytometry. All samples were incubated with Fc block for 5 minutes on ice followed by incubation with fluorophore conjugated antibody H2Kb (APC-eFluor780, 1:200, ThermoFisher) for 30 minutes. Cells were then stained with Propidium Iodide (PI, 1:10,000, ThermoFisher). Data for this assay was acquired on a Becton Dickinson LSRII machine in the NCSU flow Cytometry Core and data analyzed using FlowJo software v10.8.

5.2.7 $CD8^+$ T cell Isolation from Spleen

Mouse spleens were strained though 100-µm filters with FACS buffer and pelleted. Pellets were washed with FACS buffer and pelleted again. Pellets were then incubated with ACK lysing buffer on ice for 5 mins. After incubation FACS buffer was added and cells pelleted. Pellets were then washed twice and strained through a cell strainer cap and prepared for T cell activation assays.

5.2.8 $CD8^+$ T Cell Activation Assay

Isolated $CD8^+$ T cells from NASH spleens were plated in 96 well plates at $5x10^4$ per well and stained with a cell trace violet proliferation dye and cocultured with $1x10^4$ of peptide treated RMA-S cells as previously described. Cells were plated in a total of 200 µL of T cell media containing RPMI medium (Corning) supplemented with 10% FBS, L-glutamine (400 mM), penicillin (100 U/ml), streptomycin (100 µg/ml), 2-mercaptoethanol (50 µM), and IL-2 (100 ng). Cells were cultured at 37°C and harvested after 5 days and prepared for flow cytometry. Cells were washed twice with FACS buffer and incubated with Fc block before staining. Cells were stained with the following panel: CD8a (PE-Cy7, 1:200, BD Biosciences), TCRb (APC-Cy7, 1:200, BD Biosciences), CD44 (A700, 1:200, BD Biosciences), CD62L (APC, 1:200, BD Biosciences) and propidium iodide (PI). Flow data was obtained on the Beckman Coulter CytoFLEX machine at the NCSU flow Cytometry Core and was analyzed using FlowJo software v10.8.

5.2.9 Statistical Analysis

All statistical analyses were performed by GraphPad Prism 9.3.1 software. All graphs are displayed as the mean ± SEM. Two-way ANOVA statistical analysis was performed and

considered statistically significant for P<0.05 (*), P<0.01 (**), P<0.001(***), and P<0.0001(****).

5.3 Results

5.3.1 H2Kb is a therapeutic target for NASH

We examined the role of $CD8^+$ T cells in the development of NASH using low density lipoprotein receptor knockout (LDLRKO) on chow (control) or western diet (NASH) for 8 weeks. The LDLRKO mice on WD represent an obese hyperlipidemic model of MASH and display a mild inflammation, fibrosis, and increased hepatic $CD8^+$ T cells [81]. After 8 wks, livers from control and MASH mice were collected to examine changes in the H2Kb immunopeptidome. By using H2Kb immunoaffinity chromatography and liquid chromatography with tandem mass spectrometry (LC-MS/MS), we identified antigens from normal and NASH mouse livers (**Fig. 5.1A**). Candidate antigens were selected by searching the mouse proteome. The antigen datasets for all groups displayed the characteristic 8 to 11 amino acid length distribution for H2Kb restricted antigens. BioVenn filtering analysis revealed 59 unique chow (control), 227 unique NASH, and 219 shared peptides. Of these peptides the Ncf2 (sequence: VHYKYTVV) and Gpnmb (sequence: FVYVFHTL) peptides were only identified in the NASH mouse model. NetMHCPan-4.1 was used to predict H2Kb binding affinities predicting both the Ncf2 and Gpnmb peptides to be strong binders (**Figure 5.1B**).

To confirm H2Kb peptide binding, a peptide binding assay was performed. Flow cytometry analysis confirmed H2Kb binding for both the Ncf2 and Gpnmb peptides. The Gpnmb peptide also demonstrated a stronger affinity for H2Kb compared to positive H2Kb binding control Ovalbumin (Ova) (sequence: SIINFEKL) and Ncf2 peptide (**Fig. 5.1C**). The Ncf2

peptide increased NASH spleen $CD8^+$ T cell activation. In contrast, the Gpnmb peptide had no impact on the activation or proliferation of $CD8^+$ T cell activation (**Fig. 5.1D**).

The Gpnmb peptide was selected as a model peptide to initiate the development of our blocking peptides on the basis that Gpnmb peptide has a high H2Kb binding capability, and it is non-reactive towards NASH $CD8^+$ T cells. The protein glycoprotein non-metastatic melanoma protein B (GPNMB) is an endogenous transmembrane glycoprotein that is upregulated during liver injury and fibrosis in mice [40, 179]. GPNMB undergoes cleavage and releases its extracellular domain into circulation [180]. The extracellular domain can be detected in the serum and is upregulated in NASH mice serving as a potential biomarker for NASH [40]. Interestingly, the identified peptide sequence for Gpnmb is in the extracellular domain region. Therefore, we did not select the Gpnmb peptide as potential blocking peptide because it was identified in NASH livers and may have other functions in NASH development.

5.3.2 Molecular modeling and computational identification of blocking peptides

PepBD or *Pep*tide *B*inding *D*esign is a Monte-Carlo based search algorithm that uses an iterative procedure to identify high affinity peptide binders for a biomolecular target. The input to the algorithm is the structure of the complex formed by an initial peptide sequence (reference peptide) and the target biomolecule. PepBD generates peptide variants by implementing sequence and conformation change moves on the peptide chain. A score function, Γ_{score}, that measures the binding energy of the peptide to the receptor and the conformational stability of the peptide when bound to the receptor is used to accept, or reject newly generated peptide sequences. Details of the algorithm are provided in *Methods*.

The reference peptide and input structure needed to initiate the PepBD search were determined by performing explicit-solvent atomistic molecular dynamics simulations of the Ncf2:H2Kb and Gpnmb:H2Kb peptide-protein complexes and evaluating their $\Delta G_{binding}$. To build the initial input files for performing molecular simulations, we obtained the coordinate file of peptide Ova bound to H2Kb from the Protein Data Bank (PDB ID: 1VAC). The Ova peptide residues from the PDB file: 1VAC were mutated using the Pymol software to obtain the coordinate files of the Ncf2:H2Kb and Gpnmb:H2-Kb complexes. Three independent simulations were carried out for both the Ncf2:H2Kb and Gpnmb:H2Kb complexes for 100 ns to ensure that the system reaches an equilibrated state. The simulations were performed at 298K using the AMBER ff14SB forcefield and the AMBER18 package. We calculated the $\Delta G_{binding}$ of the peptide:receptor complex following the MD simulations using the MMGBSA protocol and variable dielectric constant method (See details *Methods* and Supplementary material). The $\Delta G_{binding}$ of Ncf2:H2Kb and Gpnb:H2Kb were found to be -1.36 kcal/mol and -7.97 kcal/mol respectively. These values confirmed our peptide binding assay results that Gpnmb peptide binds with a stronger affinity than Ncf2 to H2Kb. The representative snapshot from the last 5ns MD simulation of the Gpnmb:H2Kb complex obtained by performing a hierarchical clustering algorithm **(Fig. 5.2A).**

We selected peptide Gpnmb as the reference peptide and the Gpnmb:H2Kb complex **(Fig. 5.2A)** as the input structure for our PepBD algorithm. The goal here was to generate new peptide sequences using PepBD that bind to H2Kb with higher binding affinity than Gpnmb. The individual contributions from the residues on Gpnmb to the interaction energy with H2Kb are plotted **(Fig. 5.2B).** For our designs, we considered five different cases for PepBD that specify different amino acid composition by residue type for the peptide chain. Amino acids are

classified into five types: hydrophobic, hydrophilic, positive charge, negative charge, and glycine. The numbers of each type are fixed during the design process to improve peptide stability and increase the likelihood that the peptide will bind to the target. For example, the number of hydrophobic residues is fixed to enhance the likelihood that the peptide will be soluble, and the number/position of charged amino acids is fixed to complement the charge state of the protein. The five cases are as follows. Case One: $N_{\text{hydrophobic}} = 3$, $N_{\text{hydrophilic}} = 2$, $N_{\text{positive}} = 2$, $N_{\text{negative}} = 1$, $N_{\text{other}} = 0$ and $N_{\text{glycine}} = 0$, Case Two: $N_{\text{hydrophobic}} = 3$, $N_{\text{hydrophilic}} = 2$, $N_{\text{positive}} = 1$, $N_{\text{negative}} = 1$, $N_{\text{other}} = 0$ and $N_{\text{glycine}} = 1$, Case Three: $N_{\text{hydrophobic}} = 3$, $N_{\text{hydrophilic}} = 2$, $N_{\text{negative}} = 2$, $N_{\text{positive}} = 1$, $N_{\text{negative}} = 2$, $N_{\text{other}} = 0$ and $N_{\text{glycine}} = 0$, Case Four: $N_{\text{hydrophobic}} = 4$, $N_{\text{hydrophilic}} = 2$, $N_{\text{negative}} = 3$, $N_{\text{positive}} = 1$, $N_{\text{negative}} = 1$, $N_{\text{other}} = 0$ and $N_{\text{glycine}} = 0$ and Case Five: $N_{\text{hydrophobic}} = 5$, $N_{\text{hydrophilic}} = 3$, $N_{\text{negative}} = 0$, $N_{\text{positive}} = 0$, $N_{\text{negative}} = 0$, $N_{\text{other}} = 0$ and $N_{\text{glycine}} = 0$. (Here, $N_{\text{residue-type}}$ stands for the number of residues specific to that residue type on the peptide chain). For each case we performed the PepBD search with three different initial random seed numbers that randomize the initial peptide sequence. We do this to let PepBD, which is a Monte Carlo search, sample peptides from a large pool of peptide sequences and conformations to avoid getting trapped in local minima. As the *in-silico* search proceeds and new peptide sequences and conformers are generated, the Γ_{score} is recorded at each step. A lower Γ_{score} means stronger binding affinity of the peptide to the bound target. **Figure 5.2C** shows the Γ_{score} vs the number of sequence and conformation change moves performed with random seed-1 for Case 4. **Figure 5.2D** shows the structure of one of the top performing peptides, MHCP3 (sequence: EIFRFHQL) complexed with H2Kb from Case 5. **Figure 5.2E** shows the Γ_{score} vs the number steps performed with random seed-2 for Case 5. The MHCP5: *HVMQFFNM* complexed with H2Kb, obtained from the corresponding search, is shown in **Figure 5.2F**.

Once the *in-silico* evolution of the peptide sequence is complete, we performed explicit-solvent atomistic molecular dynamics (MD) simulations of the lowest scoring peptides complexed with the H2Kb protein to predict their binding affinity, $\Delta G_{binding}$. We performed three 100 ns independent simulations for each peptide:H2Kb complex. Each independent simulation starts with the same initial coordinates of the peptide:H2Kb complex but with randomized velocities drawn from a Gaussian distribution. The $\Delta G_{binding}$ of the peptide:receptor complex following the MD simulations was evaluated by using the MMGBSA protocol and variable dielectric constant method . Details of our atomistic MD simulation and $\Delta G_{binding}$ calculation procedure are provided in *Methods*. **Table 5.1** reports the top peptides that we obtain from our computational procedure and their corresponding Γ_{score} and $\Delta G_{binding}$ values.

5.3.3 Computational analysis of the biorecognition mechanism of MCHP3 and MHCP5 bound to H2Kb

Next, we analyzed the ability of two of the designed peptides MHCP3 and MHCP5 to bind to H2Kb with particular focus on which amino acids are key to the binding. The focus is on peptides MHPC3 and MHCP5 because, as we show in the next sections, these featured moderate-to-high binding affinity for H2Kb and protected against Ncf2 $CD8^+$ T cell activation. The $\Delta G_{binding}$ of MHCP3:H2Kb **(Fig. 5.3A)** and MHCP5:H2Kb (**Fig. 5.3B**) from atomistic molecular dynamics simulation was predicted to be -13.97 kcal/mol and -13.72 kcal/mol respectively. To draw further insights on the binding mechanism of MHPC3 and MHCP5 to H2Kb, we constructed the residue-wise decomposition of the interaction energy between MHCP3:H2Kb (**Fig. 5.3C**) and MHCP5:H2Kb (**Fig. 5.3D**) binding interface. **In Figure 5.3E** and **Figure 5.3F,** we also constructed energy panels detailing the pair-wise interactions of MHCP3:H2Kb and MHCP5:H2Kb complexes, respectively.

The critical MHCP3 residues involved in H2Kb binding are Glu1, Phe3, Gln7 and Leu8 while the critical residues on MHCP5 are His1, Asn7 and Met8. Glu 1 on MHCP3 interacts strongly with Tyr15, Tyr167, Trp175 and Tyr179 on H2Kb. Since, Glu1 (negatively charged) is forming strong interactions with Tyr and Trp, which are both aromatic amino acids, we suspect that these interactions are via anion-π contacts. Phe3 on MHCP3 preferentially interacts with Arg163, Leu164 and Tyr167, possibly via cation-π, Van der Waals contacts and π-π interaction respectively. Gln7 (polar) on MHCP3 interacts with polar Ser81 and Asp85 on H2Kb via hydrogen bonds and with Trp155 via polar-π interaction. Leu8 on MHCP3 forms strong interactions with Asp85, Thr151 and Lys154. His1 on MHCP5 interacts with Tyr15 and Tyr167 via polar-π interactions and with Glu71 via hydrogen bonding. Asn7 on MHCP5 interacts strongly with Ser81 and Asp85 on H2Kb via hydrogen bonding and with Trp155 on H2-Kb via polar- π interaction. Met8 on MHCP5 interacts with Asp85, Thr151 and Lys154. Notably, both MHCP3 and MHCP5 contain two Phe (large aromatic amino acid) residues and may provide conformational stability to the peptide chain.

5.3.4 Experimental Evaluation of the Ability of Blocking Peptides MHCP3 and MHCP5 to bind to H2Kb

We synthesized blocking peptides MHCP1 to MHCP11 and determined their ability to bind to H2Kb by using NetMHC predictions (**Fig. 5.4A**) and H2Kb peptide binding by flow cytometry analysis (**Fig. 5.4B**). MHCP -3, -4, -5 and -6 were all predicted to be strong binders by NetMHC. By pulsing RMA-S cells with the blocking peptides and detecting stabilization of H2Kb on the cell surface via flow analysis, the blocking peptides MHCP3 and MHCP5 bound to H2Kb. The binding of MHCP4 to H2Kb was not as strong as that experienced by MHCP3 and MHCP5. Interestingly, the presence of phenylalanine in the fifth position of the blocking peptide

plays an important role in the binding strength of the blocking peptides as peptides MHCP 1, 2, 6, 7, 8, 9, 10, and 11 did not bind to H2Kb.

5.3.5 Blocking peptides MHCP3 and MHCP5 protect against Ncf2 CD8 T cell activation

To determine the ability of the blocking peptides to prevent Ncf2 induced $CD8^+$ T cell activation, RMA-S cells were treated with blocking peptides MHCP3 or MHCP5 and the Ncf2 peptide. RMA-S cells were either pretreated with MHCP3 or MHCP5 for 1 hour (PreT) and then loaded with Ncf2 peptide or simultaneously treated with MHCP3 or MHCP5 and Ncf2 peptide for 5 hours (CoT). RMA-S cells were then cultured with isolated NASH splenic $CD8^+$ T cells and analyzed for $CD8^+$ T cell activation and proliferation. Both blocking peptides showed no $CD8^+$ T cell reactivity on their own. Additionally, both MHCP3 and MHCP5 were able to prevent Ncf2 induced $CD8^+$ T cell activation regardless of being pre-treated or co-treated with the Ncf2 peptide (**Figure 5.5A-B, 5.6A-B**). Our findings demonstrate that MHCP3 and MHCP5 are competitively effective in preventing Ncf2 peptide-induced activation of $CD8^+$ T cells *in vitro*.

5.4 Discussion

$CD8^+$ T cells play a critical role in the development of nonalcoholic steatohepatitis (NASH). Identifying NASH-specific immunopeptides that regulate $CD8^+$ T cell activation has opened new possibilities for immunotherapies targeting specific antigens bound to MHC class I. Blocking peptides may be a better therapy due to their smaller size and ease of altering the stability and specificity compared to antibody therapy. Developing competitive binding blocking peptides with higher binding affinity to MHC class I molecules H2Kb may prevent $CD8^+$ T cell activation and treatment for NASH. We discovered two synthetic blocking peptides containing 8

amino acids that specifically interact with H2Kb using the PepBD algorithm, which identifies peptides with higher affinity and selectivity to H2Kb. Both blocking peptides have a strong binding affinity H2Kb and competitively inhibit antigen activation of NASH $CD8^+$ T cells.

Computational design strategies are beneficial for developing targeted blocking peptides. This approach allows for developing blocking peptides that bind to the target of interest with higher specificity and efficacy. By using the Gpnmb peptide as a reference due to its stronger binding affinity and the PepBD algorithm coupled with molecular-level simulations, we were able to design peptides with stronger binding affinity to H2Kb compared to the Ncf2 and Gpnmb peptide. Interestingly, NetMHC 4.0 predicted MHCP3 and MHCP5 to be strong binders by NetMHC 4.0. In addition, both blocking peptides demonstrated stable binding to the H2Kb receptor on RMA-S cells *in vitro* compared to the other predicted blocking peptides. The stable binding may be due to critical amino acids in the MHCP3 and MHCP5, as both contain Phe5 compared to the binding affinity. Future studies mutating Phe5 in the blocking peptides may help determine the functional significance of this amino acid to help develop stable and effective blocking peptides.

Several groups have demonstrated that the stability of the peptide to the MHC I and II molecules control immunogenicity versus affinity [181-194]. We discovered that the blocking peptides did not induce an immunogenic response in hepatic isolated T cells. In addition, we analyzed if the blocking peptide sequences were present in the immunopeptidome of normal, steatosis, or NASH mouse livers and could not identify the sequence under these conditions. This further supports the possibility that these blocking peptides may be effective *in vivo* for treating NASH. Future *in vivo* testing will confirm the immunogenic capacity of MHCP3 and MHCP5.

Delivery of peptides can be challenging as certain amino acids lead to poor bioavailability, membrane permeability, and short half-life [195-197]. Modifications to enhance protease stability by incorporating D-amino acid or adding acetyl or propionyl groups to the N- and C- terminal amino acids may improve the delivery and effectiveness of the blocking peptides *in vivo* [195]. Exosomes or nanoparticles are a possible peptide delivery method [197]. We have demonstrated that myeloid cells are a critical antigen-presenting cell in regulating $CD8^+$ T cell activation in NASH [169]. Thus, developing exosomes containing MHCP3 and MHCP5 may effectively target antigen-presenting cells, preventing $CD8^+$ T cell activation. These exosomes may be delivered by systemic administration of macrophage-derived exosomes, encapsulated exosomes in carriers such as nanoparticles, or modification of the membrane of exosomes to enhance their binding to receptors on antigen-presenting cells. With the lack of FDA-approved therapies, the blocking peptides we designed may be an effective treatment for NASH and other metabolic diseases dependent on antigen presentation and $CD8^+$ T cell function.

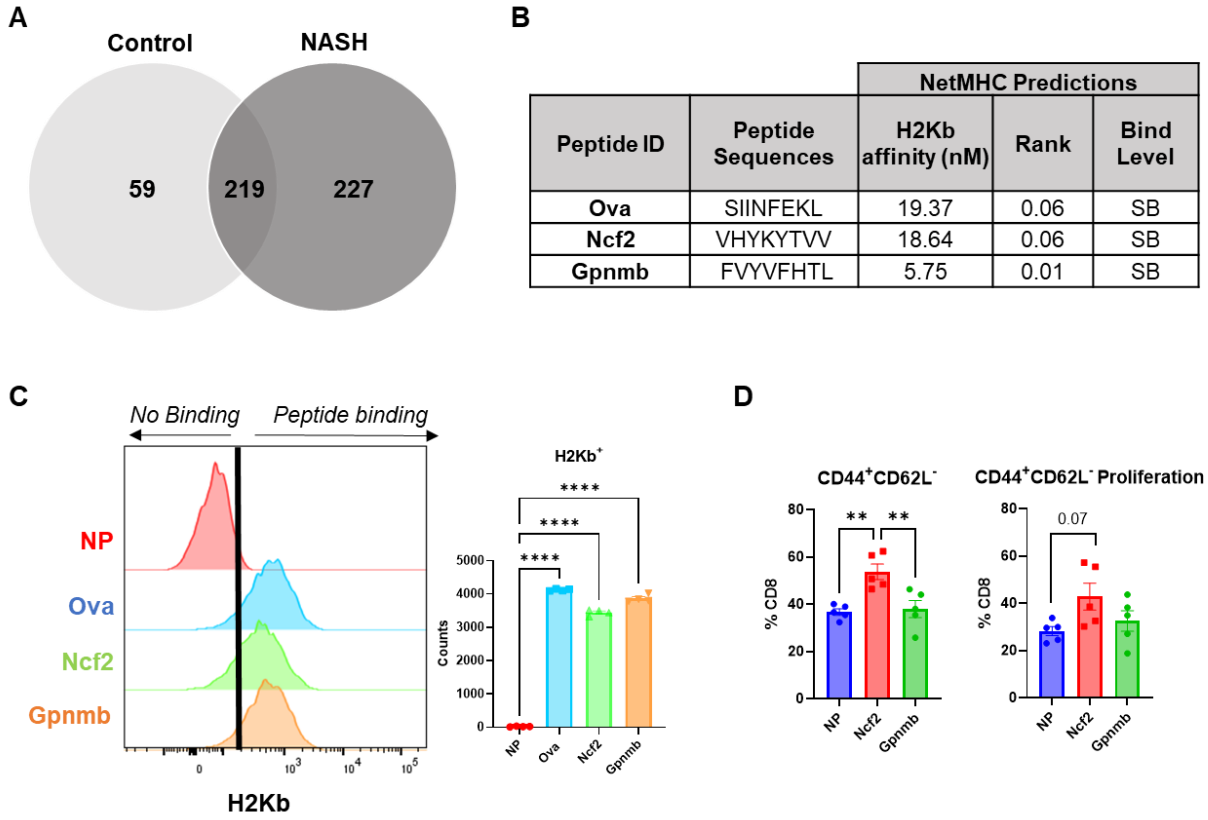

Peptide ID	Peptide Sequences	NetMHC Predictions		
		H2Kb affinity (nM)	Rank	Bind Level
Ova	SIINFEKL	19.37	0.06	SB
Ncf2	VHYKYTVV	18.64	0.06	SB
Gpnmb	FVYVFHTL	5.75	0.01	SB

Figure 5.1. H2Kb restricted peptides in NASH. LDLRKO mice on chow (control) or WD (NASH) for 12 wks (n = 3-4 mice per group, 2 replicate studies). **(A)** BioVenn filtered unique control and NASH peptides. **(B)** NetMHC predicted binding affinities for Ovalbumin (Ova), Ncf2, and Gpnmb peptide to H2Kb. **(C)** Flow cytometry analysis of H2Kb expression to determine binding with NP, Ova, Ncf2, and Gpnmb peptide pulsed RMA-S cells. **(D)** T cell activation assay of hepatic $CD8^+$ T cells co-cultured with NP, Ncf2, or Gpnmb peptide pulsed RMA-S cells. Cells were harvested on day 3 for flow cytometry analysis of $CD8^+$ T cells (*$CD8^+TCR\beta^+$)* and gated for activation (*$CD44^+$ $CD62L^-$*) and proliferation. Data shown as the mean ± SEM. Two-way ANOVA was performed and data was considered statistically significant for $P<0.01$ (**) and $P<0.0001$(****).

Figure 5.2. Molecular modeling and design of H2Kb blocking peptides. (A) Peptide Gpnmb (FVYVFHTL) bound to MHC Class I H2Kb. The α_1, α_2 and α_3 domains are shown in green. The β_2 domain is shown in orange. Peptide Gpnmb at the peptide-binding cleft of MHC Class I H2Kb is enlarged to highlight the molecular interactions between the peptide and H2Kb. **(B)** The residue-wise interaction energy decomposition of Gpnmb when bound to H2Kb. The Γ_{score} vs the number of steps for **(C)** Case 4 (random seed-1) resulting in **(D)** MHCP3:H2Kb complex, and for **(E)** Case 5 (random seed-2) resulting in **(F)** MHCP5:H2Kb complex.

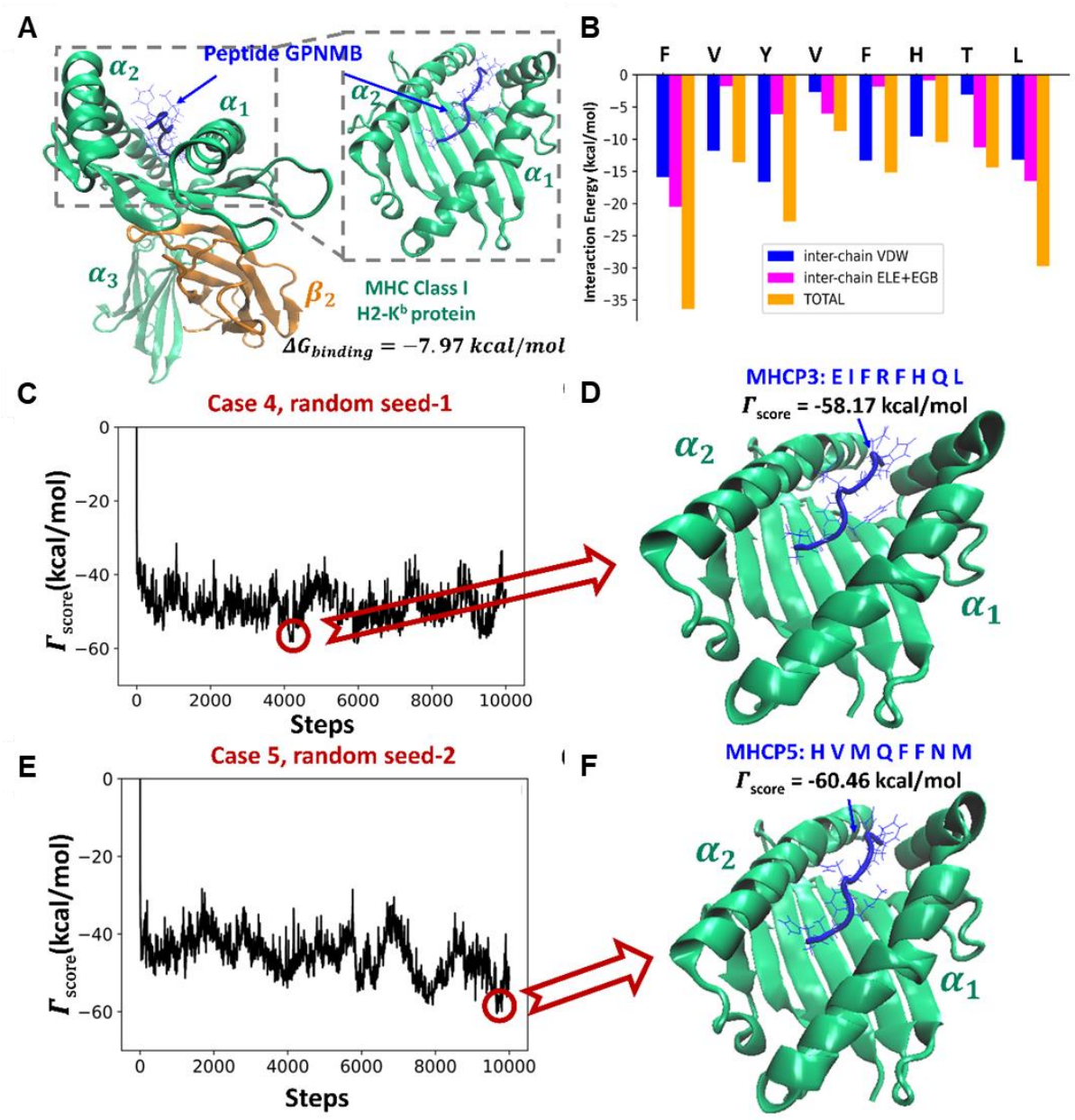
A
Peptide GPNMB
α_2
α_1
α_3
β_2
MHC Class I
H2-K^b protein
$\Delta G_{binding} = -7.97\ kcal/mol$
B
F V Y V F H T L
Interaction Energy (kcal/mol)
0 −5 −10 −15 −20 −25 −30 −35
inter-chain VDW
inter-chain ELE+EGB
TOTAL
C
Case 4, random seed-1
Γ_{score}(kcal/mol)
0 −20 −40 −60
0 2000 4000 6000 8000 10000
Steps
D
MHCP3: E I F R F H Q L
Γ_{score} = -58.17 kcal/mol
α_2
α_1
E
Case 5, random seed-2
Γ_{score}(kcal/mol)
0 −20 −40 −60
0 2000 4000 6000 8000 10000
Steps
F
MHCP5: H V M Q F F N M
Γ_{score} = -60.46 kcal/mol
α_2
α_1

Table 5.1. Top Blocking Peptide Candidates. The initial peptide sequence (Gpnmb) and the list of peptide sequences identified by PepBD screening with their corresponding $\Delta\Gamma_{score}$ and $\Delta G_{binding}$ values.

Peptide	**Case**	**Sequence**	$\boldsymbol{\Gamma_{score}\left(\frac{kcal}{mol}\right)}$	$\boldsymbol{\Delta G_{binding}\left(\frac{kcal}{mol}\right)}$
Gpnmb		FVYVFHTL		-7.97 ± 0.36
MHCP1	1	WIHEFHRR	-58.74	-14.92 ± 0.37
MHCP2	1	EHMYNFRK	-51.78	-14.65 ± 0.39
MHCP3	4	EIFRFHQL	-58.17	-13.97 ± 0.37
MHCP4	4	HIHEFFRL	-58.65	-13.86 ± 0.38
MHCP5	5	HVMQFFNM	-60.46	-13.72 ± 0.32
MHCP6	5	HIFWMHNM	-55.62	-13.65 ± 0.31
MHCP7	3	EIHEMHRM	-54.69	-13.22 ± 0.36
MHCP8	4	EIHYHWRM	-56.76	-12.79 ± 0.41
MHCP9	2	WMHQGERM	-56.83	-12.75 ± 0.34
MHCP10	2	FHHEGYRM	-53.52	-9.35 ± 0.35
MHCP11	3	EIHFQERM	-56.90	-9.01 ± 0.36

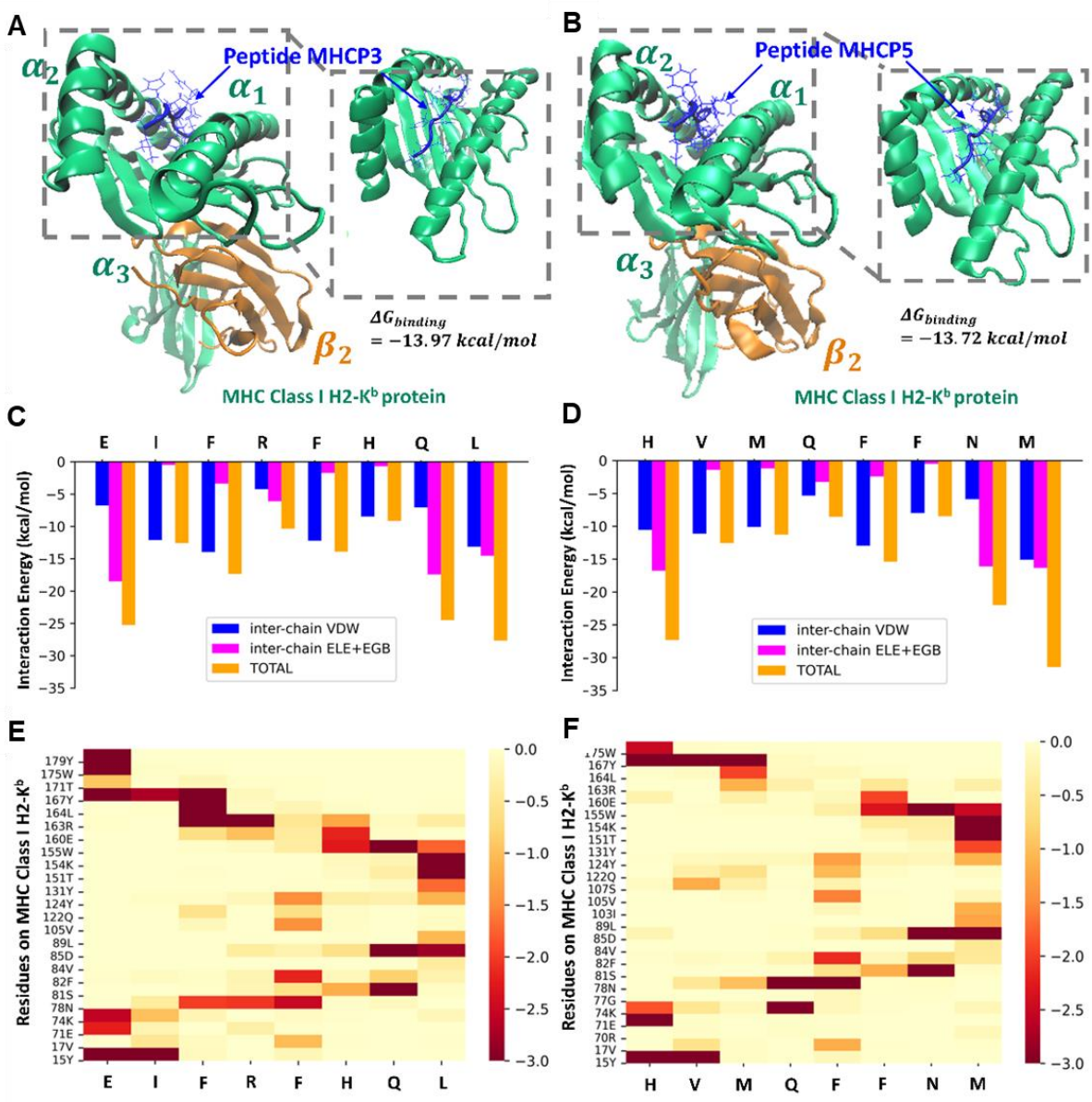

Figure 5.3. Computational analysis of MHCP3 and MHCP5. The structure of **(A)** MHCP3:H2Kb and **(B)** MHCP5:H2Kb obtained from molecular dynamics simulations. The residue-wise interaction energy decomposition of **(C)** MHCP3:H2Kb and (D) MHCP5:H2Kb complexes. Energy panel detailing the pair-wise interactions in **(E)** MHCP3:H2Kb and **(F)** MHCP5:H2Kb complexes.

Figure 5.4. Blocking peptides MHCP3 and MHCP5 bind to H2Kb. (A) NetMHC predicted binding affinities for generated blocking peptides compared to Gpnmb peptide. **(B)** Flow cytometry analysis of H2Kb expression to determine binding with blocking peptides (n=6, in 3 replicate studies). Data shown as the mean ± SEM. Two-way ANOVA was performed and data was considered statistically significant for <0.0001(****).

A

Peptide ID	Peptide Sequences	$\Delta G_{binding}$	NetMHC Predictions		
			H2Kb affinity (nM)	Rank	Bind Level
Gpnmb	FVYVFHTL	-7.97	5.75	0.01	SB
MHCP1	WIHEFHRR	-14.92	16425.07	14.856	NB
MHCP2	EHMYNFRK	-14.65	23411.35	24.818	NB
MHCP3	EIFRFHQL	-13.97	24.62	0.02	SB
MHCP4	HIHEFFRL	-13.86	57.23	0.05	SB
MHCP5	HVMQFFNM	-13.72	28.43	0.091	SB
MHCP6	HIFWMHNM	-13.65	148.46	0.3	SB
MHCP7	EIHEMHRM	-13.22	11705.55	3.485	NB
MHCP8	EIHYHWRM	-12.79	7215.29	3.745	NB
MHCP9	WMHQGERM	-12.75	12798.61	11.835	NB
MHCP10	FHHEGYRM	-9.35	7758.53	3.831	NB
MHCP11	EIHFQERM	-9.01	13696.71	4.507	NB

B

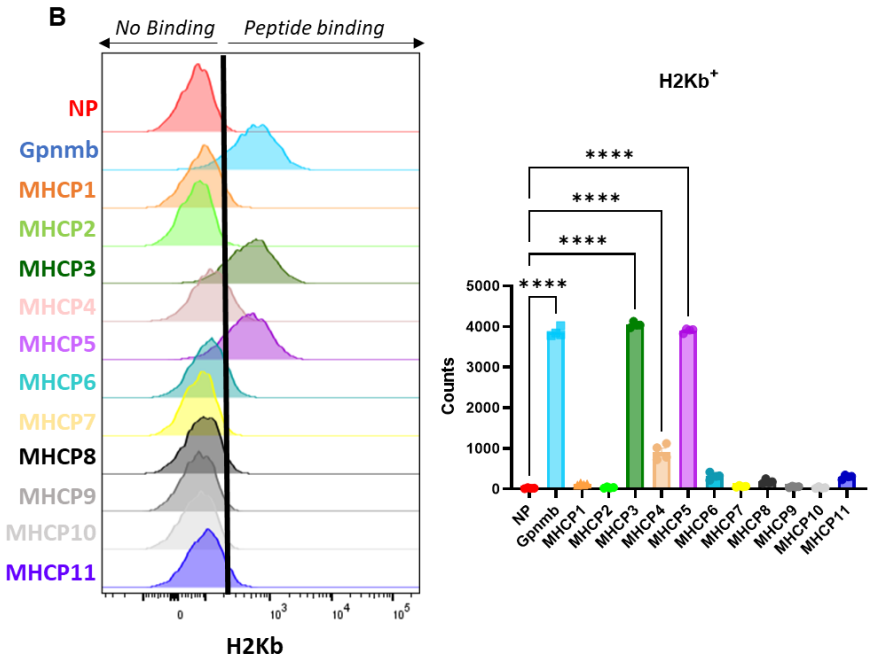

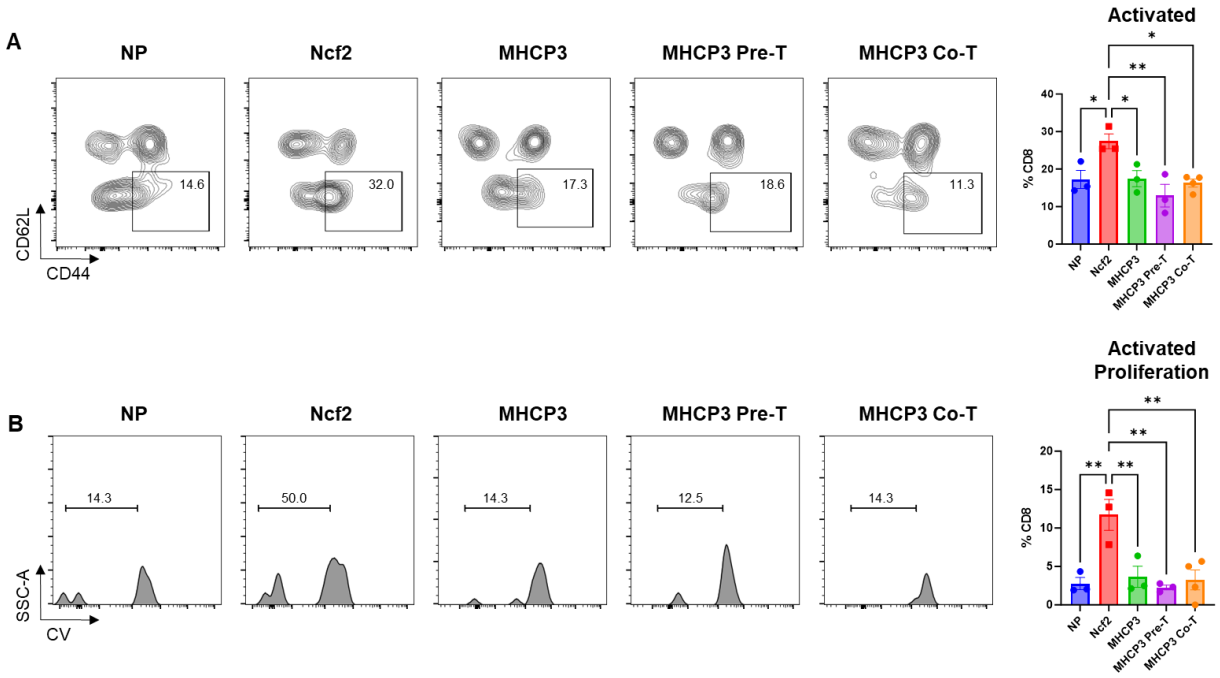

Figure 5.5. **MHCP3 blocks Ncf2 peptide CD8$^+$ T cell activation *in vitro*.** Taconic mice on amylin diet (NASH) for 28 wks (3 replicate studies). CD8 T cells were isolated from spleens of Taconic NASH mice and co-cultured with RMA-S pulsed with vehicle/no peptide (NP), Ncf2, MHCP3, MHCP3 1 hr pre-treatment then pulsed with Ncf2 (MHCP3 Pre-T), and MHCP3 pulsed with Ncf2 (MHCP3 Co-T). Representative flow plots for T cell activation assay with MHCP3 blocking peptide **(A)** CD8$^+$ T cell activation (*CD44*$^+$, *CD62L*$^-$) and **(B)** proliferation. Data shown as the mean ± SEM. Two-way ANOVA was performed and data was considered statistically significant for P<0.05 (*) and P<0.01 (**).

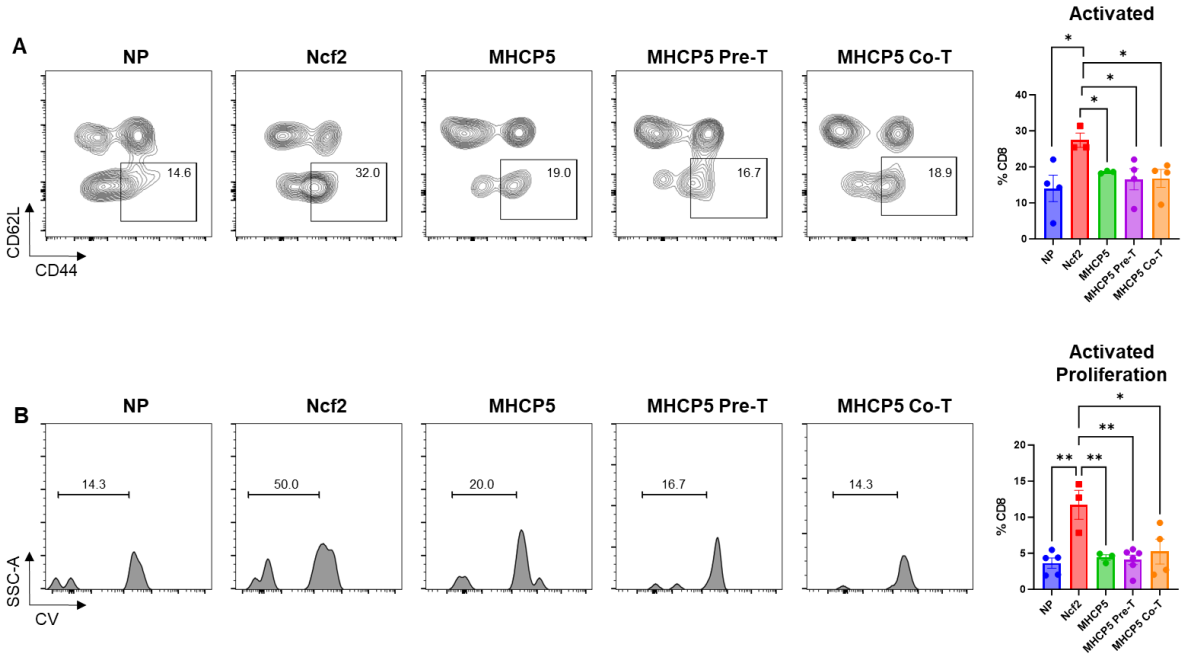

Figure 5.6. MHCP5 blocks Ncf2 peptide CD8$^+$ T cell activation *in vitro*. Taconic mice on amylin diet (NASH) for 28 wks (3 replicate studies). CD8 T cells were isolated from spleens of Taconic NASH mice and co-cultured with RMA-S pulsed with vehicle/no peptide (NP), Ncf2, MHCP5, MHCP5 1 hr pre-treatment then pulsed with Ncf2 (MHCP5 Pre-T), and MHCP5 pulsed with Ncf2 (MHCP5 Co-T). Representative flow plots for T cell activation assay with MHCP5 blocking peptide **(A)** CD8$^+$ T cell activation (*CD44*$^+$, *CD62L*$^-$) and **(B)** proliferation. Data shown as the mean ± SEM. Two-way ANOVA was performed and data was considered statistically significant for P<0.05 (*) and P<0.01 (**).

CHAPTER 6: Conclusions and Future Directions

6.1 Summary

The importance of myeloid specific H2Kb expression for $CD8^+$ T cell activation in NASH was highlighted in these studies. Here we showed that myeloid cells have increased H2Kb expression under NASH conditions. Knocking out H2Kb and H2Db provided protective effects against inflammation and fibrosis in a diet-induced NASH mouse model. Targeting myeloid cell H2Kb expression protected only against fibrosis and not inflammation suggesting additional cells types may be involved in regulating inflammation under NASH conditions. Seeing how myeloid cell H2Kb knockout provided protection against fibrosis in NASH, we proposed that H2Kb expression is driving changes in NASH through antigen presentation to activate $CD8^+$ T cells. MHC I KO and myeloid cell Kb KO prevented $CD8^+$ T cell activation in NASH emphasizing that $CD8^+$ T cell activation may be antigen dependent and $CD8^+$ T cells are the primary driver of fibrosis. Using immunoaffinity chromatography, we identified 59 unique NASH peptides across 3 different mouse models of diet induced NASH. Of these peptides, the peptide Ncf2 was identified and confirmed to be a strong H2Kb binding peptide. *In vitro* studies showed that this peptide could activate both hepatic and splenic $CD8^+$ T cells with increased T cell activation, proliferation, and cytokine secretion. Additionally, we were able to identify Ncf2 peptide reactive $CD8^+$ T cells *in vivo* through the use of an Ncf2-H2Kb tetramer. More specifically, T cell effector (TEM) and resident memory (TRM) cells showed increased Ncf2 tetramer staining in NASH livers suggesting the role of T cell memory cells in NASH. Further studies showed through using a model of NASH resolution that Ncf2 peptide generation was dependent on dietary signals. The Ncf2 peptide was only found in NASH mice and when the diet is removed NASH resolution occurs reducing body weight, inflammation, and fibrosis. Here we

did not find the Ncf2 peptide suggesting its formation is dependent on dietary signals. Thus, we hypothesize that the CD8+ T cell activation mechanism in NASH is driven by myeloid cell H2Kb antigen presentation of the Ncf2 peptide **(Fig. 6.1)**. Future studies targeting the Ncf2 protein or peptide may serve as a promising therapeutic target for regulating fibrosis in NASH.

6.2 Future Directions

6.2.1 Role of antigen presentation and other APCs

In the present studies we identified increased H2Kb expression on myeloid cells but it remains to be determined if this increased expression increases antigen presentation capability directly. Further studies are required to evaluate antigen presentation on these cells and confirm the extent to which they activate $CD8^+$ T cells in NASH. Additionally, with MHC I being expressed on any nucleated cell, this highlights a wide variety of cell types that could be presenting antigens to $CD8^+$ T cells in NASH. In the NASH liver microenvironment, you have other immune and local cells capable of MHC I antigen presentation such as dendritic cells, B cells, hepatocytes, and hepatic stellate cells (HSCs) [39, 48, 179]. The role of antigen presentation in other cells types can be evaluated through the use of the KbLoxP mouse model system and adoptive transfer studies.

6.2.2 Source of the Ncf2 Peptide

Our studies identified unique NASH peptide Ncf2 capable of $CD8^+$ T cell activation. However, these studies did not identify the source of the peptide or what cells, tissues, or signals are required for the generation of this peptide. With the Ncf2 peptide being an H2Kb restricted peptide, it is possible that multiple types of cells could be presenting it. The Ncf2 protein is largely expressed by hepatocytes, hepatic stellate cells, and kupffer cells [166, 198]. This highlights some targets of interest due to their expression of NOX2. Some preliminary work has

been done to evaluate both hepatocyte and immune cell gene expression of Ncf2 in the liver during NASH. This data shows that both the immune cell and hepatocyte fractions have increased Ncf2 expression in NASH **(Fig. 6.2)**. Additional studies are required to further identify if the peptide is being produced in hepatocytes and what specific immune cells are expressing Ncf2 at higher levels in the liver. Confirmation of peptide generation can be confirmed through peptide isolation of target cells and evaluation of protein ubiquitination.

We have isolated peptides from the livers of chow and NASH mice and identified unique NASH peptide Ncf2. However, peptides from other tissues during NASH have not been evaluated for overlapping unique NASH peptides identified in the liver or the Ncf2 peptide. It is unknown if the Ncf2 peptide is unique to the liver or generated in other metabolic tissues such as the intestine or adipose tissue. Gut microbes and oxidative stress related antigens may be generated in the intestine and travel to the liver driving $CD8^+$ T cells. The microbiome is an active player in human physiology made up of a complex ecosystem largely consisting of bacteria inhabiting the intestines known as the gut microbiome [199]. The gut microbiome is more than 90% populated by two phyla of bacteria which include Firmicutes and Bacteroidetes [199]. With advances in molecular biology techniques, characterization and detailed composition of the gut microbiome is possible. This is important as the microbiome can be altered due to lifestyle, medications, or diet and understanding changes in the microbiome can identify key factors in disease progression.

Alterations in the microbiome can have negative impacts on the host and has been highlighted as a contributor to NAFLD progression. This is supported through various animal studies showing different microbial strains inoculated in adult germ-free mice directly impact energy and adiposity regardless of reduced food intake [200]. Additionally, germ free mice were

shown to be protected from western diet induced obesity [201]. Many studies in humans have begun characterizing the microbiome in NAFLD and have found correlations between increased Gram-negative microbes, proteobacteria, and decreased Firmicutes with advanced fibrosis [202]. Additionally, studies that have combined microbial species information with clinical parameters and have been able to predict level of fibrosis indicating microbial markers could serve as potential biomarkers [202]. Although much work has been done to characterize the microbiome in NAFLD, it is yet to be determined how microbes impact the MHC I immunopeptidome and antigen presentation in NASH. Additionally, Ncf2 peptide generation from specific dietary factors such as fructose or cholesterol have not been evaluated. Further work is required to identify the Ncf2 antigen presenting cell and the possible signals that initiate peptide formation.

6.2.3 Targeting the Ncf2 protein

Since identifying the Ncf2 peptide, we have also found that Ncf2 gene and protein levels are increased in the liver. To better understand the role of the Ncf2 protein in NASH, future studies are going to be focused on Ncf2 protein regulation and degradation. Additionally, we have proposed to develop an Ncf2 knockout mouse model with hopes of seeing improvements in diet induced NASH.

6.2.4 $CD8^+$ T cell characterization

We have shown that $CD8^+$ T cells are significantly increased in the liver during NASH and can be regulated by H2Kb expression. Much of our work has been focused on antigen presentation, however additional work is required to characterize $CD8^+$ T cells in NASH. Single cell RNA-sequencing can be used to evaluate key gene expression changes in $CD8^+$ T cells and provide invaluable information on metabolic changes, changes in distinct subsets, activation

states, and T cell receptor clonality. Additional studies are in progress to evaluate the effectiveness of an Ncf2 peptide vaccine and if mice are able to generate Ncf2 reactive $CD8^+$ T cells *in vivo*. Outside out the Ncf2 peptide, we have other candidate NASH peptides that have not been evaluated for $CD8^+$ T cell reactivity. Additionally, previous studies have identified resolution specific peptides that could be involved in promoting the activation of beneficial TRMs for fibrosis resolution and hepatic stellate cell apoptosis.

6.2.5 Human Relevance

Our data has highlighted Ncf2 as a potential therapeutic target for NASH. In humans with NASH $CD8^+$ T cells are also upregulated and are key players in regulating fibrosis. Mechanisms for $CD8^+$ T cell activation in humans is also unknown. More work is necessary to evaluate MHC I antigen presentation in humans. To address the relevance of this mechanism to humans, current progress is being made to isolate MHC I peptides and determine if the Nf2 peptide is also present in humans during NASH. Preliminary data suggests that Ncf2 could also be playing a role in NASH in humans. Hepatic gene expression of normal, steatotic, and NASH livers from humans demonstrated significant increases in Ncf2 expression in NASH patients compared to controls **(Fig. 6.3)**. However, further work is required to complete the identification of human MHC I peptides and evaluate them for $CD8^+$ T cell reactivity.

6.3 Conclusions

Overall, this body of work highlights the importance of MHC I expression in NASH. Our data supports the mechanism of antigen presentation for $CD8^+$ T cell activation and a unique MHC I immunopeptidome. These unique peptides have the potential to be used for biomarkers and help identify specific $CD8^+$ T cell subsets driving NASH progression.

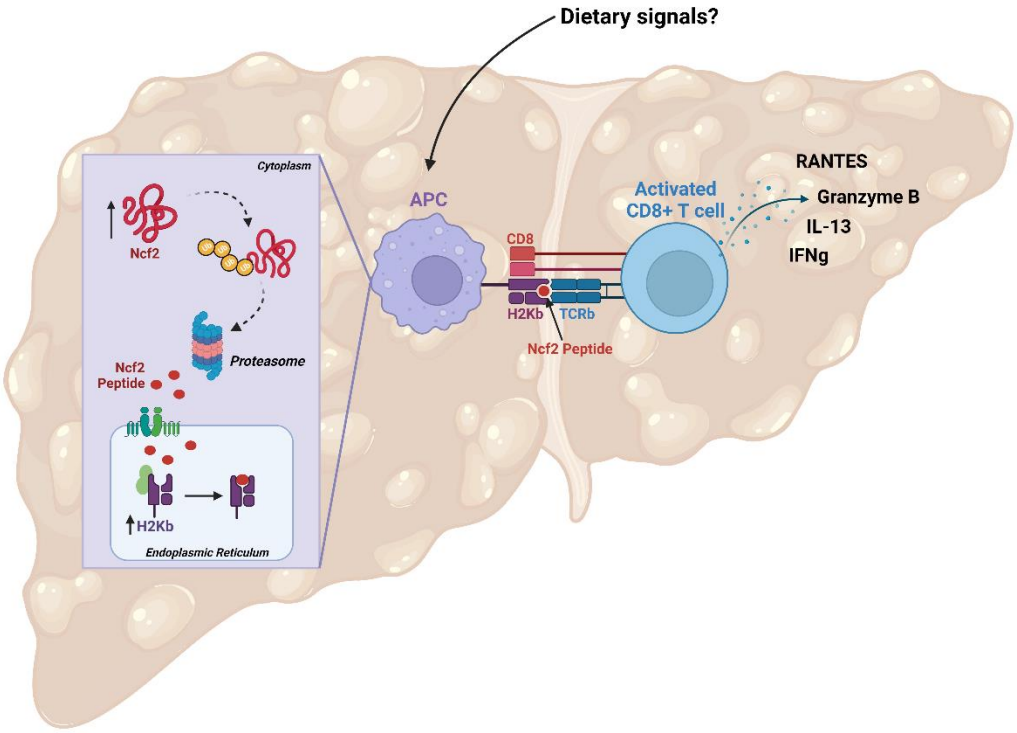

Figure 6.1. Proposed mechanism. We propose that NASH conditions lead to myeloid cell upregulation of H2Kb. Dietary signals increase Ncf2 expression leading to the development of the Ncf2 peptide. The Ncf2 peptide is then presented on myeloid cells to $CD8^+$ T cells leading to activation promoting NASH-induced fibrosis.

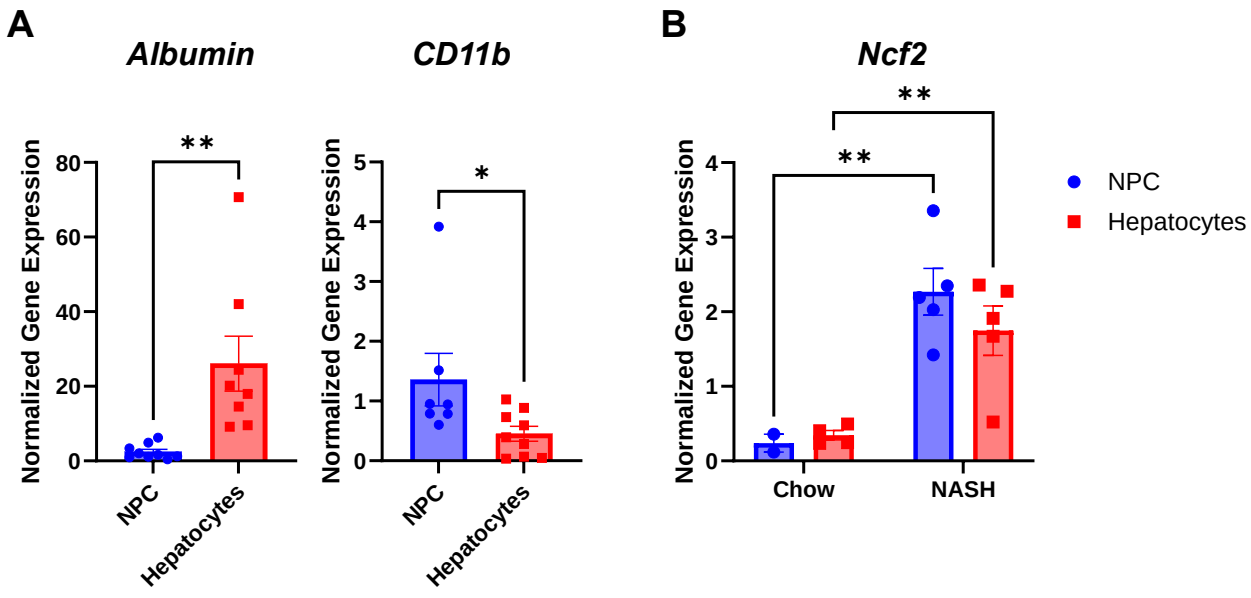

Figure 6.2. Ncf2 is increased in hepatocytes and immune cells during NASH. LDLRKO mice on chow or WD for 16 wks (n=3-5 mice per group). **(A)** Total liver gene expression of hepatocyte marker *Albumin* and NPC marker *CD11b* to confirm separation. **(B)** Ncf2 gene expression of NPCs and hepatocytes from chow or NASH mice. Data shown as the mean ± SEM. Two-tailed unpaired Student's t-tests was performed for data sets with 2 groups and Two-way ANOVA was performed with data sets with more than 2 groups and considered statistically significant for $P<0.05$ (*) and $P<0.01$ (**)

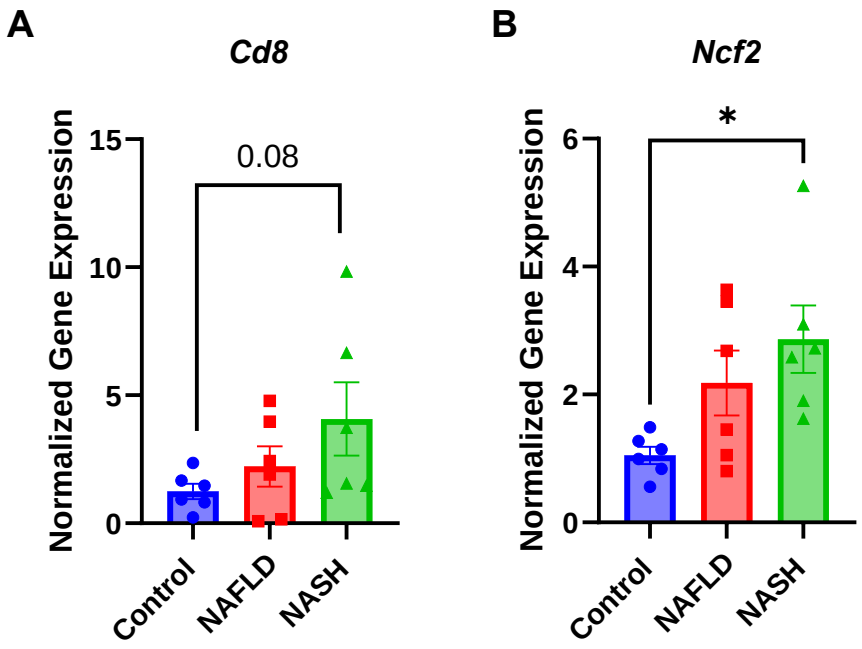

Figure 6.3. Ncf2 is increased during NASH in humans. Human liver gene expression for patients characterized as normal (Control), NAFLD (Steatosis no fibrosis), and NASH (with fibrosis). Data shown as the mean ± SEM. Two-way ANOVA was performed and considered statistically significant for $P<0.05$ (*).

REFERENCES

1. Machado, A.P., *Metabolic syndrome, atherosclerosis and thrombogenic risk.* Rev Port Cardiol, 2006. **25**(2): p. 173-8.
2. Rinella, M.E., *Nonalcoholic fatty liver disease: a systematic review.* JAMA, 2015. **313**(22): p. 2263-73.
3. Lindenmeyer, C.C. and A.J. McCullough, *The Natural History of Nonalcoholic Fatty Liver Disease-An Evolving View.* Clin Liver Dis, 2018. **22**(1): p. 11-21.
4. Horn, C.L., et al., *Role of Cholesterol-Associated Steatohepatitis in the Development of NASH.* Hepatol Commun, 2022. **6**(1): p. 12-35.
5. Huang, Y., et al., *Nonalcoholic fatty liver disease is associated with atherosclerosis in middle-aged and elderly Chinese.* Arterioscler Thromb Vasc Biol, 2012. **32**(9): p. 2321-6.
6. Brecelj, J. and R. Orel, *Non-Alcoholic Fatty Liver Disease in Children.* Medicina (Kaunas), 2021. **57**(7).
7. Shaunak, M., et al., *Non-alcoholic fatty liver disease and childhood obesity.* Arch Dis Child, 2021. **106**(1): p. 3-8.
8. Bonora, E. and G. Targher, *Increased risk of cardiovascular disease and chronic kidney disease in NAFLD.* Nat Rev Gastroenterol Hepatol, 2012. **9**(7): p. 372-81.
9. Alkhouri, N., et al., *The inflamed liver and atherosclerosis: a link between histologic severity of nonalcoholic fatty liver disease and increased cardiovascular risk.* Dig Dis Sci, 2010. **55**(9): p. 2644-50.
10. Eslam, M., et al., *A new definition for metabolic dysfunction-associated fatty liver disease: An international expert consensus statement.* J Hepatol, 2020. **73**(1): p. 202-209.

11. Fouad, Y., et al., *What's in a name? Renaming 'NAFLD' to 'MAFLD'.* Liver Int, 2020. **40**(6): p. 1254-1261.

12. Younes, R. and E. Bugianesi, *Should we undertake surveillance for HCC in patients with NAFLD?* J Hepatol, 2018. **68**(2): p. 326-334.

13. Estes, C., et al., *Modeling NAFLD disease burden in China, France, Germany, Italy, Japan, Spain, United Kingdom, and United States for the period 2016-2030.* J Hepatol, 2018. **69**(4): p. 896-904.

14. Clark, R. and T. Kupper, *Old meets new: the interaction between innate and adaptive immunity.* J Invest Dermatol, 2005. **125**(4): p. 629-37.

15. Turvey, S.E. and D.H. Broide, *Innate immunity.* J Allergy Clin Immunol, 2010. **125**(2 Suppl 2): p. S24-32.

16. Bonilla, F.A. and H.C. Oettgen, *Adaptive immunity.* J Allergy Clin Immunol, 2010. **125**(2 Suppl 2): p. S33-40.

17. Théry, C. and S. Amigorena, *The cell biology of antigen presentation in dendritic cells.* Curr Opin Immunol, 2001. **13**(1): p. 45-51.

18. Kumar, B.V., T.J. Connors, and D.L. Farber, *Human T Cell Development, Localization, and Function throughout Life.* Immunity, 2018. **48**(2): p. 202-213.

19. Mauri, C. and A. Bosma, *Immune regulatory function of B cells.* Annu Rev Immunol, 2012. **30**: p. 221-41.

20. Wang, Y., et al., *B Cell Development and Maturation.* Adv Exp Med Biol, 2020. **1254**: p. 1-22.

21. Machado, M. and H. Cortez-Pinto, *Non-alcoholic steatohepatitis and metabolic syndrome.* Curr Opin Clin Nutr Metab Care, 2006. **9**(5): p. 637-42.

22. Giles, D.A., et al., *Regulation of Inflammation by IL-17A and IL-17F Modulates Non-Alcoholic Fatty Liver Disease Pathogenesis.* PLoS One, 2016. **11**(2): p. e0149783.

23. Liu, Y., et al., *3, 3'-Diindolylmethane alleviates steatosis and the progression of NASH partly through shifting the imbalance of Treg/Th17 cells to Treg dominance.* Int Immunopharmacol, 2014. **23**(2): p. 489-98.

24. Ma, X., et al., *A high-fat diet and regulatory T cells influence susceptibility to endotoxin-induced liver injury.* Hepatology, 2007. **46**(5): p. 1519-29.

25. Rolla, S., et al., *The balance between IL-17 and IL-22 produced by liver-infiltrating T-helper cells critically controls NASH development in mice.* Clin Sci (Lond), 2016. **130**(3): p. 193-203.

26. Tang, Y., et al., *Interleukin-17 exacerbates hepatic steatosis and inflammation in non-alcoholic fatty liver disease.* Clin Exp Immunol, 2011. **166**(2): p. 281-90.

27. Mantovani, A., et al., *Neutrophils in the activation and regulation of innate and adaptive immunity.* Nat Rev Immunol, 2011. **11**(8): p. 519-31.

28. Borregaard, N., *Neutrophils, from marrow to microbes.* Immunity, 2010. **33**(5): p. 657-70.

29. Nathan, C., *Neutrophils and immunity: challenges and opportunities.* Nat Rev Immunol, 2006. **6**(3): p. 173-82.

30. Daley, J.M., et al., *Use of Ly6G-specific monoclonal antibody to deplete neutrophils in mice.* J Leukoc Biol, 2008. **83**(1): p. 64-70.

31. Boivin, G., et al., *Durable and controlled depletion of neutrophils in mice.* Nat Commun, 2020. **11**(1): p. 2762.

32. Ou, R., et al., *Neutrophil depletion improves diet-induced non-alcoholic fatty liver disease in mice.* Endocrine, 2017. **57**(1): p. 72-82.

33. Zang, S., et al., *Neutrophils Play a Crucial Role in the Early Stage of Nonalcoholic Steatohepatitis via Neutrophil Elastase in Mice.* Cell Biochem Biophys, 2015. **73**(2): p. 479-487.

34. Lavin, Y., et al., *Tissue-resident macrophage enhancer landscapes are shaped by the local microenvironment.* Cell, 2014. **159**(6): p. 1312-26.

35. Heymann, F., et al., *Liver inflammation abrogates immunological tolerance induced by Kupffer cells.* Hepatology, 2015. **62**(1): p. 279-91.

36. Krenkel, O. and F. Tacke, *Liver macrophages in tissue homeostasis and disease.* Nat Rev Immunol, 2017. **17**(5): p. 306-321.

37. Scott, C.L., et al., *Bone marrow-derived monocytes give rise to self-renewing and fully differentiated Kupffer cells.* Nat Commun, 2016. **7**: p. 10321.

38. Shapouri-Moghaddam, A., et al., *Macrophage plasticity, polarization, and function in health and disease.* J Cell Physiol, 2018. **233**(9): p. 6425-6440.

39. Remmerie, A., et al., *Osteopontin Expression Identifies a Subset of Recruited Macrophages Distinct from Kupffer Cells in the Fatty Liver.* Immunity, 2020. **53**(3): p. 641-657.e14.

40. Xiong, X., et al., *Landscape of Intercellular Crosstalk in Healthy and NASH Liver Revealed by Single-Cell Secretome Gene Analysis.* Mol Cell, 2019. **75**(3): p. 644-660.e5.

41. Ramachandran, P., et al., *Resolving the fibrotic niche of human liver cirrhosis at single-cell level.* Nature, 2019. **575**(7783): p. 512-518.

42. Daemen, S., et al., *Dynamic Shifts in the Composition of Resident and Recruited Macrophages Influence Tissue Remodeling in NASH.* Cell Rep, 2021. **34**(2): p. 108626.

43. Tran, S., et al., *Impaired Kupffer Cell Self-Renewal Alters the Liver Response to Lipid Overload during Non-alcoholic Steatohepatitis.* Immunity, 2020. **53**(3): p. 627-640.e5.

44. David, B.A., et al., *Combination of Mass Cytometry and Imaging Analysis Reveals Origin, Location, and Functional Repopulation of Liver Myeloid Cells in Mice.* Gastroenterology, 2016. **151**(6): p. 1176-1191.

45. Revelo, X.S., et al., *Nucleic Acid-Targeting Pathways Promote Inflammation in Obesity-Related Insulin Resistance.* Cell Rep, 2016. **16**(3): p. 717-30.

46. Henning, J.R., et al., *Dendritic cells limit fibroinflammatory injury in nonalcoholic steatohepatitis in mice.* Hepatology, 2013. **58**(2): p. 589-602.

47. Heier, E.C., et al., *Murine CD103+ dendritic cells protect against steatosis progression towards steatohepatitis.* J Hepatol, 2017. **66**(6): p. 1241-1250.

48. Deczkowska, A., et al., *XCR1+ type 1 conventional dendritic cells drive liver pathology in non-alcoholic steatohepatitis.* Nat Med, 2021. **27**(6): p. 1043-1054.

49. Hofmann, K., A.K. Clauder, and R.A. Manz, *Targeting B Cells and Plasma Cells in Autoimmune Diseases.* Front Immunol, 2018. **9**: p. 835.

50. Gadd, V.L., et al., *The portal inflammatory infiltrate and ductular reaction in human nonalcoholic fatty liver disease.* Hepatology, 2014. **59**(4): p. 1393-405.

51. Faggioli, F., et al., *B lymphocytes limit senescence-driven fibrosis resolution and favor hepatocarcinogenesis in mouse liver injury.* Hepatology, 2018. **67**(5): p. 1970-1985.

52. Bruzzì, S., et al., *B2-Lymphocyte responses to oxidative stress-derived antigens contribute to the evolution of nonalcoholic fatty liver disease (NAFLD).* Free Radic Biol Med, 2018. **124**: p. 249-259.

53. Martin, M.D. and V.P. Badovinac, *Defining Memory CD8 T Cell.* Front Immunol, 2018. **9**: p. 2692.

54. Dijkgraaf, F.E., L. Kok, and T.N.M. Schumacher, *Formation of Tissue-Resident CD8.* Cold Spring Harb Perspect Biol, 2021. **13**(8).

55. Berg, R.E. and J. Forman, *The role of CD8 T cells in innate immunity and in antigen non-specific protection.* Curr Opin Immunol, 2006. **18**(3): p. 338-43.

56. Dudek, M., et al., *Auto-aggressive CXCR6+ CD8 T cells cause liver immune pathology in NASH.* Nature, 2021. **593**(7860): p. E14.

57. Freeman, B.E., et al., *Regulation of innate CD8+ T-cell activation mediated by cytokines.* Proc Natl Acad Sci U S A, 2012. **109**(25): p. 9971-6.

58. Raué, H.P., et al., *Activation of virus-specific CD8+ T cells by lipopolysaccharide-induced IL-12 and IL-18.* J Immunol, 2004. **173**(11): p. 6873-81.

59. Micallef, M.J., et al., *Interferon-gamma-inducing factor enhances T helper 1 cytokine production by stimulated human T cells: synergism with interleukin-12 for interferon-gamma production.* Eur J Immunol, 1996. **26**(7): p. 1647-51.

60. Ahn, H.J., et al., *A mechanism underlying synergy between IL-12 and IFN-gamma-inducing factor in enhanced production of IFN-gamma.* J Immunol, 1997. **159**(5): p. 2125-31.

61. Guo, Y., et al., *Metabolic reprogramming of terminally exhausted CD8.* Nat Immunol, 2021. **22**(6): p. 746-756.

62. Raud, B., et al., *Fatty acid metabolism in CD8.* Immunol Rev, 2018. **283**(1): p. 213-231.

63. Feng, Q., et al., *Lactate increases stemness of CD8 + T cells to augment anti-tumor immunity.* Nat Commun, 2022. **13**(1): p. 4981.

64. Sebastiani, G., K. Gkouvatsos, and K. Pantopoulos, *Chronic hepatitis C and liver fibrosis.* World J Gastroenterol, 2014. **20**(32): p. 11033-53.

65. Stuart, J.D., E. Salinas, and A. Grakoui, *Immune system control of hepatitis C virus infection.* Curr Opin Virol, 2021. **46**: p. 36-44.

66. Chen, D.Y., et al., *Hepatitis C virus-specific CD4+ T cell phenotype and function in different infection outcomes.* J Clin Invest, 2020. **130**(2): p. 768-773.

67. Aregay, A., et al., *Elimination of hepatitis C virus has limited impact on the functional and mitochondrial impairment of HCV-specific CD8+ T cell responses.* J Hepatol, 2019. **71**(5): p. 889-899.

68. Abdel-Hakeem, M.S., et al., *Selective expansion of high functional avidity memory CD8 T cell clonotypes during hepatitis C virus reinfection and clearance.* PLoS Pathog, 2017. **13**(2): p. e1006191.

69. Utzschneider, D.T., et al., *T Cell Factor 1-Expressing Memory-like CD8(+) T Cells Sustain the Immune Response to Chronic Viral Infections.* Immunity, 2016. **45**(2): p. 415-27.

70. Wieland, D., et al., *TCF1.* Nat Commun, 2017. **8**: p. 15050.

71. Thommen, D.S. and T.N. Schumacher, *T Cell Dysfunction in Cancer.* Cancer Cell, 2018. **33**(4): p. 547-562.

72. Wherry, E.J. and M. Kurachi, *Molecular and cellular insights into T cell exhaustion.* Nat Rev Immunol, 2015. **15**(8): p. 486-99.

73. Hashimoto, M., et al., *CD8 T Cell Exhaustion in Chronic Infection and Cancer: Opportunities for Interventions.* Annu Rev Med, 2018. **69**: p. 301-318.

74. El-Khoueiry, A.B., et al., *Nivolumab in patients with advanced hepatocellular carcinoma (CheckMate 040): an open-label, non-comparative, phase 1/2 dose escalation and expansion trial.* Lancet, 2017. **389**(10088): p. 2492-2502.

75. Zhu, A.X., et al., *Pembrolizumab in patients with advanced hepatocellular carcinoma previously treated with sorafenib (KEYNOTE-224): a non-randomised, open-label phase 2 trial.* Lancet Oncol, 2018. **19**(7): p. 940-952.

76. Bhattacharjee, J., et al., *Hepatic Natural Killer T-cell and CD8+ T-cell Signatures in Mice with Nonalcoholic Steatohepatitis.* Hepatol Commun, 2017. **1**(4): p. 299-310.

77. Wolf, M.J., et al., *Metabolic activation of intrahepatic CD8+ T cells and NKT cells causes nonalcoholic steatohepatitis and liver cancer via cross-talk with hepatocytes.* Cancer Cell, 2014. **26**(4): p. 549-64.

78. Safadi, R., et al., *Immune stimulation of hepatic fibrogenesis by CD8 cells and attenuation by transgenic interleukin-10 from hepatocytes.* Gastroenterology, 2004. **127**(3): p. 870-82.

79. Casini, A., et al., *Immune mechanisms for hepatic fibrogenesis. T-lymphocyte-mediated stimulation of fibroblast collagen production in chronic active hepatitis.* Liver, 1985. **5**(3): p. 134-41.

80. Hirsova, P., et al., *Emerging Roles of T Cells in the Pathogenesis of Nonalcoholic Steatohepatitis and Hepatocellular Carcinoma.* Front Endocrinol (Lausanne), 2021. **12**: p. 760860.

81. Breuer, D.A., et al., *CD8(+) T cells regulate liver injury in obesity-related nonalcoholic fatty liver disease.* Am J Physiol Gastrointest Liver Physiol, 2020. **318**(2): p. G211-g224.

82. Fu, J., et al., *Increased regulatory T cells correlate with CD8 T-cell impairment and poor survival in hepatocellular carcinoma patients.* Gastroenterology, 2007. **132**(7): p. 2328-39.

83. van der Leun, A.M., D.S. Thommen, and T.N. Schumacher, *Cd8(+) T cell states in human cancer: insights from single-cell analysis.* Nat Rev Cancer, 2020. **20**(4): p. 218-232.

84. Pfister, D., et al., *NASH limits anti-tumour surveillance in immunotherapy-treated HCC.* Nature, 2021. **592**(7854): p. 450-456.

85. Hernandez-Gea, V. and S.L. Friedman, *Pathogenesis of liver fibrosis.* Annu Rev Pathol, 2011. **6**: p. 425-56.

86. Tsuchida, T. and S.L. Friedman, *Mechanisms of hepatic stellate cell activation.* Nat Rev Gastroenterol Hepatol, 2017. **14**(7): p. 397-411.

87. Arthur, M.J., *Reversibility of liver fibrosis and cirrhosis following treatment for hepatitis C.* Gastroenterology, 2002. **122**(5): p. 1525-8.

88. Koda, Y., et al., *CD8+ tissue-resident memory T cells promote liver fibrosis resolution by inducing apoptosis of hepatic stellate cells.* Nat Commun, 2021. **12**(1): p. 4474.

89. Roche, P.A. and P. Cresswell, *Antigen Processing and Presentation Mechanisms in Myeloid Cells.* Microbiol Spectr, 2016. **4**(3).

90. Klein, J., *The major histocompatibility complex of the mouse.* Science, 1979. **203**(4380): p. 516-21.

91. Hewitt, E.W., *The MHC class I antigen presentation pathway: strategies for viral immune evasion.* Immunology, 2003. **110**(2): p. 163-9.

92. Schuster, H., et al., *A tissue-based draft map of the murine MHC class I immunopeptidome.* Sci Data, 2018. **5**: p. 180157.

93. Granados, D.P., et al., *The nature of self for T cells-a systems-level perspective.* Curr Opin Immunol, 2015. **34**: p. 1-8.

94. Adamopoulou, E., et al., *Exploring the MHC-peptide matrix of central tolerance in the human thymus.* Nat Commun, 2013. **4**: p. 2039.

95. de Verteuil, D., et al., *Deletion of immunoproteasome subunits imprints on the transcriptome and has a broad impact on peptides presented by major histocompatibility complex I molecules.* Mol Cell Proteomics, 2010. **9**(9): p. 2034-47.

96. McDonnell, W.J., et al., *High CD8 T-Cell Receptor Clonality and Altered CDR3 Properties Are Associated With Elevated Isolevuglandins in Adipose Tissue During Diet-Induced Obesity.* Diabetes, 2018. **67**(11): p. 2361-2376.

97. Kent, S.C., et al., *Expanded T cells from pancreatic lymph nodes of type 1 diabetic subjects recognize an insulin epitope.* Nature, 2005. **435**(7039): p. 224-8.

98. Yang, H., et al., *Obesity accelerates thymic aging.* Blood, 2009. **114**(18): p. 3803-12.

99. Durgeau, A., et al., *Recent Advances in Targeting CD8 T-Cell Immunity for More Effective Cancer Immunotherapy.* Front Immunol, 2018. **9**: p. 14.

100. Nair, R. and J. Westin, *CAR T-Cells.* Adv Exp Med Biol, 2020. **1244**: p. 215-233.

101. Chemical, C., *Research Tools for Fatty Liver Diseases [Brochure]*. 2017: www.caymanchem.com. p. 1-4.

102. Zhong, X., et al., *State of CD8+ T cells in progression from nonalcoholic steatohepatitis to hepatocellular carcinoma: From pathogenesis to immunotherapy.* Biomed Pharmacother, 2023. **165**: p. 115131.

103. Nardo, G., M.C. Trolese, and C. Bendotti, *Major Histocompatibility Complex I Expression by Motor Neurons and Its Implication in Amyotrophic Lateral Sclerosis.* Front Neurol, 2016. **7**: p. 89.

104. Machado, M.V. and A.M. Diehl, *Pathogenesis of Nonalcoholic Steatohepatitis.* Gastroenterology, 2016. **150**(8): p. 1769-77.

105. Luedde, T., N. Kaplowitz, and R.F. Schwabe, *Cell death and cell death responses in liver disease: mechanisms and clinical relevance.* Gastroenterology, 2014. **147**(4): p. 765-783.e4.

106. Zimmermann, H.W. and F. Tacke, *Modification of chemokine pathways and immune cell infiltration as a novel therapeutic approach in liver inflammation and fibrosis.* Inflamm Allergy Drug Targets, 2011. **10**(6): p. 509-36.

107. Puri, P., et al., *A lipidomic analysis of nonalcoholic fatty liver disease.* Hepatology, 2007. **46**(4): p. 1081-90.

108. Tan, H.L., et al., *Allele HLA-DQB1*06 reduces fibrosis score in patients with non-alcoholic fatty liver disease.* Hepatol Res, 2020. **50**(8): p. 947-954.

109. Gough, S.C. and M.J. Simmonds, *The HLA Region and Autoimmune Disease: Associations and Mechanisms of Action.* Curr Genomics, 2007. **8**(7): p. 453-65.

110. Jones, D.E. and P.T. Donaldson, *Genetic factors in the pathogenesis of primary biliary cirrhosis.* Clin Liver Dis, 2003. **7**(4): p. 841-64.

111. Kamatani, Y., et al., *A genome-wide association study identifies variants in the HLA-DP locus associated with chronic hepatitis B in Asians.* Nat Genet, 2009. **41**(5): p. 591-5.

112. Karlsen, T.H., et al., *Genome-wide association analysis in primary sclerosing cholangitis.* Gastroenterology, 2010. **138**(3): p. 1102-11.

113. Karrar, A., et al., *Analysis of human leukocyte antigen allele polymorphism in patients with non alcoholic fatty liver disease.* Medicine (Baltimore), 2019. **98**(32): p. e16704.

114. Govaere, O., et al., *Transcriptomic profiling across the nonalcoholic fatty liver disease spectrum reveals gene signatures for steatohepatitis and fibrosis.* Sci Transl Med, 2020. **12**(572).

115. Willemin, G., et al., *Major Histocompatibility Class II Pathway Is Not Required for the Development of Nonalcoholic Fatty Liver Disease in Mice.* Int J Endocrinol, 2013. **2013**: p. 972962.

116. Barrow, F., et al., *Microbiota-Driven Activation of Intrahepatic B Cells Aggravates NASH Through Innate and Adaptive Signaling.* Hepatology, 2021. **74**(2): p. 704-722.

117. Wen, Y., et al., *Hepatic macrophages in liver homeostasis and diseases-diversity, plasticity and therapeutic opportunities.* Cell Mol Immunol, 2021. **18**(1): p. 45-56.

118. Nati, M., K.J. Chung, and T. Chavakis, *The Role of Innate Immune Cells in Nonalcoholic Fatty Liver Disease.* J Innate Immun, 2022. **14**(1): p. 31-41.

119. Duffield, J.S., et al., *Selective depletion of macrophages reveals distinct, opposing roles during liver injury and repair.* J Clin Invest, 2005. **115**(1): p. 56-65.

120. Pradere, J.P., et al., *Hepatic macrophages but not dendritic cells contribute to liver fibrosis by promoting the survival of activated hepatic stellate cells in mice.* Hepatology, 2013. **58**(4): p. 1461-73.

121. Wynn, T.A., A. Chawla, and J.W. Pollard, *Macrophage biology in development, homeostasis and disease.* Nature, 2013. **496**(7446): p. 445-55.

122. Cai, B., et al., *Macrophage MerTK Promotes Liver Fibrosis in Nonalcoholic Steatohepatitis.* Cell Metab, 2020. **31**(2): p. 406-421.e7.

123. He, W., et al., *Identifying a distinct fibrosis subset of NAFLD via molecular profiling and the involvement of profibrotic macrophages.* J Transl Med, 2023. **21**(1): p. 448.

124. Theisen, D.J., et al., *WDFY4 is required for cross-presentation in response to viral and tumor antigens.* Science, 2018. **362**(6415): p. 694-699.

125. Netea, M.G., et al., *Trained immunity: A program of innate immune memory in health and disease.* Science, 2016. **352**(6284): p. aaf1098.

126. Dai, H., et al., *PIRs mediate innate myeloid cell memory to nonself MHC molecules.* Science, 2020. **368**(6495): p. 1122-1127.

127. Arindkar, S., et al., *Antigen peptide transporter 1 is involved in the development of fructose-induced hepatic steatosis in mice.* J Gastroenterol Hepatol, 2013. **28**(8): p. 1403-9.

128. Kotsiliti, E., et al., *Intestinal B cells license metabolic T-cell activation in NASH microbiota/antigen-independently and contribute to fibrosis by IgA-FcR signalling.* J Hepatol, 2023. **79**(2): p. 296-313.

129. Ortiz-López, N., et al., *The immune response as a therapeutic target in non-alcoholic fatty liver disease.* Front Immunol, 2022. **13**: p. 954869.

130. Bhattacharjee, J., et al., *Role of immunodeficient animal models in the development of fructose induced NAFLD.* J Nutr Biochem, 2014. **25**(2): p. 219-26.

131. Malo, C.S., et al., *Non-equivalent antigen presenting capabilities of dendritic cells and macrophages in generating brain-infiltrating CD8.* Nat Commun, 2018. **9**(1): p. 633.

132. Duan, L., et al., *Prioritize biologically relevant ions for data-independent acquisition (BRI-DIA) in LC-MS/MS-based lipidomics analysis.* Metabolomics, 2022. **18**(8): p. 55.

133. Vugmeyster, Y., et al., *Major histocompatibility complex (MHC) class I KbDb -/- deficient mice possess functional CD8+ T cells and natural killer cells.* Proc Natl Acad Sci U S A, 1998. **95**(21): p. 12492-7.

134. Kärre, K., et al., *Selective rejection of H-2-deficient lymphoma variants suggests alternative immune defence strategy.* Nature, 1986. **319**(6055): p. 675-8.

135. Salcedo, M., et al., *Fine tuning of natural killer cell specificity and maintenance of self tolerance in MHC class I-deficient mice.* Eur J Immunol, 1998. **28**(4): p. 1315-21.

136. Dorfman, J.R., et al., *The basis for self-tolerance of natural killer cells in beta2-microglobulin- and TAP-1- mice.* J Immunol, 1997. **159**(11): p. 5219-25.

137. Nguyen, P., et al., *Liver lipid metabolism.* J Anim Physiol Anim Nutr (Berl), 2008. **92**(3): p. 272-83.

138. Ganz, M., et al., *Progression of non-alcoholic steatosis to steatohepatitis and fibrosis parallels cumulative accumulation of danger signals that promote inflammation and liver tumors in a high fat-cholesterol-sugar diet model in mice.* J Transl Med, 2015. **13**: p. 193.

139. Gan, L.T., et al., *Hepatocyte free cholesterol lipotoxicity results from JNK1-mediated mitochondrial injury and is HMGB1 and TLR4-dependent.* J Hepatol, 2014. **61**(6): p. 1376-84.

140. Tacke, F., *Targeting hepatic macrophages to treat liver diseases.* J Hepatol, 2017. **66**(6): p. 1300-1312.

141. Koda, Y., et al., *CD8.* Nat Commun, 2021. **12**(1): p. 4474.

142. Fujii, T., et al., *Expression and Function of the Cholinergic System in Immune Cells.* Front Immunol, 2017. **8**: p. 1085.

143. Fain, C.E., *H-2Kb and H-2Db class I molecules on cerebral endothelium differentially modulate CD8 T cells dynamics and pathological outcomes in experimental cerebral malaria.* The Journal of Immunology, 2022. **208**.

144. Tritz, Z.P., et al., *Conditional Silencing of H-2D.* J Immunol, 2020. **205**(5): p. 1228-1238.

145. Huseby Kelcher, A.M., et al., *Brain atrophy in picornavirus-infected FVB mice is dependent on the H-2D.* FASEB J, 2017. **31**(6): p. 2267-2275.

146. Altintas, A., et al., *Differential expression of H-2K and H-2D in the central nervous system of mice infected with Theiler's virus.* J Immunol, 1993. **151**(5): p. 2803-12.

147. Xu, H.C., et al., *Single MHC-I Expression Promotes Virus-Induced Liver Immunopathology.* Hepatol Commun, 2022. **6**(7): p. 1620-1633.

148. Bassani-Sternberg, M., et al., *Direct identification of clinically relevant neoepitopes presented on native human melanoma tissue by mass spectrometry.* Nat Commun, 2016. **7**: p. 13404.

149. Boon, T., et al., *Human T cell responses against melanoma.* Annu Rev Immunol, 2006. **24**: p. 175-208.

150. Dutoit, V., et al., *Exploiting the glioblastoma peptidome to discover novel tumour-associated antigens for immunotherapy.* Brain, 2012. **135**(Pt 4): p. 1042-54.

151. Kowalewski, D.J., et al., *HLA ligandome analysis identifies the underlying specificities of spontaneous antileukemia immune responses in chronic lymphocytic leukemia (CLL).* Proc Natl Acad Sci U S A, 2015. **112**(2): p. E166-75.

152. Löffler, M.W., et al., *Mapping the HLA Ligandome of Colorectal Cancer Reveals an Imprint of Malignant Cell Transformation.* Cancer Res, 2018. **78**(16): p. 4627-4641.

153. Gonzalez-Duque, S., et al., *Conventional and Neo-antigenic Peptides Presented by β Cells Are Targeted by Circulating Naïve CD8+ T Cells in Type 1 Diabetic and Healthy Donors.* Cell Metab, 2018. **28**(6): p. 946-960.e6.

154. Nishimura, S., et al., *CD8+ effector T cells contribute to macrophage recruitment and adipose tissue inflammation in obesity.* Nat Med, 2009. **15**(8): p. 914-20.

155. Yang, H., et al., *Obesity increases the production of proinflammatory mediators from adipose tissue T cells and compromises TCR repertoire diversity: implications for systemic inflammation and insulin resistance.* J Immunol, 2010. **185**(3): p. 1836-45.

156. Chen, X., et al., *Obesity Reshapes Visceral Fat-Derived MHC I Associated-Immunopeptidomes and Generates Antigenic Peptides to Drive CD8.* iScience, 2020. **23**(4): p. 100977.

157. Sutti, S. and E. Albano, *Adaptive immunity: an emerging player in the progression of NAFLD.* Nat Rev Gastroenterol Hepatol, 2020. **17**(2): p. 81-92.

158. Haas, J.T., et al., *Transcriptional Network Analysis Implicates Altered Hepatic Immune Function in NASH development and resolution.* Nat Metab, 2019. **1**(6): p. 604-614.

159. Wang, T., et al., *The immunoregulatory effects of CD8 T-cell-derived perforin on diet-induced nonalcoholic steatohepatitis.* FASEB J, 2019. **33**(7): p. 8490-8503.

160. Kowalewski, D.J. and S. Stevanović, *Biochemical large-scale identification of MHC class I ligands.* Methods Mol Biol, 2013. **960**: p. 145-157.

161. Jiang, J.X. and N.J. Török, *NADPH Oxidases in Chronic Liver Diseases.* Adv Hepatol, 2014. **2014**.

162. Feng, D., et al., *Increased expression of NAD(P)H oxidase subunit p67(phox) in the renal medulla contributes to excess oxidative stress and salt-sensitive hypertension.* Cell Metab, 2012. **15**(2): p. 201-8.

163. Ming, W., et al., *The Rac effector p67phox regulates phagocyte NADPH oxidase by stimulating Vav1 guanine nucleotide exchange activity.* Mol Cell Biol, 2007. **27**(1): p. 312-23.

164. Ashraf, N.U. and T.A. Sheikh, *Endoplasmic reticulum stress and Oxidative stress in the pathogenesis of Non-alcoholic fatty liver disease.* Free Radic Res, 2015. **49**(12): p. 1405-18.

165. Arroyave-Ospina, J.C., et al., *Role of Oxidative Stress in the Pathogenesis of Non-Alcoholic Fatty Liver Disease: Implications for Prevention and Therapy.* Antioxidants (Basel), 2021. **10**(2).

166. Del Ben, M., et al., *NOX2-generated oxidative stress is associated with severity of ultrasound liver steatosis in patients with non-alcoholic fatty liver disease.* BMC Gastroenterol, 2014. **14**: p. 81.

167. Deczkowska, A., et al., *XCR1.* Nat Med, 2021. **27**(6): p. 1043-1054.

168. Sundara Rajan, S. and M.P. Longhi, *Dendritic cells and adipose tissue.* Immunology, 2016. **149**(4): p. 353-361.

169. Adams, V.R., et al., *Myeloid cell MHC I expression drives CD8+ T cell activation in nonalcoholic steatohepatitis.* Frontiers in Immunology, 2023. **14**.

170. Wang, Y., et al., *A TNF-α blocking peptide that reduces NF-κB and MAPK activity for attenuating inflammation.* Bioorg Med Chem, 2023. **92**: p. 117420.

171. Zhou, Q., T. Gwag, and S. Wang, *Thrombospondin1 antagonist peptide treatment attenuates obesity-associated chronic inflammation and metabolic disorders in a diet-induced obese mouse model.* Sci Rep, 2023. **13**(1): p. 20193.

172. von Herrath, M.G., et al., *In vivo treatment with a MHC class I-restricted blocking peptide can prevent virus-induced autoimmune diabetes.* J Immunol, 1998. **161**(9): p. 5087-96.

173. Havasi, A., et al., *Blocking peptides and molecular mimicry as treatment for kidney disease.* Am J Physiol Renal Physiol, 2017. **312**(6): p. F1016-F1025.

174. Sarma, S., et al., *Computational Design and Experimental Validation of ACE2-Derived Peptides as SARS-CoV-2 Receptor Binding Domain Inhibitors.* J Phys Chem B, 2022. **126**(41): p. 8129-8139.

175. Xiao, X., C.K. Hall, and P.F. Agris, *The design of a peptide sequence to inhibit HIV replication: a search algorithm combining Monte Carlo and self-consistent mean field techniques.* J Biomol Struct Dyn, 2014. **32**(10): p. 1523-36.

176. Xiao, X., P.F. Agris, and C.K. Hall, *Designing peptide sequences in flexible chain conformations to bind RNA: a search algorithm combining Monte Carlo, self-consistent mean field and concerted rotation techniques.* J Chem Theory Comput, 2015. **11**(2): p. 740-52.

177. Xiao, X., et al., *Adding energy minimization strategy to peptide-design algorithm enables better search for RNA-binding peptides: Redesigned λ N peptide binds boxB RNA.* J Comput Chem, 2016. **37**(27): p. 2423-35.

178. Xiao, X., et al., *Extended Concerted Rotation Technique Enhances the Sampling Efficiency of the Computational Peptide-Design Algorithm.* J Chem Theory Comput, 2017. **13**(11): p. 5709-5720.

179. Xiong, X., et al., *Mapping the molecular signatures of diet-induced NASH and its regulation by the hepatokine Tsukushi.* Mol Metab, 2019. **20**: p. 128-137.

180. van der Lienden, M.J.C., et al., *Glycoprotein Non-Metastatic Protein B: An Emerging Biomarker for Lysosomal Dysfunction in Macrophages.* Int J Mol Sci, 2018. **20**(1).

181. van der Burg, S.H., et al., *Immunogenicity of peptides bound to MHC class I molecules depends on the MHC-peptide complex stability.* J Immunol, 1996. **156**(9): p. 3308-14.

182. Micheletti, F., et al., *Selective amino acid substitutions of a subdominant Epstein-Barr virus LMP2-derived epitope increase HLA/peptide complex stability and immunogenicity: implications for immunotherapy of Epstein-Barr virus-associated malignancies.* Eur J Immunol, 1999. **29**(8): p. 2579-89.

183. Burrows, J.M., et al., *The impact of HLA-B micropolymorphism outside primary peptide anchor pockets on the CTL response to CMV.* Eur J Immunol, 2007. **37**(4): p. 946-53.

184. Nicholls, S., et al., *Secondary anchor polymorphism in the HA-1 minor histocompatibility antigen critically affects MHC stability and TCR recognition.* Proc Natl Acad Sci U S A, 2009. **106**(10): p. 3889-94.

185. Spierings, E., et al., *Steric hindrance and fast dissociation explain the lack of immunogenicity of the minor histocompatibility HA-1Arg Null allele.* J Immunol, 2009. **182**(8): p. 4809-16.

186. Lipford, G.B., et al., *In vivo CTL induction with point-substituted ovalbumin peptides: immunogenicity correlates with peptide-induced MHC class I stability.* Vaccine, 1995. **13**(3): p. 313-20.

187. van Stipdonk, M.J., et al., *Design of agonistic altered peptides for the robust induction of CTL directed towards H-2Db in complex with the melanoma-associated epitope gp100.* Cancer Res, 2009. **69**(19): p. 7784-92.

188. Lazarski, C.A., et al., *The kinetic stability of MHC class II:peptide complexes is a key parameter that dictates immunodominance.* Immunity, 2005. **23**(1): p. 29-40.

189. Hall, F.C., et al., *Relationship between kinetic stability and immunogenicity of HLA-DR4/peptide complexes.* Eur J Immunol, 2002. **32**(3): p. 662-70.

190. Pogue, R.R., et al., *Amino-terminal alteration of the HLA-A*0201-restricted human immunodeficiency virus pol peptide increases complex stability and in vitro immunogenicity.* Proc Natl Acad Sci U S A, 1995. **92**(18): p. 8166-70.

191. Brooks, J.M., et al., *HLA-B27 subtype polymorphism and CTL epitope choice: studies with EBV peptides link immunogenicity with stability of the B27:peptide complex.* J Immunol, 1998. **161**(10): p. 5252-9.

192. Abdel-Motal, U.M., et al., *Dendritic cell vaccination induces cross-reactive cytotoxic T lymphocytes specific for wild-type and natural variant human immunodeficiency virus type 1 epitopes in HLA-A*0201/Kb transgenic mice.* Clin Immunol, 2001. **101**(1): p. 51-8.

193. Vertuani, S., et al., *Improved immunogenicity of an immunodominant epitope of the HER-2/neu protooncogene by alterations of MHC contact residues.* J Immunol, 2004. **172**(6): p. 3501-8.

194. Grohmann, U., et al., *Immunogenicity of tumor peptides: importance of peptide length and stability of peptide/MHC class II complex.* Cancer Immunol Immunother, 1999. **48**(4): p. 195-203.

195. Bruno, B.J., G.D. Miller, and C.S. Lim, *Basics and recent advances in peptide and protein drug delivery.* Ther Deliv, 2013. **4**(11): p. 1443-67.

196. Berillo, D., et al., *Peptide-Based Drug Delivery Systems.* Medicina (Kaunas), 2021. **57**(11).

197. Wang, L., et al., *Therapeutic peptides: current applications and future directions.* Signal Transduct Target Ther, 2022. **7**(1): p. 48.

198. Gabbia, D., L. Cannella, and S. De Martin, *The Role of Oxidative Stress in NAFLD-NASH-HCC Transition-Focus on NADPH Oxidases.* Biomedicines, 2021. **9**(6).

199. De Filippis, F., et al., *High-level adherence to a Mediterranean diet beneficially impacts the gut microbiota and associated metabolome.* Gut, 2016. **65**(11): p. 1812-1821.

200. Bäckhed, F., et al., *The gut microbiota as an environmental factor that regulates fat storage.* Proc Natl Acad Sci U S A, 2004. **101**(44): p. 15718-23.

201. Bäckhed, F., et al., *Mechanisms underlying the resistance to diet-induced obesity in germ-free mice.* Proc Natl Acad Sci U S A, 2007. **104**(3): p. 979-84.

202. Loomba, R., et al., *Gut Microbiome-Based Metagenomic Signature for Non-invasive Detection of Advanced Fibrosis in Human Nonalcoholic Fatty Liver Disease.* Cell Metab, 2017. **25**(5): p. 1054-1062.e5.